On the structural and dynamical properties of a new class of galaxy models with a central BH
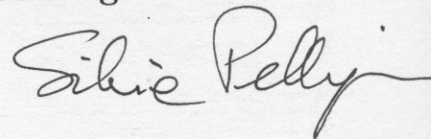
TESI DI LAUREA MAGISTRALE

PRESENTATA DA:
Antonio Mancino

RELATORE:
**Chiar.mo Prof.
Luca Ciotti**

CORRELATORE:
**Chiar.ma Prof.ssa
Silvia Pellegrini**

ABSTRACT

This thesis work focuses on the dynamical properties of two-component galaxy models character-ized by a *stellar* density distribution $\rho_*(r)$ described by a Jaffe profile, and a *galaxy* (stars plus dark matter) density distribution $\rho_{\rm g}(r)$ following a r^{-3} shape at large radii. The dark matter (hereafter, DM) density profile is defined by the difference $\rho_{\rm g}(r) - \rho_*(r)$, thus the approach used to build this family of models is different from the standard one, where a DM halo is added to the stellar distribution. The advantage of this strategy is that only one integration is required to solve the Jeans equations, because the total potential is assigned. The orbital structure of the stellar component is described by the Osipkov-Merritt (OM) radial anisotropy, and that of the DM halo is assumed isotropic; a black hole (BH) is also added at the center of the galaxy.

The thesis is organized as follows. In Chapter 2 the main structural properties of the models are presented, and the conditions required to have a nowhere negative and monothonically decreasing DM halo density profile are derived; a discussion is also given of how the DM component can be built in order to have the same asymptotical behaviour, in the outer regions and near the center, as the Navarro-Frenk-White (NFW) profile. In Chapter 3 an investigation of the phase-space properties of the models is carried out, both from the point of view of the necessary and sufficient conditions for consistency, and from the direct inspection of the distribution function; the minimum value of the anisotropy radius for consistency is derived in terms of the galaxy parameters. In Chapter 4 the analytical solution of the Jeans equations with OM anisotropy is presented, together with the projection of the velocity dispersion profile at small and large radii. Finally, in Chapter 5 the global quantities entering the Virial theorem are explicitly calculated; these can be used for energetic considerations that are briefly mentioned, and allow us to determine the fiducial anisotropy limit required to prevent the onset of Radial Orbit Instability as a function of the galaxy parameters. The main results are summarized in Chapter 6, and some technical details are given in the Appendices.

Most of the main results obtained are completely analytical; when this is not possible, the asymptotic behaviour is given or a numerical inspection is presented. Furthermore this class of models, even though idealized, can be useful as a starting point for more advanced modeling of the dynamics and the mass distribution of elliptical galaxies; for example, an extension to the axisymmetric case, and an application in the field of BH accretion, are in progress.

In this thesis, the symbol "$\equiv$" stands for "is defined as", while "$=$" is used for equality between two quantities previously defined; "$\sim$" means "asymptotic to", whereas "$\simeq$" indicates approximate numerical equivalence.

SOMMARIO

In questa tesi vengono studiate le proprietà strutturali e dinamiche di una particolare famiglia di modelli di galassia a due componenti: la distribuzione di densità di massa *stellare* $\rho_*(r)$ è descritta da un profilo di Jaffe, mentre il profilo di densità della *galassia* (stelle più materia oscura) va come r^{-3} a grandi raggi. Il profilo di densità di materia oscura (DM) è definto dalla differenza $\rho_g(r) - \rho_*(r)$. Questo approccio è differente da quello standard, in cui l'alone di DM viene solitamente sommato al profilo di stelle; tuttavia, essendo il potenziale totale assegnato in partenza, ha il vantaggio di richiedere una sola integrazione per risolvere le equazioni di Jeans. La struttura orbitale della componente stellare è descritta dall'anisotropia radiale di Osipkov-Merritt (OM), mentre l'alone di DM è assunto isotropo; al centro della galassia vi è poi la presenza di un buco nero.

La tesi è organizzata come segue. Nel Capitolo 2 vengono presentate le principali proprietà dei modelli, nonché esaminate le condizioni di non-negatività e monotonicità del profilo di densità di DM; segue poi una discussione sulla possibilità di costruire un modello che abbia un profilo di DM asintoticamente equivalente, sia a piccoli raggi sia nelle regioni esterne, a quello di Navarro-Frenk-White (NFW). Il Capitolo 3 si concentra sull'analisi della consistenza, discutendo dapprima le condizioni necessarie e sufficienti per avere una funzione di distribuzione non-negativa su tutto lo spazio delle fasi, e successivamente effettuando uno studio numerico diretto della funzione di distribuzione stessa; da ultimo viene calcolato, in funzione dei parametri che definiscono il modello, il valore minimo che deve avere il raggio di anisotropia affinché sia verificata la condizione di consistenza. Nel Capitolo 4 vengono risolte le equazioni di Jeans in presenza di anisotropia di tipo OM; viene poi determinato l'andamento asintotico, vicino al centro e a grande distanza, del profilo di dispersione di velocità proiettata. Il Capitolo 5 si focalizza sull'analisi dell'energetica, calcolando esplicitamente le principali quantità che obbediscono al teorema del Viriale e determinando il valore del raggio di anisotropia minimo richiesto per prevenire il manifestarsi di orbite instabili. Nel Capitolo 6 vengono infine riassunti i principali risultati; i dettagli più tecnici vengono discussi nelle Appendici.

Molti dei risultati ottenuti sono completamente analitici; quando questo non è possibile, vengono forniti andamenti asintotici o direttamente soluzioni numeriche. Questo permette ai modelli J3 di poter essere utilizzati come punto di partenza per studi dinamici più sofisticati: una loro estensione al caso assisimmetrico e un'applicazione alla fisica dell'accrescimento sono già in fase di sviluppo.

In questa tesi, il simbolo "≡" significa "uguale per definizione", mentre "=" viene utilizzato per stabilire l'uguaglianza tra due grandezze precedentemente definite; inoltre, "∼" significa "asintotico a", mentre "≃" indica un'approssimazione numerica.

CONTENTS

CHAPTER 1

INTRODUCTION

SPHERICALLY symmetric galaxy models, thanks to their simplicity, can be useful in exploratory works in Stellar Dynamics (see, e.g., Bertin 2000, Binney & Tremaine 2008). A successful spherical model compensates its geometric limitations with other features, such as the possibilities to:

- derive manageable analytical expressions for the most important dynamical quantities;

- include a dark matter (hereafter, DM) halo with an adjustable density profile;

- model the dynamical effects of a central black hole (hereafter, BH);

- control orbital anisotropy.

A model for the density profile of the stellar distribution, once projected, should be similar to that of early-type galaxies (hereafter, ETGs), which are usually described by de Vaucouleurs's law (see de Vaucouleurs 1948). As is well known, unfortunately this law does not allow for an explicit deprojection via elementary functions. However, Jaffe's model (see Jaffe 1983), which belongs to the family of the so-called γ models (see Dehnen 1993, Tremaine et al. 1994), has the advantage of resemble, in projection, de Vaucouleurs's law with sufficient accurancy over a large range for most of applications. For this reason, Jaffe's density profile is a natural choice to describe the stellar distribution of ETGs in the spherical approximation.

Once the stellar profile of the model is considered acceptable, a second important feature of a useful spherical model is the possibility to reproduce, with a minor effort, the large scale properties of the *total* density profile (see, e.g., Bertin et al. 1994, Rix et al. 1997, Gerhard et al. 2001, Rusin et al. 2003, Treu & Koopmans 2004, Rusin & Kochanek 2005, Koopmans et al. 2006, Gavazzi et al. 2007, Czoske et al. 2008, Dye et al. 2008, Nipoti et al. 2008; see also Shankar et al. 2017). For example, simple spherical models with a flat rotation curve have been constructed (see, e.g., Kochaneck 1994, Naab & Ostriker 2007; Ciotti et al. 2009, hereafter CMZ09; see also the double power-law models of Hiotelis 1994).

Finally, since supermassive BHs with a mass of the order of $M_{\mathrm{BH}} \simeq 10^{-3} M_*$ are routinely found at the center of the stellar spheroids of total mass M_* (see, e.g., Magorrian et al. 1988, Kormendy & Ho 2013), a third significant feature of a useful spherical model is the possibility to easily compute the dynamical properties of the stellar component in presence of a central BH.

Following the arguments above, a family of models (hereafter, JJ models) with a Jaffe profile for the stellar distribution, and a galaxy (stars plus DM) density profile described by another Jaffe law has already been proposed (see Ciotti & Ziaee Lorzad 2018, hereafter CZ18). Since the

cumulative mass associated with a Jaffe profile is finite, the total mass of JJ models kept finite; at the same time, since the scale length of the galaxy density is a free parameter, the models can reproduce an r^{-2} profile over a quite arbitrary large radial range. For the JJ models in presence of a central BH, the Jeans equations with Osipkov-Merritt (hereafter, OM; see Osipkov 1979, Merritt 1985) radial anisotropy can be solved analytically; further, the projected velocity dispersion can be expressed by means of simple formulae both at small and large radii for generic values of the model parameters. Moreover, for these models also the positivity of the phase-space distribution function (hereafter, DF) can be easily studied, together with the maximum amount of radial anisotropy allowable for consistency.

One of the most interesting features of the JJ models is that in the special *minumum halo* case, the DM profile, also for this class of models defined by the difference between the galaxy and the stellar profiles, behaves like r^{-1} close to the center, similarly to the Navarro-Frenk-White profile (hereafter, NFW; see Navarro et al. 1997). At large radii, instead, the DM profile decreases as r^{-4}, at variance with the NFW profile that goes as r^{-3}. The natural question left open is then if it is possible to construct models with similar analytical properties of JJ models, but with the additional property that the DM follows the r^{-3} shape in the external regions. In this paper we show that, indeed, this *is* possible, and we call the resulting models "J3", to stress that the stellar density is again a Jaffe model, while the DM decreases as r^{-3} at large radii. In particular, we shall prove that the DM halo, in minimum halo J3 models, can be made remarkably similar to the NFW over the *whole* radial range.

CHAPTER 2

THE MODELS

IN this Chapter the main structural properties of the family of two-component galaxy models that will be used throughout the whole thesis work are presented. The Chapter is organized as follows.

In Section 2.1 the spatial distribution of the stellar mass density is introduced, and the main properties of Jaffe's profile are summarized.

In Section 2.2 the radial trend of the total mass density is studied. Particular attention is paid to the derivation of the projection quantities and their comparison with the corresponding expressions for the stellar component.

In Section 2.3 the DM halo density profile, defined as the difference between the total and the stellar profiles, is discussed. Then, the conditions required to have a nowhere negative and monotonically decreasing DM halo density profile are derived. A discussion is also given of how the DM component can be built in order to have the same asymptotical behaviour, in the outer regions and near the center, as the NFW profile.

2.1   The stellar distribution

Let the stellar component be described by a Jaffe profile (see Jaffe 1983). Thus, its density distribution is given by

$$\rho_*(r) = \frac{\rho_{\mathrm{n}}}{s^2(1+s)^2}, \qquad \rho_{\mathrm{n}} \equiv \frac{M_*}{4\pi r_*^3}, \qquad (2.1)$$

where M_* is the (finite) total stellar mass, r_* is a scale length, and $s \equiv r/r_*$ is the dimensionless radius; the quantity ρ_{n}, then, does represent the natural density scale.

One of the advanteges of the model proposed by Jaffe is the analytical computing of many of its properties. By integrating the density profile over the whole space, we obtain the cumulative mass contained within the sphere of radius r, i.e.,

$$M_*(r) = 4\pi \int_0^r \rho_*(x)x^2 dx = M_* \times \frac{s}{1+s}. \qquad (2.2)$$

Therefore, r_* is the half-mass radius and, as anticipated, $M_*(r)$ tends to M_* for $r \to \infty$. The Newtonian potential $\Psi_*(r)$ can also be easily determined, with the natural condition of vanishing at infinity, by integrating Poisson's equation $\nabla^2\Psi_*(r) = -4\pi G\rho_*(r)$, where $G \simeq 6.67 \times 10^{-8}\,\mathrm{cm}^3\,\mathrm{sec}^{-2}\,\mathrm{g}^{-1}$ is the constant of gravitation. For the density in eq. (2.1) we have

$$\Psi_*(r) = \frac{GM_*(r)}{r} + 4\pi G \int_r^\infty \rho_*(x)x\,dx = \Psi_{\mathrm{n}} \ln \frac{1+s}{s}, \qquad \Psi_{\mathrm{n}} \equiv \frac{GM_*}{r_*}, \qquad (2.3)$$

where Ψ_{n} represents the natural potential scale. Consequently the stellar potential, which is monotonic bacause of spherical symmetry, diverges logarithmically near the center, while it goes to zero like r^{-1} at large radii (see Fig. 2.4). Notice that the quantity $GM_*(r)/r$ is nothing else than the square of the circular speed $v_{\mathrm{c}*}(r)$, defined to be the speed of a test particle in circular orbit at radius r; from eq. (2.2) we readily obtain

$$v_{\mathrm{c}*}^2(r) = \frac{\Psi_{\mathrm{n}}}{1+s}, \qquad (2.4)$$

whose behaviour is shown in Fig. 2.7. The projected density profile $\Sigma_*(R)$ can be computed by integrating the spatial density distribution along the line of sight; for a Jaffe profile we find

$$\Sigma_*(R) = 2 \int_R^\infty \frac{\rho_*(r)r dr}{\sqrt{r^2 - R^2}} = \Sigma_{\mathrm{n}} \times g_*(\eta), \qquad g_*(\eta) \sim \begin{cases} \dfrac{\pi}{\eta}, & \eta \to 0, \\[2mm] \dfrac{\pi}{2\eta^3}, & \eta \to \infty, \end{cases} \qquad (2.5)$$

where $\Sigma_{\mathrm{n}} \equiv M_*/(4\pi r_*^2)$ is the natural projected density scale, and $\eta \equiv R/r_*$ is the projected radius in units of r_*. The analytical expression of the well known dimensionless function $g_*(\eta)$ is given in Appendix A, and the trend of $\Sigma_*(R)$ is shown in Fig. 2.1.
Finally, the projected mass $M_{\mathrm{p}*}(R)$ contained within the cylinder of radius R, given by

$$M_{\mathrm{p}*}(R) = 2\pi \int_0^R \Sigma_*(R')R'dR', \qquad (2.6)$$

can be derived in terms of elementary functions. We shall now prove that, for spherical systems
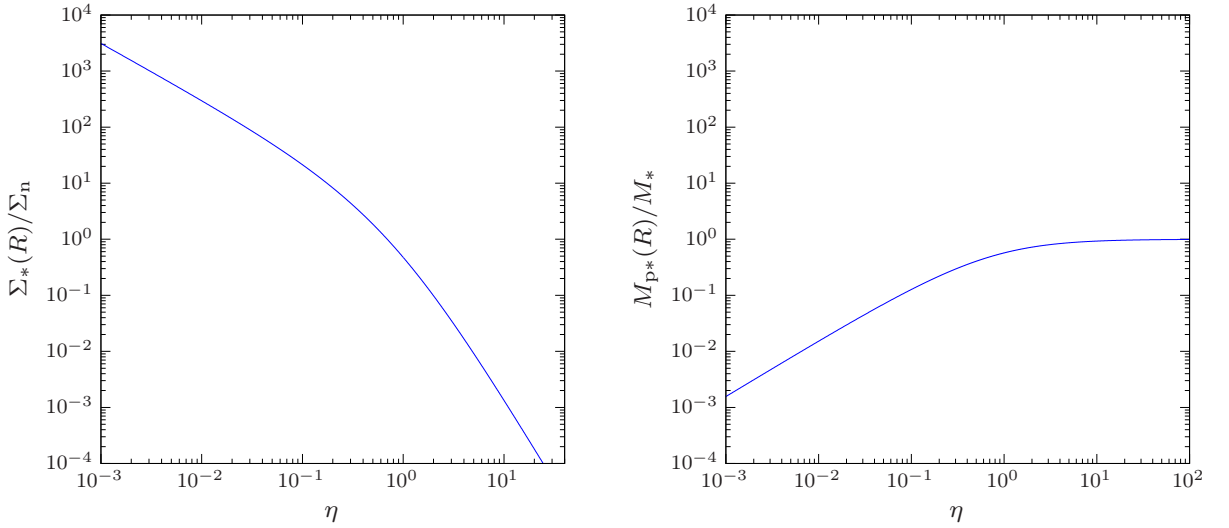
Figure 2.1. The behaviours of $\Sigma_*(R)$ (left panel) and $M_{\mathrm{p}*}(R)$ (right panel), as functions of $\eta = R/r_*$.

of *finite* total mass, this important structural property can be rewritten in a simpler form. First, inserting the expression (2.5) in eq. (2.6), and changing the order of integration, we obtain

$$M_{\mathrm{p}*}(R) = \int_0^R dx \int_x^\infty F(x,r)dr$$

$$= \int_0^R dr \int_0^r F(x,r)dx + \int_R^\infty dr \int_0^R F(x,r)dx, \qquad F(x,r) \equiv \frac{4\pi r \rho_*(r)x}{\sqrt{r^2 - x^2}}. \qquad (2.7)$$

Then, after some minor reductions, we find

$$M_{\mathrm{p}*}(R) = 4\pi \int_0^R \rho_*(r)r^2 dr + 4\pi \int_R^\infty \rho_*(r)r^2 dr - 4\pi \int_R^\infty \rho_*(r)r\sqrt{r^2 - R^2}\, dr. \qquad (2.8)$$

Now, because the total stellar mass is finite, the first two terms in the equation above can be combined to give the following expression:

$$M_{\mathrm{p}*}(R) = M_* - 4\pi \int_R^\infty \rho_*(r)r\sqrt{r^2 - R^2}\, dr. \qquad (2.9)$$

Therefore, computing the integration for the density in eq. (2.1), we obtain that the projected mass of the Jaffe stellar profile can be written as

$$M_{\mathrm{p}*}(R) = M_* \times h_*(\eta), \qquad h_*(\eta) \sim \begin{cases} \dfrac{\pi}{2}\, \eta, & \eta \to 0, \\[2mm] 1, & \eta \to \infty, \end{cases} \qquad (2.10)$$

where $h_*(\eta)$ is a well known dimensionless function, presented in Appendix A; as expected, $h_*(\eta) \to 1$ for $\eta \to \infty$ (see Fig. 2.1). In particular, the effective radius R_{e} of the Jaffe profile (i.e., the radius in the projection plane encircling half of the total mass), for which $h_*(\eta_{\mathrm{e}}) = 1/2$, is $R_{\mathrm{e}} \simeq 0.7447\, r_*$.

2.2   The total mass distribution

Let the galaxy mass density distribution be

$$\rho_{\mathrm{g}}(r) = \frac{\mathcal{R}\rho_{\mathrm{n}}}{s^2(\xi + s)}, \qquad\qquad \xi \equiv \frac{r_{\mathrm{g}}}{r_*}, \tag{2.11}$$

where $\mathcal{R}$ is a dimensionless factor, and r_{g} is the galaxy scale length; clearly, every formula in the thesis (if not differently stated) applies to positive values of ξ, even if *realistic* cases are obtained for $\xi \geq 1$. As $\xi\rho_{\mathrm{g}}(r) \sim \mathcal{R}\rho_{\mathrm{n}}/s^2$ and $\rho_*(r) \sim \rho_{\mathrm{n}}/s^2$ at small radii, the natural condition that $\rho_{\mathrm{g}}(r) \geq \rho_*(r)$ close to the center implies $\mathcal{R} \geq \xi$; however, as we shall see in the following, this condition can become more stringent when considered over the whole radial range (see Fig. 2.3).

The cumulative mass distribution associated with the density $\rho_{\mathrm{g}}(r)$ is

$$M_{\mathrm{g}}(r) = 4\pi \int_0^r \rho_{\mathrm{g}}(x)x^2 dx = M_*\mathcal{R} \int_0^s \frac{dy}{\xi + y} = M_*\mathcal{R} \ln\frac{\xi + s}{\xi}. \tag{2.12}$$

Hence, at variance with the stellar profile, the total mass is divergent. Nevertheless, the previous equation provides a method to define the dimensionless factor $\mathcal{R}$: indeed, evaluating $M_{\mathrm{g}}(r)$ for $r = r_{\mathrm{g}}$, we readily find $M_{\mathrm{g}}(r_{\mathrm{g}})/M_* = \mathcal{R}\ln 2$, which lead us to express $\mathcal{R}$ as a mass ratio. Moreover, by considering the behaviour of $\rho_{\mathrm{g}}(r)$ and $\rho_*(r)$ near the center, we find

$$\mathcal{R} = \xi \times \lim_{r \to 0} \frac{\rho_{\mathrm{g}}(r)}{\rho_*(r)}, \tag{2.13}$$

thus $\mathcal{R}$ could also be interpreted as a galaxy-to-stellar density ratio.

Also in this case we are able to determine the potential without any mathematical difficulties; even though the total mass is infinite, yet the normalization value at infinity can still be assumed equal to zero, inasmuch as the density profile at large radii is steeper than r^{-2}. With this assumption, the galaxy potential can be calculated as

$$\Psi_{\mathrm{g}}(r) = \frac{GM_{\mathrm{g}}(r)}{r} + 4\pi G \int_r^\infty \rho_{\mathrm{g}}(x)x\,dx$$

$$= \frac{\Psi_{\mathrm{n}}\mathcal{R}}{s} \ln\frac{\xi + s}{\xi} + \Psi_{\mathrm{n}}\mathcal{R} \int_s^\infty \frac{dy}{y(\xi + y)}, \tag{2.14}$$

whence, performing the integration,

$$\Psi_{\mathrm{g}}(r) = \Psi_{\mathrm{n}}\mathcal{R} \left(\frac{1}{s}\ln\frac{\xi + s}{\xi} + \frac{1}{\xi}\ln\frac{\xi + s}{s}\right). \tag{2.15}$$

In the external regions the first term in brackets dominates, which goes to zero like $(\ln s)/s$; near the center, instead, the potential runs to infinity as $-\ln s$, because of the second term's behaviour. It is of interest to note that the second term is nothing else than the rescaled Jaffe potential in eq. (2.3); indeed, by using Poisson's equation in order to find the radial density profile $\hat{\rho}_*(r)$ corresponding to this term, we obtain

$$\hat{\rho}_*(r) = -\frac{1}{4\pi G r^2}\frac{d}{dr}\left[r^2\frac{d}{dr}\left(\frac{\Psi_{\mathrm{n}}\mathcal{R}}{\xi}\ln\frac{\xi + s}{s}\right)\right] = \frac{\xi\mathcal{R}\rho_{\mathrm{n}}}{s^2(\xi + s)^2}, \tag{2.16}$$

which is clearly the rescaled Jaffe density profile in eq. (2.1).
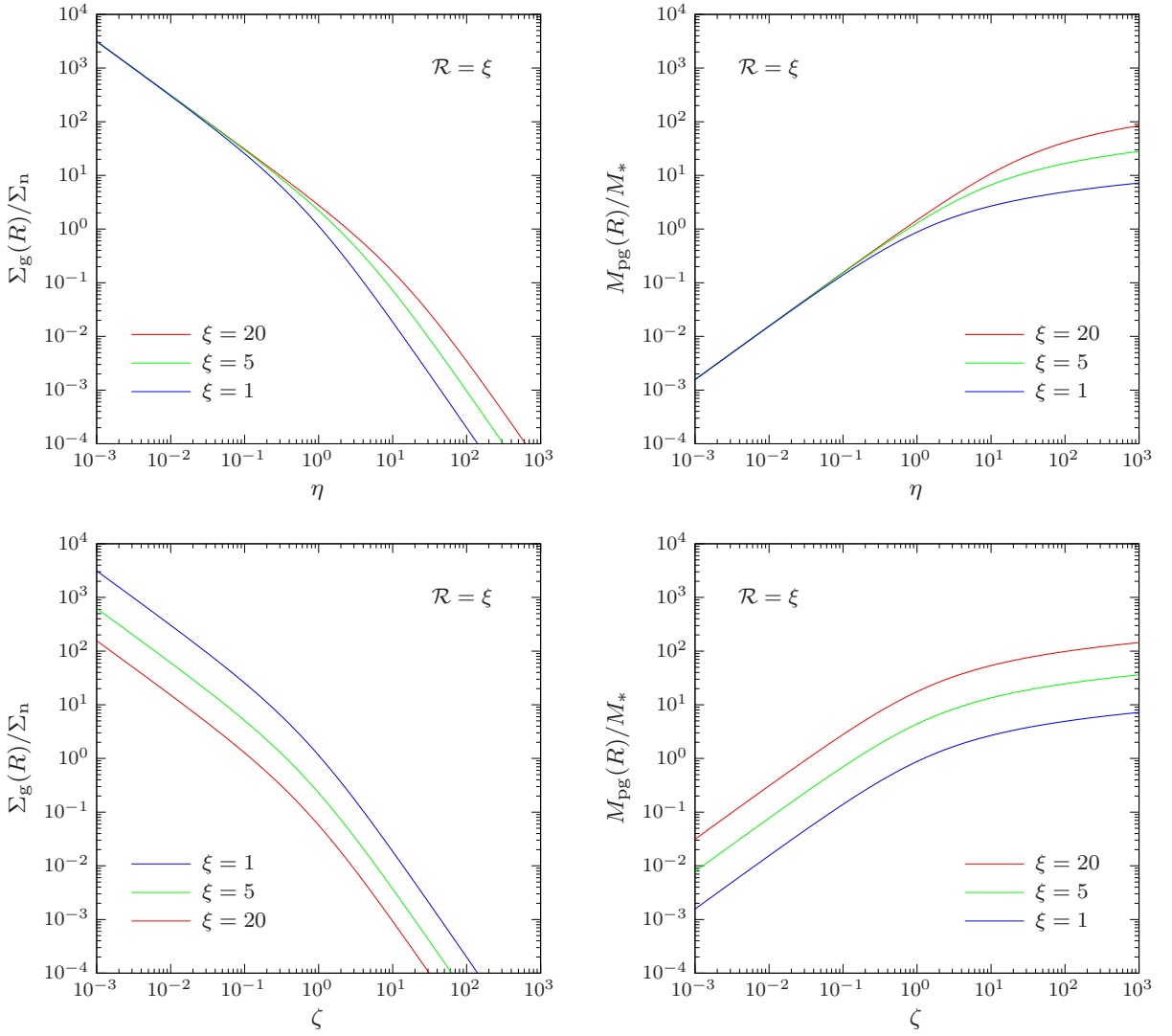
Figure 2.2. The behaviours of $\Sigma_{\mathrm{g}}(R)$ and $M_{\mathrm{pg}}(R)$, as functions of $\eta = R/r_*$ (top panels) and $\zeta = R/r_{\mathrm{g}}$ (bottom panels), for three representative models with $\mathcal{R} = \xi$.

In analogy with eq. (2.5), it is possible to derive the galaxy projected density at radius R in the projection plane. In Appendix A it is shown that

$$\Sigma_{\mathrm{g}}(R) = \Sigma_{\mathrm{n}} \times \frac{\mathcal{R}}{\xi^2} \, g_{\mathrm{g}}(\zeta), \qquad g_{\mathrm{g}}(\zeta) \sim \begin{cases} \dfrac{\pi}{\zeta}, & \zeta \to 0, \\[2mm] \dfrac{2}{\zeta^2}, & \zeta \to \infty, \end{cases} \tag{2.17}$$

where $\zeta \equiv R/r_{\mathrm{g}}$, and the analytical expression of the dimensionless function $g_{\mathrm{g}}(\zeta)$ is given in eq. (A7). Figure 2.2 shows the behaviour of $\Sigma_{\mathrm{g}}(R)$, as a function of η and $\zeta = \eta/\xi$, for three realistic models ($\xi \geq 1$) with $\mathcal{R} = \xi$.

In order to find the projected mass $M_{\mathrm{pg}}(R)$, since the cumulative mass associated with the galaxy density profile is divergent, we cannot apply the eq. (2.9) to the profile $\rho_{\mathrm{g}}(r)$; for this purpose we must necessarily integrate the projected density $\Sigma_{\mathrm{g}}(R)$ previously derived. As shown in Appendix A,

$$M_{\mathrm{pg}}(R) = M_* \mathcal{R} \times h_{\mathrm{g}}(\zeta), \qquad h_{\mathrm{g}}(\zeta) \sim \begin{cases} \dfrac{\pi}{2}\,\zeta, & \zeta \to 0, \\[2ex] \ln \zeta, & \zeta \to \infty, \end{cases} \tag{2.18}$$

where $h_{\mathrm{g}}(\zeta)$ is a dimensionless function, given in eq. (A15), and the trend of $M_{\mathrm{pg}}(R)$ is depicted in Fig. 2.2.

As a central BH of mass M_{BH} is added at the center of the galaxy, the *total* mass profile $M_{\mathrm{T}}(r) = M_{\mathrm{g}}(r) + M_{\mathrm{BH}}$ and the *total* potential $\Psi_{\mathrm{T}}(r) = \Psi_{\mathrm{g}}(r) + GM_{\mathrm{BH}}/r$ become, respectively,

$$M_{\mathrm{T}}(r) = M_* \times \left(\mathcal{R} \ln \frac{\xi + s}{\xi} + \mu \right), \qquad \Psi_{\mathrm{T}}(r) = \Psi_{\mathrm{n}} \times \left(\frac{\mathcal{R}}{s} \ln \frac{\xi + s}{\xi} + \frac{\mathcal{R}}{\xi} \ln \frac{\xi + s}{s} + \frac{\mu}{s} \right), \tag{2.19}$$

where $\mu \equiv M_{\mathrm{BH}}/M_*$ is a free parameter of the models, which we shall set equal to 0.002 (see, e.g., Magorrian et al. 1988, Kormendy & Ho 2013). For the sake of completeness, we also give the expression for the *total* mass density in presence of the central BH; this can be achieved by adding to $\rho_{\mathrm{g}}(r)$ the density distribution $\rho_{\mathrm{BH}}(r)$ of a point particle with mass M_{BH} located at $r = 0$, i.e.,

$$\rho_{\mathrm{T}}(r) = \rho_{\mathrm{g}}(r) + \rho_{\mathrm{BH}}(r), \qquad \rho_{\mathrm{BH}}(r) = M_{\mathrm{BH}} \times \frac{\delta(r)}{4\pi r^2} = \mu \rho_{\mathrm{n}} \frac{\delta(s)}{s^2}, \tag{2.20}$$

where $\delta(r)$ denotes Dirac's δ-function.

Finally, the circular speed $v_{\mathrm{c}}(r)$ of the total distribution is

$$v_{\mathrm{c}}^2(r) = \frac{GM_{\mathrm{T}}(r)}{r} = \frac{\Psi_{\mathrm{n}}}{s} \times \left(\mathcal{R} \ln \frac{\xi + s}{\xi} + \mu \right) \sim \Psi_{\mathrm{n}} \times \begin{cases} \dfrac{\mu}{s} + \dfrac{\mathcal{R}}{\xi}, & r \to 0, \\[2ex] \dfrac{\mathcal{R} \ln s}{s}, & r \to \infty. \end{cases} \tag{2.21}$$

In particular, as the asymptotic behaviour shows, the circular velocity profile goes to zero in the external regions; very close to the center, instead, while in general (i.e., for $\mu \neq 0$) the radial profile tends to infinity, in absence of the central BH it reduces to a constant. Obviously, as $M_{\mathrm{T}}(r) = M_{\mathrm{g}}(r) + M_{\mathrm{BH}}$, it follows that $v_{\mathrm{c}}^2(r) = v_{\mathrm{cg}}^2(r) + v_{\mathrm{cBH}}^2(r)$, with

$$v_{\mathrm{cg}}^2(r) = \frac{GM_{\mathrm{g}}(r)}{r} = \frac{\Psi_{\mathrm{n}} \mathcal{R}}{s} \ln \frac{\xi + s}{s}, \qquad v_{\mathrm{cBH}}^2(r) = \frac{GM_{\mathrm{BH}}}{r} = \frac{\Psi_{\mathrm{n}} \mu}{s}. \tag{2.22}$$

The trends of $v_{\mathrm{c}}(r)$ and $v_{\mathrm{cBH}}(r)$ are shown in Fig. 2.7 (right panel) for a selected choice of the model parameters.

2.3   The DM distribution

Given the stellar and the galaxy density profiles, the DM density distribution is obtained by the difference

$$\rho_{\mathrm{DM}}(r) = \rho_{\mathrm{g}}(r) - \rho_*(r) = \frac{\rho_{\mathrm{n}}}{s^2} \times \left[\frac{\mathcal{R}}{\xi + s} - \frac{1}{(1 + s)^2} \right]. \tag{2.23}$$

By construction, in general, the behaviour of $\rho_{\mathrm{DM}}(r)$ depends on ξ and $\mathcal{R}$. Nevertheless, not all values of these two parameters are compatible with a nowhere negative distribution $\rho_{\mathrm{DM}}(r)$. Expanding eq. (2.23) near the center and at large radii, we have

$$
\rho_{\mathrm{DM}}(r) \sim \rho_{\mathrm{n}} \times \begin{cases} \dfrac{\mathcal{R} - \xi}{\xi s^2} + \dfrac{2\xi^2 - \mathcal{R}}{\xi^2 s} + \dfrac{\mathcal{R} - 3\xi^3}{\xi^3}, & r \to 0, \\[3mm] \dfrac{\mathcal{R}}{s^3}, & r \to \infty. \end{cases} \tag{2.24}
$$

Therefore, while in the external regions the DM is *always* dominant over the stars, close to the center the leading order term of the expansion depends on the relation between $\mathcal{R}$ and ξ. A similar situation occurs when we consider the behaviour of the DM potential $\Psi_{\mathrm{DM}}(r) = \Psi_{\mathrm{g}}(r) - \Psi_*(r)$, whose expansion is given by

$$
\Psi_{\mathrm{DM}}(r) \sim \Psi_{\mathrm{n}} \times \begin{cases} -\dfrac{\mathcal{R} - \xi}{\xi} \ln s + \dfrac{\mathcal{R}(1 + \ln \xi)}{\xi}, & r \to 0, \\[3mm] \dfrac{\mathcal{R} \ln s}{s}, & r \to \infty. \end{cases} \tag{2.25}
$$

Before studying the dynamical properties of the models, it is important to determine the conditions for the *positivity* and radial *monotonicity* of the density distribution of the DM halo.

2.3.1 The positivity condition

The condition for the positivity of the DM halo density given in eq. (2.23) is obtained by imposing $\rho_{\mathrm{DM}}(r) \geq 0$ for $r \geq 0$, i.e.,

$$
\mathcal{R} \geq \frac{\xi + s}{(1 + s)^2} \equiv \mathcal{P}_\xi(s). \tag{2.26}
$$

Hence, $\mathcal{R}$ must be greater than or equal to the maximum $\mathcal{R}_{\mathrm{m}}(\xi)$ of the "positivity function" $\mathcal{P}_\xi(s)$; simple algebra shows that $d\mathcal{P}_\xi(s)/ds \geq 0$ if and only if $s \leq 1 - 2\xi$. Thus, while for $0 < \xi < 1/2$ the function $\mathcal{P}_\xi(s)$ exhibits a maximum in $s = 1 - 2\xi$, if $\xi \geq 1/2$ the maximum is reached in $s = 0$ (see Fig. 2.6). Consequently, the positivity condition for the DM halo density can be written as

$$
\mathcal{R} \geq \mathcal{R}_{\mathrm{m}}(\xi) = \begin{cases} \dfrac{1}{4(1 - \xi)}, & 0 < \xi < \dfrac{1}{2}, \\[3mm] \xi, & \xi \geq \dfrac{1}{2}. \end{cases} \tag{2.27}
$$

For given ξ, $\mathcal{R}_{\mathrm{m}}(\xi)$ is the *minimum* value of $\mathcal{R}$ in order to have a nowhere negative DM halo; for this reason, we call *minimum halo* a DM halo of a model with $\mathcal{R} = \mathcal{R}_{\mathrm{m}}(\xi)$. Notice that the foregoing condition for $\xi \geq 1/2$ is coincident with that obtained in Section 2.2 from the preliminary analysis in the central region; instead, for $0 < \xi < 1/2$, the condition is more stringent (see the dashed line in Fig. 2.3). This means that values of $(\xi, \mathcal{R})$ between the dashed and solid lines in Fig. 2.3 correspond to $\rho_{\mathrm{DM}}(r)$ that becomes negative off-center. Only values of $(\xi, \mathcal{R})$ located in the region above the black solid line are associated with a DM halo with a nowhere negative $\rho_{\mathrm{DM}}(r)$. The positivity condition allows to better establish the relative behaviour of $\rho_{\mathrm{DM}}(r)$ and $\rho_*(r)$ in the central region. Indeed, from eqs. (2.24) and (2.27) it follows that, for $\mathcal{R} > \mathcal{R}_{\mathrm{m}}(\xi)$,
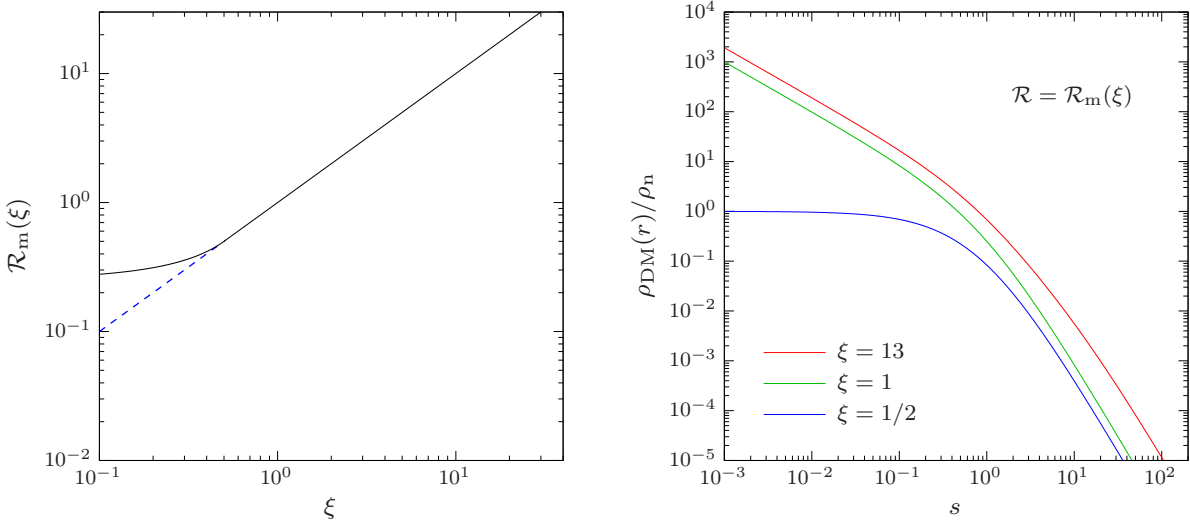
Figure 2.3. Left panel: the function $\mathcal{R}_{\mathrm{m}}(\xi)$, as given by eq. (2.27). Only models in the region above the black solid line have a DM halo with $\rho_{\mathrm{DM}}(r) \geq 0$. Right panel: radial trend of the DM halo density for three particular minimum halo models; while in the external regions $\rho_{\mathrm{DM}}(r)$ always follows a r^{-3} profile (see eq. [2.24]), at small radii it goes like r^{-1} or reduces to a constant depending on whether $\xi > 1/2$ or $\xi = 1/2$, respectively, as shown in eq. (2.28).

i.e. in non-minimum halo models, $\rho_{\mathrm{DM}}(r) \propto r^{-2}$, so the DM and stellar densities are locally proportional; in the minimum halo models, instead, where $\mathcal{R} = \mathcal{R}_{\mathrm{m}}(\xi)$, we have

$$
\rho_{\mathrm{DM}}(r) \sim \rho_{\mathrm{n}} \times \begin{cases} \dfrac{(2\xi - 1)^2}{4\xi(1 - \xi)s^2}, & 0 < \xi < \dfrac{1}{2}, \\[3mm] 1, & \xi = \dfrac{1}{2}, \\[3mm] \dfrac{2\xi - 1}{\xi s}, & \xi > \dfrac{1}{2}. \end{cases} \tag{2.28}
$$

In particular, in the physically interesting case of a minimum halo with $\xi \geq 1$, $\rho_{\mathrm{DM}}(r) \propto r^{-1}$, and so it is shallower than $\rho_*(r)$. Fig. 2.3 shows the behaviour of $\rho_{\mathrm{DM}}(r)$ for different minimum halo models; the case $0 < \xi < 1/2$ is not depicted because in this range of ξ the DM halo density profile vanishes for positive values of s.

A similar behavior at small radii is obtained for the DM potential; indeed, from eqs. (2.25) and (2.27), while in non-minimum halo models $\Psi_{\mathrm{DM}}(r) \propto -\ln s$, for $\mathcal{R} = \mathcal{R}_{\mathrm{m}}(\xi)$ we find

$$
\Psi_{\mathrm{DM}}(r) \sim \Psi_{\mathrm{n}} \times \begin{cases} -\dfrac{(2\xi - 1)^2}{4\xi(1 - \xi)} \ln s, & 0 < \xi < \dfrac{1}{2}, \\[3mm] 1 + \ln \xi, & \xi \geq \dfrac{1}{2}. \end{cases} \tag{2.29}
$$

In particular, for realistic minimum halo cases, $\Psi_{\mathrm{DM}}(r)$ is constant near the center (see Fig. 2.4).

The ratio of the DM-to-visible mass within a prescribed spatial radius r is derived from eqs. (2.12) and (2.2) as

$$
\frac{M_{\mathrm{DM}}(r)}{M_*(r)} = \mathcal{R} \frac{1 + s}{s} \ln \frac{\xi + s}{\xi} - 1, \tag{2.30}
$$
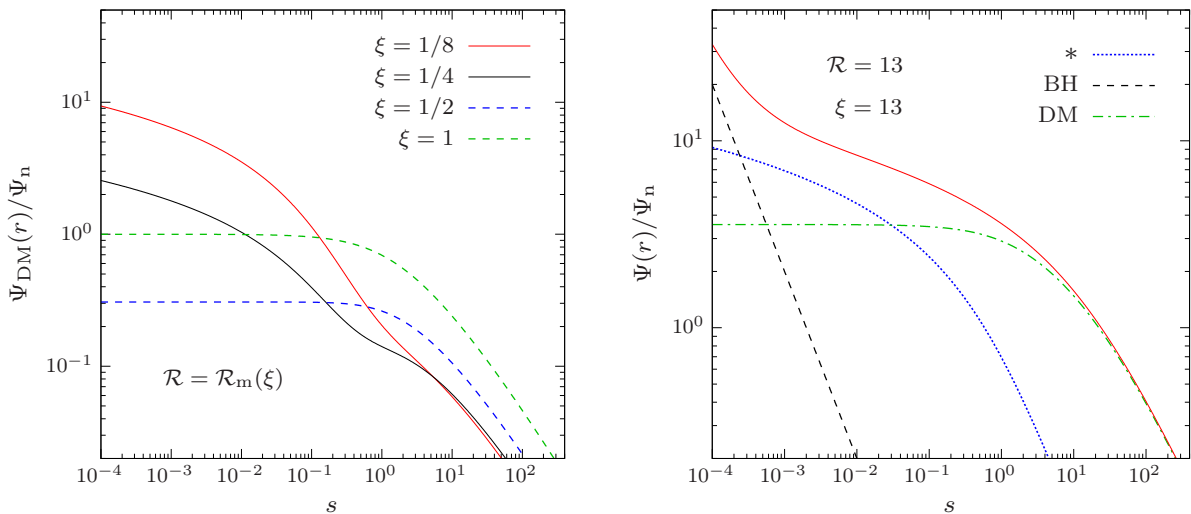
Figure 2.4. Left panel: radial trend of the DM potential $\Psi_{\mathrm{DM}}(r) = \Psi_{\mathrm{g}}(r) - \Psi_*(r)$, in case of minimum halo models, for different values of ξ; while at large radii the behaviour is proportional to $(\ln s)/s$ independently of ξ, close to the center it diverges logarithmically or reduces to a constant depending on whether $0 < \xi < 1/2$ or $\xi \geq 1/2$, respectively, as shown in eq. (2.29). Right panel: total potential profile for a minimum halo galaxy model with $\xi = 13$ and $\mu = 0.002$ (red solid line), as given in eq. (2.19), with the separate contributions of stars, BH, and the DM halo; notice that, in accordance with eq. (2.29), $\Psi_{\mathrm{DM}}(r) \sim (1 + \ln 13)\Psi_{\mathrm{n}} \simeq 3.56\,\Psi_{\mathrm{n}}$ at small radii.

where $M_{\mathrm{DM}}(r) = M_{\mathrm{g}}(r) - M_*(r)$. A similar behaviour is obtained for the ratio of the projected DM-to-visible mass within an aperture R; from eqs. (2.18) and (2.10) we obtain

$$\frac{M_{\mathrm{pDM}}(R)}{M_{\mathrm{p}*}(R)} = \mathcal{R}\,\frac{h_{\mathrm{g}}(\zeta)}{h_*(\eta)} - 1, \tag{2.31}$$

where $M_{\mathrm{pDM}}(R) = M_{\mathrm{pg}}(R) - M_{\mathrm{p}*}(R)$. The application of the condition eq. (2.27) therefore gives

$$\frac{M_{\mathrm{DM}}(r)}{M_*(r)} \geq \mathcal{R}_{\mathrm{m}}(\xi)\,\frac{1+s}{s}\ln\frac{\xi+s}{\xi} - 1, \qquad \frac{M_{\mathrm{pDM}}(R)}{M_{\mathrm{p}*}(R)} \geq \mathcal{R}_{\mathrm{m}}(\xi)\,\frac{h_{\mathrm{g}}(\zeta)}{h_*(\eta)} - 1. \tag{2.32}$$

In Fig. 2.5 the trends of the *minimum* values of $M_{\mathrm{DM}}(r)/M_*(r)$ and $M_{\mathrm{pDM}}(R)/M_{\mathrm{p}*}(R)$ are shown as functions of ξ for three representative choices of r and R, respectively. Even if the two profiles, in general, are non monotonic functions of ξ, for fixed $\xi \geq 1$ the minimum values in eq. (2.32) increases for increasing chosen (spatial or projected) radius.

Finally, the contribution of the DM component to the circular velocity $v_{\mathrm{c}}(r)$ reads

$$v_{\mathrm{cDM}}^2(r) = \frac{GM_{\mathrm{DM}}(r)}{r} = \frac{\Psi_{\mathrm{n}}}{s} \times \left(\mathcal{R}\ln\frac{\xi+s}{\xi} - \frac{s}{1+s}\right). \tag{2.33}$$

In Fig. 2.7, for reasons that will be clear in the following, this quantity is shown in case of minimum halo with $\xi = 13$.

2.3.2 The monotonicity condition

While the request of positivity for $\rho_{\mathrm{DM}}(r)$ is a first "natural" condition for the viability of the model, a brief comment is in order to justify a second important requirement. This request,
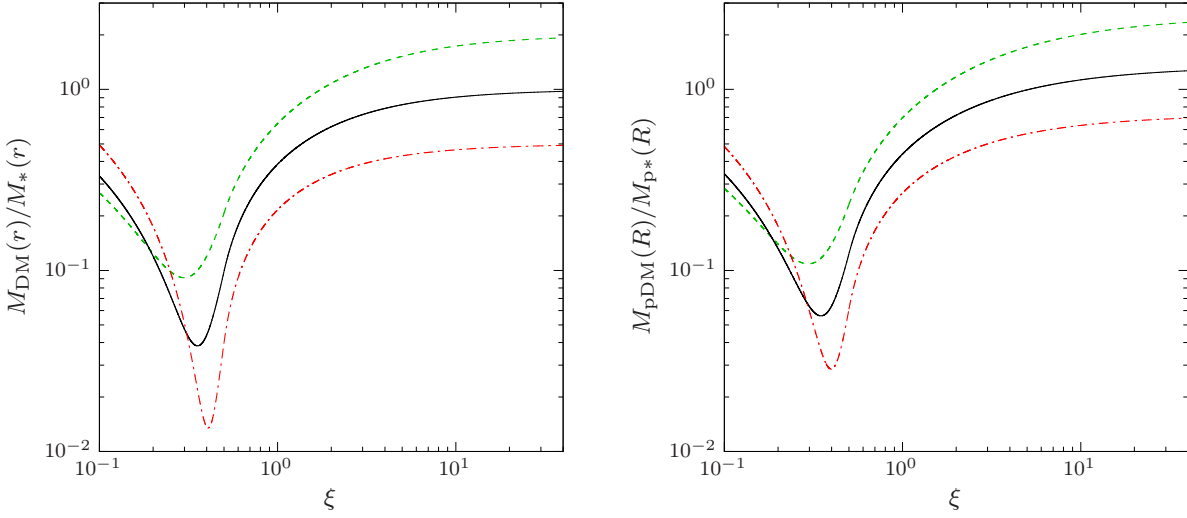
Figure 2.5. Left panel: the minimum value of the volumic DM-to-stellar mass ratio, given in eq. (2.32), inside a sphere of radius $r = 0.5r_*, r_*, 2r_*$ (red dashdotted, black solid and green dashed lines, respectively), as a function of ξ. Right panel: the minimum value of the projected DM-to-stellar mass ratio, given in eq. (2.32), inside the circle of radius $R = 0.5R_{\rm e}, R_{\rm e}, 2R_{\rm e}$ (red dashdotted, black solid and green dashed lines, respectively), as a function of ξ.

based on dynamical arguments, is the *monotonicity* of the DM halo density, which reduces to the determination of the minimum value $\mathcal{R}_{\rm mon}(\xi)$ so that $d\rho_{\rm DM}(r)/dr \leq 0$ for $r \geq 0$. As we shall see in Chapter 3, it can be shown that monotonicity of $\rho_{\rm DM}(r)$ is necessary for the positivity of the phase-space DF.

By differentiating $\rho_{\rm DM}(r)$ with respect to s, we obtain

$$\frac{d\rho_{\rm DM}(r)}{ds} = \rho_{\rm n} \frac{2(\xi + s)^2(1 + 2s) - \mathcal{R}(1 + s)^3(2\xi + 3s)}{s^3(\xi + s)^2(1 + s)^3}. \tag{2.34}$$

Therefore, imposing $d\rho_{\rm DM}(r)/dr \leq 0$ we have

$$\mathcal{R} \geq \frac{2(\xi + s)^2(1 + 2s)}{(1 + s)^3(2\xi + 3s)} \equiv \mathcal{M}_\xi(s). \tag{2.35}$$

As the foregoing inequality must be verified for all values of $r \geq 0$, it follows that $\mathcal{R}$ must be greater than or equal to the maximum $\mathcal{R}_{\rm mon}(\xi)$ of the "monotonicity function" $\mathcal{M}_\xi(s)$. In order to find $\mathcal{R}_{\rm mon}(\xi)$, we have to determine the sign of $d\mathcal{M}_\xi(s)/ds$; by differentiating the monotonicity function $\mathcal{M}_\xi(s)$ with respect to s, we find

$$\frac{d\mathcal{M}_\xi(s)}{ds} = -\frac{2(\xi + s)[6s^3 + 6(3\xi - 1)s^2 + (4\xi + 3)(2\xi - 1)s + \xi(2\xi - 1)]}{(1 + s)^4(2\xi + 3s)}. \tag{2.36}$$

Hence,

$$\frac{d\mathcal{M}_\xi(s)}{ds} \geq 0 \quad \Leftrightarrow \quad 6s^3 + 6(3\xi - 1)s^2 + (4\xi + 3)(2\xi - 1)s + \xi(2\xi - 1) \leq 0. \tag{2.37}$$

The explicit solution of the inequality above presents no formal difficulty; however, important information can be easily obtained without solving it.
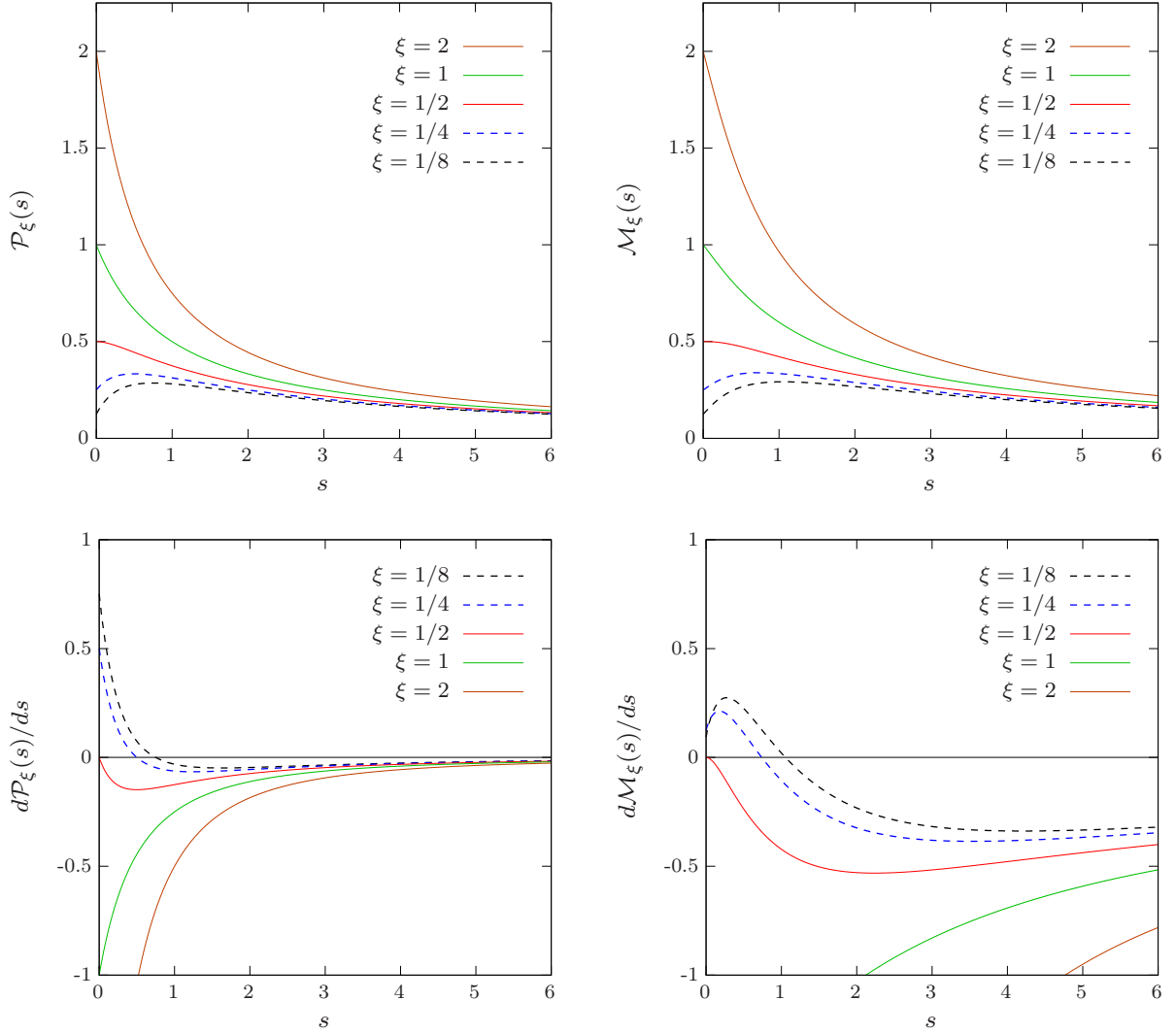
Figure 2.6. The functions $\mathcal{P}_\xi(s)$ and $\mathcal{M}_\xi(s)$, and their derivatives with respect to s, for different values of ξ.

- For $0 < \xi < 1/2$ the cubic function in eq. (2.37) is negative for small values of s, and positive for large values of s, and so $\mathcal{M}_\xi(s)$ has at least one maximum for $s \geq 0$, inasmuch as $d\mathcal{M}_\xi(s)/ds$ has at least one zero for non-negative values of s. Moreover, by Descartes's theorem it is found that at most one positive zero of the cubic exists (see Fig. 2.6), therefore corresponding to the single maximum $\mathcal{R}_{\mathrm{mon}}(\xi)$. As we are mainly interested in realistic models with $\xi \geq 1$, we do not discuss further this case;

- For $\xi \geq 1/2$ the cubic function in eq. (2.37) is nowhere negative (see Fig. 2.6), thus the maximum is reached at $s = 0$, with $\mathcal{R}_{\mathrm{mon}}(\xi) = \mathcal{M}_\xi(0) = \xi$.

Thus, in practice, *for $\xi \geq 1/2$ the positivity and monotonicity conditions coincide.*

2.3.3 Comparison with the NFW profile

We shall now compare the DM halo profile $\rho_{\mathrm{DM}}(r)$ with the NFW profile (see Navarro et al. 1997) $\rho_{\mathrm{NFW}}(r)$, which we write in general form as
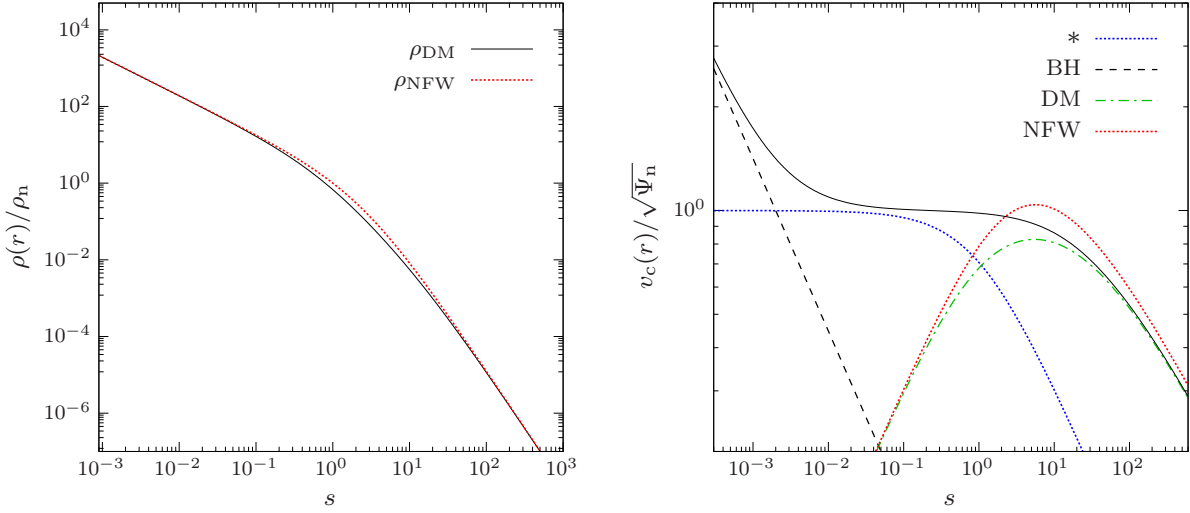
Figure 2.7. Left panel: comparison between the minimum halo DM profile of J3 models (black solid line) and the NFW profile (red dotted line), for $\xi = 13$ and $c = 10$. Right panel: circular velocity profile for the same minimum halo galaxy model with $\mu = 0.002$ (black solid line), with the separate contributions of BH, stars and the DM halo for the J3 model; the circular velocity profile associated with the density $\rho_{\mathrm{NFW}}(r)$ in the left panel (red dotted line) is also shown.

$$\rho_{\mathrm{NFW}}(r) = \frac{A}{r\left(r_{\mathrm{NFW}} + r\right)^2}, \tag{2.38}$$

where A is a normalization constant, and r_{NFW} a scale length. The cumulative mass distribution associated with this density profile reads

$$M_{\mathrm{NFW}}(r) = 4\pi \int_0^r \rho_{\mathrm{NFW}}(x)x^2 dx = 4\pi A\left(\ln \frac{\xi_{\mathrm{NFW}} + s}{\xi_{\mathrm{NFW}}} - \frac{s}{\xi_{\mathrm{NFW}} + s}\right), \tag{2.39}$$

where $\xi_{\mathrm{NFW}} \equiv r_{\mathrm{NFW}}/r_*$ is the NFW scale length in units of r_*. The mass profile is therefore logarithmically divergent; however, by choosing a truncation radius r_{t}, we readily find

$$M_{\mathrm{NFW}}(r_{\mathrm{t}}) = 4\pi A f(c), \qquad f(c) \equiv \ln(1+c) - \frac{c}{1+c}, \tag{2.40}$$

where $c \equiv r_{\mathrm{t}}/r_{\mathrm{NFW}}$ is the so-called "concentration parameter". Therefore, the constant A can be easily determined in order to obtain a NFW profile rewritten as

$$\rho_{\mathrm{NFW}}(r) = \frac{\rho_{\mathrm{n}}\mathcal{R}_{\mathrm{NFW}}}{f(c)s(\xi_{\mathrm{NFW}} + s)^2} \sim \rho_{\mathrm{n}}\frac{\mathcal{R}_{\mathrm{NFW}}}{f(c)} \times \begin{cases} \dfrac{1}{\xi_{\mathrm{NFW}}^2\, s}, & r \to 0, \\[2mm] \dfrac{1}{s^3}, & r \to \infty, \end{cases} \tag{2.41}$$

where we have defined $\mathcal{R}_{\mathrm{NFW}} \equiv M_{\mathrm{NFW}}(r_{\mathrm{t}})/M_*$. By construction, $\rho_{\mathrm{DM}}(r)$ and $\rho_{\mathrm{NFW}}(r)$ have the same behaviour at large radii. Moreover, in the central region, where $\rho_{\mathrm{NFW}}(r) \propto r^{-1}$, in the minimum halo case with $\xi > 1/2$, one also has $\rho_{\mathrm{DM}}(r) \propto r^{-1}$, as shown in eq. (2.28). Comparing the leading order terms of the expansions of $\rho_{\mathrm{NFW}}(r)$ and $\rho_{\mathrm{DM}}(r)$, for $\mathcal{R} = \mathcal{R}_{\mathrm{m}}(\xi)$ and $\xi > 1/2$, it follows that the two profiles can be made *asymptotically* coincident in the outer regions *and* near the center by imposing

$$\frac{\mathcal{R}_{\mathrm{NFW}}}{f(c)} = \xi, \qquad\qquad \xi_{\mathrm{NFW}} = \frac{\xi}{\sqrt{2\xi - 1}}. \qquad\qquad (2.42)$$

Hence, once a specific minimum halo galaxy model is considered, and then ρ_{n} and ξ are chosen, eqs. (2.41) and (2.42) allow to determine the NFW profile that best reproduces $\rho_{\mathrm{DM}}(r)$ by tuning the value of the ratio $\mathcal{R}_{\mathrm{NFW}}/f(c)$. While cosmological simulations predict $c \simeq 10$ (see, e.g., Bullock & Boylan-Kolchin 2017), Cosmology gives $\mathcal{R}_{\mathrm{NFW}} \simeq 15 \div 30$; therefore, in order to have a cosmologically motivated asymptotic coincidence, we *must* consider models with $\xi \simeq 10 \div 20$. Figure 2.7 (left panel) shows an example of how well a NFW profile can reproduce a minimum halo $\rho_{\mathrm{DM}}(r)$; in this figure $\xi = 13$ and $c = 10$, which give, from eq. (2.42), $\mathcal{R}_{\mathrm{NFW}} \simeq 20$ and $r_{\mathrm{NFW}} = 2.6\, r_*$. The right panel, instead, shows the different contributions of the variour mass component to the circular velocity $v_{\mathrm{c}}(r)$, given in eq. (2.21). The circular velocity profile corresponding to the NFW density distribution is given by

$$v^2_{\mathrm{cNFW}}(r) = \frac{GM_{\mathrm{NFW}}(r)}{r} = \frac{\Psi_{\mathrm{n}}\mathcal{R}_{\mathrm{NFW}}}{f(c)s} \times \left(\ln \frac{\xi_{\mathrm{NFW}} + s}{\xi_{\mathrm{NFW}}} - \frac{s}{\xi_{\mathrm{NFW}} + s} \right), \qquad (2.43)$$

which is shown in Fig. 2.7 once the relations in eq. (2.42) are used.

CHAPTER 3

THE PHASE-SPACE DF

IN this Chapter some properties of the phase-space distribution function of J3 models are discussed in order to exclude dynamically inconsistent combinations of parameters. The Chapter is organized as follows.

In Section 3.1 a minimum theoretical background is drawn, recalling the main properties of the DF of a stellar system, and the multi-component decomposition of galaxy models. Then, some general conditions for the consistency of spherical OM anisotropic systems are presented.

In Section 3.2 the investigation of the phase-space properties of J3 models is carried out, both from the point of view of the necessary and sufficient conditions for consistency.

In Section 3.3 the DF of the stellar component of J3 models is derived numerically for different choices of the model parameters.

3.1   The consistency of multi-component OM systems

In general, any collisionless system subject to a total potential $\Psi = \Psi(\mathbf{x}, t)$ is completely described by its *phase-space distribution function* (DF) $f = f(\mathbf{x}, \mathbf{v}, t)$, which satisfies the *Collisionless Boltzmann Equation* $Df(\mathbf{x}, \mathbf{v}, t)/Dt = 0$ (see Appendix B). We call *consistently generated* any system derived from a non-negative DF. Moreover, if the total mass density $\rho = \rho(\mathbf{x}, t)$ is related to the total potential by Poisson's equation, the system is called *self-consistently generated*.

Now suppose that the system, subject to a total potential $\Psi_\mathrm{T} = \Psi_\mathrm{T}(\mathbf{x}, t)$, is composed by n mass density components $\rho_1(\mathbf{x}, t), \rho_2(\mathbf{x}, t), \ldots, \rho_n(\mathbf{x}, t)$, each corresponding to a distribution function $f_1(\mathbf{x}, \mathbf{v}, t), f_2(\mathbf{x}, \mathbf{v}, t), \ldots, f_n(\mathbf{x}, \mathbf{v}, t)$, i.e.,

$$\int_{\mathbb{R}^3} f_k(\mathbf{x}, \mathbf{v}, t) d^3\mathbf{v} = \rho_k(\mathbf{x}, t), \qquad\qquad (k = 1, \ldots, n). \qquad\qquad (3.1)$$

Since each $f_k(\mathbf{x}, \mathbf{v}, t)$ represents the probability density of finding some star in the volume $d^3\mathbf{x}\, d^3\mathbf{v}$ centred on $(\mathbf{x}, \mathbf{v})$ at the time t, it *must* be nowhere negative. This observation implies that if the k-th DF takes a negative value somewhere over the accessible phase-space, then the model is physically unfounded. For this reason, the function

$$f_\mathrm{T}(\mathbf{x}, \mathbf{v}, t) \equiv \sum_{k=1}^{n} f_k(\mathbf{x}, \mathbf{v}, t) \qquad\qquad (3.2)$$

is said to be the DF of the n-component system *if and only if*

$$\frac{Df_k(\mathbf{x}, \mathbf{v}, t)}{Dt} = 0, \qquad\qquad f_k(\mathbf{x}, \mathbf{v}, t) \geq 0, \qquad\qquad (k = 1, \ldots, n). \qquad\qquad (3.3)$$

In this case, each component $f_k(\mathbf{x}, \mathbf{v}, t)$ is said to be a *consistent component*. Moreover, if

$$\nabla^2 \Psi_\mathrm{T}(\mathbf{x}, t) = -4\pi G \rho_\mathrm{T}(\mathbf{x}, t), \qquad\qquad \rho_\mathrm{T}(\mathbf{x}, t) \equiv \sum_{k=1}^{n} \rho_k(\mathbf{x}, t), \qquad\qquad (3.4)$$

the n-component system is defined *self-consistent*.

The phase-space consistency is an essential requirement to have a physically acceptable model, and so it represents an important check of the validity of the whole model. In general, when studying the self-consistency of dynamical models, several strategies can be adopted (see, e.g., Bertin 2000, Binney & Tremaine 2008). In this thesis work we shall adopt the approach known as "ρ-to-f", an investigation method motivated by the fact that the density distribution is the quantity which is best constrained by the observations. Indeed, once a mass density profile is assumed, its free parameters can be determined by deprojecting the observed luminosity profile and specifing a certain mass-to-ligth ratio. Nevertheless, the DF is generally difficult to recover, which in many cases makes it impossible to carry out a simple consistency analysis. Indeed, the general problem can be formuled as the problem of inverting the integral equation (3.1) for an assigned density profile. Once the DF is recovered, in order to guarantee the consistency of the constructed galaxy model, i.e. its physical validity, the non-negativity of the DF should be checked; however, since the difficulties inherent in the operation of recovering analytically the DF prevent a simple consistency analysis, a numerical exploration is usually needed. Thus, it would be noteworthy to have a technique permitting to check the non-negativity of the distribution function without the explicit calculation of it. As we shall see in the following, such a technique, when the orbital anisotropy of each component is of the OM form, has been developed by Ciotti and Pellegrini, which have shown that in this case it is possible to obtain lower bounds for the

anisotropy radius as a function of the stellar density slope and the total mass profile[1] (see CP92), without actually recovering the DF.

In case of anisotropic OM spherical systems, the (stationary) DF f_k of each density component depends on the *relative energy* (per unit mass) $\mathcal{E} \equiv \Psi_{\mathrm{T}} - |\mathbf{v}|^2/2$ and on the angular momentum modulus (per unit mass) $J \equiv |\mathbf{x} \times \mathbf{v}|$ only through a linear combination of them, that is

$$
f_k = \begin{cases} f_k(Q_k), & Q_k > 0, \\ \\ 0, & Q_k \leq 0, \end{cases} \qquad Q_k \equiv \mathcal{E} - \frac{J^2}{2r_{\mathrm{ak}}^2}, \tag{3.5}
$$

where r_{ak} is the *anisotropy radius* associated with the k-th component. Moreover, for the k-th component the radial and tangential components of the velocity dispersion tensor (see Appendix B) in OM models are related as

$$
\beta_k(r) \equiv \frac{r^2}{r^2 + r_{\mathrm{ak}}^2}. \tag{3.6}
$$

As a consequence, the velocity dispersion tensor is isotropic at the center independently of the particular value of the anisotropy radius. The fully isotropic case is obtained for $r_{\mathrm{ak}} \to \infty$, while for $r_{\mathrm{ak}} = 0$ the galaxy is supported by radial orbits only. For finite values of r_{ak}, the velocity dispersion tensor becomes isotropic in the limit $r \to 0$ (in practice, for $r \ll r_{\mathrm{ak}}$), and fully radially anisotropic for $r \to \infty$ (in practice, for $r \gg r_{\mathrm{ak}}$).

One of the advantages of the OM parametrization is that a simple inversion formula to recover the DF of the k-component from the associated mass density profile can be derived. Indeed, by introducing the *augmented density*

$$
\varrho_k(r) \equiv \rho_k(r) \times \left(1 + \frac{r^2}{r_{\mathrm{ak}}^2} \right), \tag{3.7}
$$

it is found that

$$
f_k(Q_k) = \frac{1}{\sqrt{8}\pi^2} \frac{d}{dQ_k} \int_0^{Q_k} \frac{d\varrho_k}{d\Psi_{\mathrm{T}}} \frac{d\Psi_{\mathrm{T}}}{\sqrt{Q_k - \Psi_{\mathrm{T}}}}. \tag{3.8}
$$

where it is intended that ϱ_k is expressed in terms of Ψ_{T}. By integrating by parts the integral in the foregoing equation, and performing the differentiation with respect to Q_k, we obtain that eq. (3.8) can be rewritten as[2]

$$
f_k(Q_k) = \frac{1}{\sqrt{8}\pi^2} \left[\int_0^{Q_k} \frac{d^2\varrho_k}{d\Psi_{\mathrm{T}}^2} \frac{d\Psi_{\mathrm{T}}}{\sqrt{Q_k - \Psi_{\mathrm{T}}}} + \frac{1}{\sqrt{Q_k}} \left(\frac{d\varrho_k}{d\Psi_{\mathrm{T}}} \right)_{\Psi_{\mathrm{T}}=0} \right]. \tag{3.9}
$$

---

[1]We recall that the CP92 result has been shown to be a special case of a class of more general inequalities connecting the local density slope and the anisotropy profile in consistent spherical models: the so-called Global Density Slope-Anisotropy Inequality (GDSAI; see, e.g., de Bruijne et al. 1996, An & Evans 2006, Ciotti & Morganti 2009, van Hese et al. 2011).

[2]Let $\varphi(x, \alpha)$ be a continuous functions of the two variables x and α when x varies from X and Y, and α varies between cerain limits α_1 and α_2. If the limits X and Y are themselves functions of α, i.e., $X = X(\alpha)$ and $Y = Y(\alpha)$, it follows that

$$
\frac{d}{d\alpha} \int_X^Y \varphi(x, \alpha) dx = \int_X^Y \frac{\partial\varphi(x, \alpha)}{\partial\alpha} dx + \frac{dY}{d\alpha} \varphi(Y, \alpha) - \frac{dX}{d\alpha} \varphi(X, \alpha),
$$

which is the general formula for *differentiation under the integral sign* (see, e.g., Goursat 1904).

Note that, although the previous equation seem rather complicated, for untruncated systems of finite total mass the second term in square brackets in eq. (3.9) vanishes.

It is important to stress the fact that the recovered DFs $f_k(Q_k)$ are not guaranteed to be non-negative definite. For, we shall now proceed to discuss about the limitations on r_{ak} imposed by the request of phase-space consistency, i.e., $f_k(Q_k) \geq 0$ over the accessible phase-space. Following CP92, a *necessary condition* (hereafter, NC) for the non-negativity of the DF of each of the mass components in the total potential is that, for all values of $r \geq 0$,

$$\frac{d\varrho_k(r)}{dr} \leq 0, \qquad (k = 1, \ldots, n). \tag{3.10}$$

Note that the NC for the k-component is *independent of the behaviour of the other* $(n-1)$ *density components of the system*, therefore its violation is related only to the radial trend of the augmented density $\varrho_k(r)$ and the value of the anisotropy radius r_{ak}. Since this condition is only necessary, $f_k(Q_k)$ can be negative even for values of model parameters allowed by the NC, and so the k-th component *may be* inconsistent. On the other hand, a *weak sufficient condition* (hereafter, WSC) for consistency is obtained by requiring that the derivative inside the last integral in eq. (3.9) be non-negative; therefore, by expressing this condition as a function of radius, the WSC requires that, for $r \geq 0$,

$$\frac{d}{dr}\left[\frac{d\varrho_k(r)}{dr}\frac{r^2}{M_{\mathrm{T}}(r)}\right] \geq 0, \qquad (k = 1, \ldots, n), \tag{3.11}$$

where $M_{\mathrm{T}}(r)$ is the total mass distribution[3]. Note that, at variance with the NC, the WSC for the k-component depends also on the radial density profile of all the other components, and so a model failing the WSC *may be* consistent. Summarizing, a model failing eq. (3.10) is *certainly inconsistent*, while a model obeying eq. (3.11) is *certainly consistent*. Consequently, it follows that *the true boundary in the parameter space separating consistent and inconsistent models is "bracketed" by the* NC *and* WSC *limits*.

Before embarking on the analysis of the consistency, some interesting consideration is in order. First, expanding the derivative in eq. (3.11) we have, for each component,

$$\frac{d}{dr}\left[\frac{d\varrho_k(r)}{dr}\frac{r^2}{M_{\mathrm{T}}(r)}\right] = \frac{\dfrac{d}{dr}\left[r^2\dfrac{d\varrho_k(r)}{dr}\right]\displaystyle\sum_{i=1}^{n}M_i(r) - r^2\dfrac{d\varrho_k(r)}{dr}\dfrac{d}{dr}\displaystyle\sum_{i=1}^{n}M_i(r)}{M_{\mathrm{T}}^2(r)}$$

$$= \frac{1}{M_{\mathrm{T}}^2(r)}\sum_{i=1}^{n}\left\{\frac{d}{dr}\left[r^2\frac{d\varrho_k(r)}{dr}\right]M_i(r) - r^2\frac{d\varrho_k(r)}{dr}\frac{dM_i(r)}{dr}\right\}, \tag{3.12}$$

or, after some rearrangements,

---

[3]The NC and WSC can be proven by simple arguments. One writes the density as an integral of the OM DF, and derives the identity with respect to the total potential. If the DF is non-negative, it follows that necessarily the derivative of the augmented density in terms of the total potential is non-negative. But the potential is monotonically decreasing, and so one gets eq. (3.10) with the condition to be less than or equal to zero. Next, if one performs the Abel inversion, and assumes a non-truncated (or regularly truncated) density distribution, then to have a positive second derivative of the augmented density with respect to the potential, it is sufficient to have a non-negative DF. Fore more details, see CP92.

$$\frac{d}{dr}\left[\frac{d\varrho_k(r)}{dr}\frac{r^2}{M_{\rm T}(r)}\right] = \frac{1}{M_{\rm T}^2(r)}\sum_{i=1}^{n}M_i^2(r)\frac{d}{dr}\left[\frac{d\varrho_k(r)}{dr}\frac{r^2}{M_i(r)}\right], \qquad (k=1,\ldots,n). \qquad (3.13)$$

Therefore, since the WSC for the k-component requires the non-negativity of the left-hand side of the foregoing equation, if all the n derivatives at the right-hand side are non-negative for fixed k, it follows that $f_k(Q_k) \geq 0$. A second consideration is about the effect of the orbital anisotropy. Indeed, the investigation of the NC and WSC, and the study of the consistency condition in eq. (3.9), all lead to consider inequalities that can be written as

$$F + \frac{G}{r_{\rm ak}^2} \geq 0, \qquad (3.14)$$

and that must hold over the domain $\mathcal{C}$ spanned by the arguments of the functions F and G. In practice, these two functions are functions of r (in the case of the NC and WSC), or functions of Q_k (in the case of the DF). From eq. (3.14) it then follows that all OM models can be divided in two families. When F is nowhere negative over $\mathcal{C}$ (e.g., in the case of a consistent isotropic DF), consistency in the anisotropic case is obtained for

$$r_{\rm ak} \geq r_{\rm ak}^- \equiv \sqrt{\max\left[0,\,\sup_{\mathcal{C}}\left(-\frac{G}{F}\right)\right]}. \qquad (3.15)$$

If G is also positive over $\mathcal{C}$, then $r_{\rm ak} = 0$ and the system can be supported by radial orbits only. In the second case, $F > 0$ over some subset $\mathcal{C}_+$ of $\mathcal{C}$, and negative (or zero) over the complementary subset $\mathcal{C}_-$. If also $G < 0$ somewhere on $\mathcal{C}_-$, then eq. (3.14) cannot be satisfied and the model is inconsistent. If $G \geq 0$ on $\mathcal{C}_-$ one must consider not only the lower limit $r_{\rm ak}^-$ evaluated over $\mathcal{C}_+$ as above, but also the condition

$$r_{\rm ak} \leq r_{\rm ak}^+ = \sqrt{\inf_{\mathcal{C}_-}\left(-\frac{G}{F}\right)}, \qquad (3.16)$$

and consistency is possible only if $r_{\rm ak}^- < r_{\rm ak}^+$. Summarizing,

- If $F \geq 0$, then $r_{\rm ak} \geq r_{\rm ak}^-$ for consistency;

- If $F \leq 0$ over $\mathcal{C}_-$ and $G \geq 0$ there, then the inequality $r_{\rm ak}^- \leq r_{\rm ak} \leq r_{\rm ak}^+$ must be verified;

- If $G < 0$ somewhere over $\mathcal{C}_-$, or $r_{\rm ak}^+ < r_{\rm ak}^-$, then the inequality in eq. (3.14) cannot be satisfied, and the model must be rejected as inconsistent.

3.2 The necessary and sufficient conditions for J3 models

After the general presentation given in the previous Section, we shall now proceed to discuss the application of the NC and WSC to J3 models. We *assume* for the stellar component a DF with the OM parametrization (see eq. [3.5])

$$f_* = \begin{cases} f_*(Q), & Q > 0, \\ \\ 0, & Q \leq 0, \end{cases} \qquad Q \equiv \mathcal{E} - \frac{J^2}{2r_{\rm a}^2}, \qquad (3.17)$$

associated with an orbital structure described by

$$\beta(r) = \frac{r^2}{r^2 + r_\mathrm{a}^2}. \tag{3.18}$$

Note that, to avoid overloading the notation, we have set $Q_* \equiv Q$, $r_{\mathrm{a}*} \equiv r_\mathrm{a}$, and $\beta_* \equiv \beta$; as a natural consequence, we also define $r_{\mathrm{a}*}^- \equiv r_\mathrm{a}^-$, and $r_{\mathrm{a}*}^+ \equiv r_\mathrm{a}^+$. For what concerns the DM distribution, instead, for simplicity we shall restrict to the isotropic case (i.e., $r_{\mathrm{aDM}} = \infty$).

Before embarking on the analysis of the consistency, a brief consideration about the effect of the central BH is in order. Since $M_\mathrm{T}(r) = M_\mathrm{g}(r) + M_\mathrm{BH}$, eq. (3.13) becomes

$$\frac{d}{dr}\left[\frac{d\varrho_k(r)}{dr}\frac{r^2}{M_\mathrm{T}(r)}\right] = \frac{1}{M_\mathrm{T}^2(r)}\left\{M_\mathrm{g}^2(r)\frac{d}{dr}\left[\frac{d\varrho_k(r)}{dr}\frac{r^2}{M_\mathrm{g}(r)}\right] + M_\mathrm{BH}\frac{d}{dr}\left[r^2\frac{d\varrho_k(r)}{dr}\right]\right\}, \tag{3.19}$$

which is valid both for $\varrho_*(r)$ and $\varrho_\mathrm{DM}(r)$. Therefore, *if*

$$1) \quad \frac{d}{dr}\left[\frac{d\varrho_k(r)}{dr}\frac{r^2}{M_\mathrm{g}(r)}\right] \geq 0, \qquad\qquad 2) \quad \frac{d}{dr}\left[r^2\frac{d\varrho_k(r)}{dr}\right] \geq 0, \tag{3.20}$$

then the WSC in eq. (3.11) is satisfied for arbitrary values of M_BH; in other words, the model with central BH is certainly consistent. Nothe that, while point 1) refers to the WSC for the investigated density component in absence of the central BH, point 2) is nothing else than the WSC for the considered density profile interpreted as a tracer in the gravitational field of the central BH itself; we shall use this result in the following discussion.

3.2.1 The consistency of the stellar profile

We now move to case of the NC and WSC for the stellar component of OM anisotropic J3 models.

The NC requires that, for all values of $r \geq 0$,

$$\frac{d\varrho_*(r)}{dr} \leq 0, \qquad\qquad \varrho_*(r) \equiv \rho_*(r) \times \left(1 + \frac{r^2}{r_\mathrm{a}^2}\right). \tag{3.21}$$

Simple algebra shows that this condition can be rewritten as

$$s_\mathrm{a}^2 \geq -\frac{s^3}{1 + 2s}, \tag{3.22}$$

where $s_\mathrm{a} \equiv r_\mathrm{a}/r_*$ is the anisotropy radius in units of r_*. Thus, the NC produces the case described by eq. (3.15), with $s_\mathrm{a}^- \equiv r_\mathrm{a}^-/r_*$. Since the right-hand side of eq. (3.22) is nowhere positive for non-negative values of s, the NC leads to $s_\mathrm{a} \geq 0$. In words: *the NC for the stellar component of J3 models is always satisfied, even in the purely radial case.*

The WSC, instead, leads to an analytical but cumbersome expression. Indeed, in absence of the central BH, it reads

$$\frac{d}{dr}\left[\frac{d\varrho_*(r)}{dr}\frac{r^2}{M_\mathrm{g}(r)}\right] \geq 0, \qquad\qquad (s \geq 0), \tag{3.23}$$

where $\varrho_*(r)$ and $M_\mathrm{g}(r)$ are given in eqs. (3.21) and (2.12), respectively. Then, performing the differentiation and rearranging, we obtain

$$s_{\mathrm{a}}^2 \geq -\frac{s^3[(\xi + s)(s - 2)\ln(1 + s/\xi) + s(1 + s)]}{(\xi + s)(6s^2 + 4s + 1)\ln(1 + s/\xi) + s(1 + s)(2 + 2s)}. \tag{3.24}$$

Again, we are in presence of an inequality of the type (3.15). Moreover, note that, when restricting to the case $\mu = 0$, the limit on anisotropy is independent of $\mathcal{R}$. By a numerical inspection of eq. (3.24) we obtain the trend of s_{a}^- as a function of ξ, which is depicted in Fig. 3.1; for a galaxy model with $\xi = 13$ we find the approximate value $s_{\mathrm{a}}^- \simeq 0.0502$ (see red circle in Fig. 3.1).

Lastly, in case of a dominant BH, only M_{BH} is retained in eq. (3.11). In this case, the WSC actually coincides with point 2) in eq. (3.20), and so it reduces to

$$s_{\mathrm{a}}^2 \geq -\frac{s^3(s - 2)}{6s^2 + 4s + 1} \equiv \mathcal{W}_*(s), \tag{3.25}$$

which is obviously independent of ξ and μ, and quite easy to examine. Since the foregoing inequality must be verified for all values of $s \geq 0$, it follows that s_{a}^2 must be greater than or equal to the maximum of the function $\mathcal{W}_*(s)$. For, we have to determine the sign of $\mathcal{W}_*(s)$; by differentiating with respect to s, it is readily found that

$$\frac{d\mathcal{W}_*(s)}{ds} = -\frac{6s^2(2s^3 - 2s - 1)}{(6s^2 + 4s + 1)^2}. \tag{3.26}$$

Therefore,

$$\frac{d\mathcal{W}_*(s)}{ds} \geq 0 \qquad \Leftrightarrow \qquad 2s^3 - 2s - 1 \leq 0. \tag{3.27}$$

A numerical exploration show that the inequality above is satisfied when $0 \leq s \lesssim 1.19$, i.e., that $\mathcal{W}_*(s)$ exhibits a maximum in $s \simeq 1.19$. Then, the WSC reduces to $s_{\mathrm{a}} \geq s_{\mathrm{a}}^- \simeq 0.31$. Therefore, by virtue of the discussion after eq. (3.11), from comparison with Fig. 3.1 we conclude that *the stellar component of J3 models is certainly consistent for $s_{\mathrm{a}} \gtrsim 0.31$.*

3.2.2 The consistency of the DM halo

The second application of the NC and WSC to J3 models concerns the consistency of the DM halo.

Since we assume an isotropic DM halo, the NC requires that, for $r \geq 0$,

$$\frac{d\varrho_{\mathrm{DM}}(r)}{dr} \leq 0, \qquad\qquad \varrho_*(r) \equiv \rho_{\mathrm{DM}}(r). \tag{3.28}$$

Then, the NC coincides with the request of monotonicity of the DM density profile. As we have seen in Chapter 2, following the discussion after eq. (2.37), for $\xi \geq 1/2$ the NC is satisfied once just positivity is assured, i.e. for $\mathcal{R} \geq \xi$. In words: *for the isotropic DM halo of J3 models, positivity condition, monotonicity condition and NC coincide when $\xi \geq 1/2$, holding for $\mathcal{R} \geq \xi$.*

The discussion of the WSC for the DM component is more complicated. By restricting to the case $\mu = 0$, in order to test the consistency we have to consider the following inequality:

$$\frac{d}{dr}\left[\frac{d\rho_{\mathrm{DM}}(r)}{dr}\frac{r^2}{M_{\mathrm{g}}(r)}\right] \geq 0, \qquad\qquad (s \geq 0). \tag{3.29}$$

By expanding the expression on the left-hand side we obtain, after some minor reductions,

$$\mathcal{R} \geq \frac{2(\xi+s)^2[(\xi+s)(6s^2+4s+1)\ln(1+s/\xi)+s(1+s)(1+2s)]}{(1+s)^4[2(3s^2+3\xi s+\xi^2)\ln(1+s/\xi)+s(2\xi+3s)]}. \tag{3.30}$$

As the inequality above must be verified for all values of $s \geq 0$, it follows that $\mathcal{R}$ must be greater than or equal to the maximum of the radial function at the right-hand side. A numerical study indicates that for $\xi \geq 1$ the WSC holds when $\mathcal{R} \geq \xi$.

Finally, in analogy with eq. (3.25), the WSC for the isotropic halo in the potential of a dominant central mass reduces to

$$\mathcal{R} \geq \frac{(\xi+s)^3(6s^2+4s+1)}{(1+s)^4(3s^2+3\xi s+\xi^2)} \equiv \mathcal{W}_{\text{DM}}(s). \tag{3.31}$$

Again, following the same strategy adopted to discuss the WSC for the stellar component in case of dominant BH, we have to study the sign of $\mathcal{W}_{\text{DM}}(s)$ to find its maximum. By differentiating $\mathcal{W}_{\text{DM}}(s)$ with respect to s we find

$$\frac{d\mathcal{W}_{\text{DM}}(s)}{ds} = -\frac{(\xi+s)^2 s^2[18s^3+6(12\xi-5)s^2+3(16\xi^2-5)s+3(4\xi^3-1)]}{(1+s)^5(3s^2+3\xi s+\xi^2)^2}. \tag{3.32}$$

whence,

$$\frac{d\mathcal{W}_{\text{DM}}(s)}{ds} \geq 0 \qquad \Leftrightarrow \qquad 18s^3+6(12\xi-5)s^2+3(16\xi^2-5)s+3(4\xi^3-1) \leq 0. \tag{3.33}$$

The explicit solution of the foregoing inequality presents no formal difficulty. By arguments similar to those used to discuss eq. (2.37), the application of Descartes's theorem shows that the maximum of $\mathcal{W}_{\text{DM}}(s)$ is reached at $s = 0$, i.e. again for $\mathcal{R} \geq \xi$. Therefore, following the discussion after eq. (3.11), we conclude that the DM component for a model with $\xi \geq 1$ and $\mathcal{R} \geq \xi$ is certainly consistent. Summarizing, *for isotropic* DM *halos of* J3 *models with a central* BH *of arbitrary mass and* $\xi \geq 1$, *the requirements of positivity, monotonicity, and* WSC *for phase-space consistency coincide, and are all satisfied once* $\mathcal{R} \geq \xi$.

3.3   The explicit phace-space DF

As we have seen in the previous Section, *the presence of a diffuse halo increases the model ability to sustain radial anisotropy, while for concentrated halos the consistency of the stellar distribution requires a more isotropic velocity dispersion tensor*, in agreement with the results obtained for other two-component OM models (see, e.g., Ciotti 1999, CMZ09, CZ18).

We now return to the eq. (3.9) to determine the explicit form of the DF of the stellar component. It is convenient to define the following dimensionless quantities:

$$\tilde{\rho}_*(s) \equiv \frac{\rho_*(r)}{\rho_{\text{n}}} = \frac{1}{s^2(1+s)^2}, \qquad\qquad \tilde{\varrho}_*(s) \equiv \frac{\varrho_*(r)}{\rho_{\text{n}}} = \tilde{\rho}_*(s) \times \left(1+\frac{s^2}{s_{\text{a}}^2}\right). \tag{3.34}$$

Further, we also define the dimensionless total potential

$$\psi(s) \equiv \frac{\Psi_{\text{T}}(r)}{\Psi_{\text{n}}} = \mathcal{R}\left(\frac{1}{s}\ln\frac{\xi+s}{\xi}+\frac{1}{\xi}\ln\frac{\xi+s}{s}\right)+\frac{\mu}{s}. \tag{3.35}$$
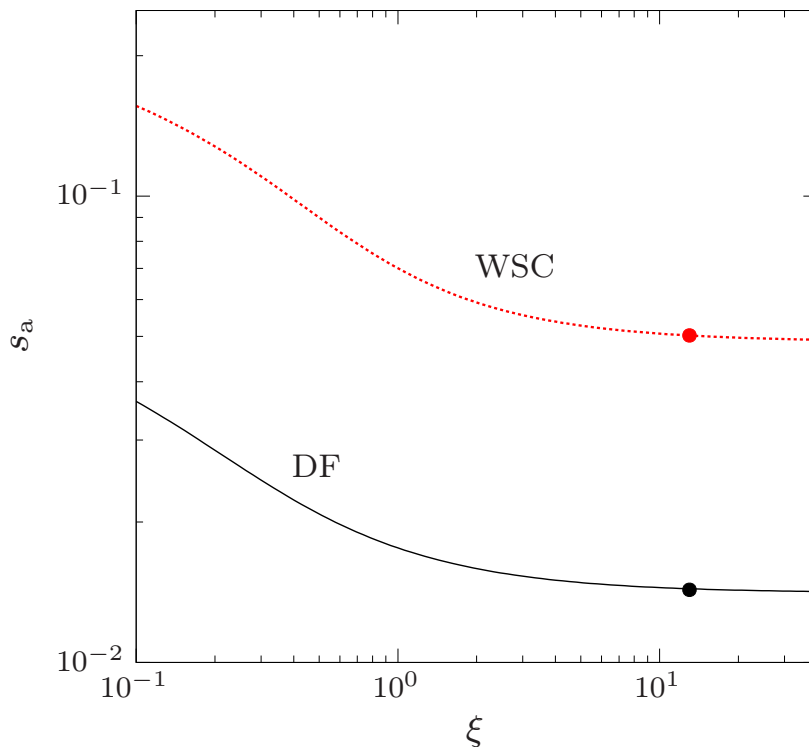
Figure 3.1. Different limitations on the anisotropy radius $s_\mathrm{a} = r_\mathrm{a}/r_*$ of the stellar component of J3 models, as a function of $\xi = r_\mathrm{g}/r_*$. The lines refer to $\mu = 0$, i.e. in absence of the central BH. The black solid line and the red dotted line represent the minimum value of s_a obtained directly from the DF and from the WSC (see eq. [3.24]), respectively. The circles correspond to models with $\xi = 13$, for which we find $s_\mathrm{a}^- \simeq 0.0143$ (DF) and $s_\mathrm{a}^- \simeq 0.0502$ (WSC). Notice how the shape of the critical consistency curve parallels the WSC condition. For reference, the minimum value for consistency for the Jaffe model is $s_\mathrm{a}^- \simeq 0.02205$.

By using these definitions, eq. (3.9) becomes

$$f_*(q) = \frac{\rho_\mathrm{n}}{\sqrt{8}\pi^2 \Psi_\mathrm{n}^{3/2}} \int_0^q \frac{d^2 \tilde{\varrho}_*}{d\psi^2} \frac{d\psi}{\sqrt{q-\psi}}, \qquad q \equiv \frac{Q}{\Psi_\mathrm{n}}. \tag{3.36}$$

Note that the second term in eq. (3.9) is absent, since the cumulative mass associated with the stellar component is finite. Unfortunately, for J3 models the integral in eq. (3.36) cannot be solved via elementary functions. Hence, in the following discussion we shall proceed with the numerical integration of eq. (3.36) for a selected choice of the model parameters. First, by changing the integration variable from total dimensionless potential ψ to dimensionless radius s, we obtain

$$f_*(q) = \frac{\rho_\mathrm{n}}{\sqrt{8}\pi^2 \Psi_\mathrm{n}^{3/2}} \int_\infty^s \left(\frac{d\psi}{dx}\right)^{-1} \frac{d}{dx}\left[\frac{d\tilde{\varrho}_*}{dx}\left(\frac{d\psi}{dx}\right)^{-1}\right] \frac{d\psi}{dx} \frac{dx}{\sqrt{\psi(s)-\psi(x)}}, \tag{3.37}$$

where it is intended that $s = s(q)$. Next, by differentiating eq. (3.35) with respect to s, and inserting it in eq. (3.37), we find

$$f_*(q) = \frac{\rho_\mathrm{n}}{\sqrt{8}\pi^2 \Psi_\mathrm{n}^{3/2}} \int_s^\infty \frac{d}{dx}\left[\frac{d\tilde{\varrho}_*}{dx} \frac{x^2}{\mathcal{R}\ln(1+x/\xi)+\mu}\right] \frac{dx}{\sqrt{\psi(s)-\psi(x)}}. \tag{3.38}$$

Moreover, in order to rewrite $f_*(q)$ in a more convenient form, we define
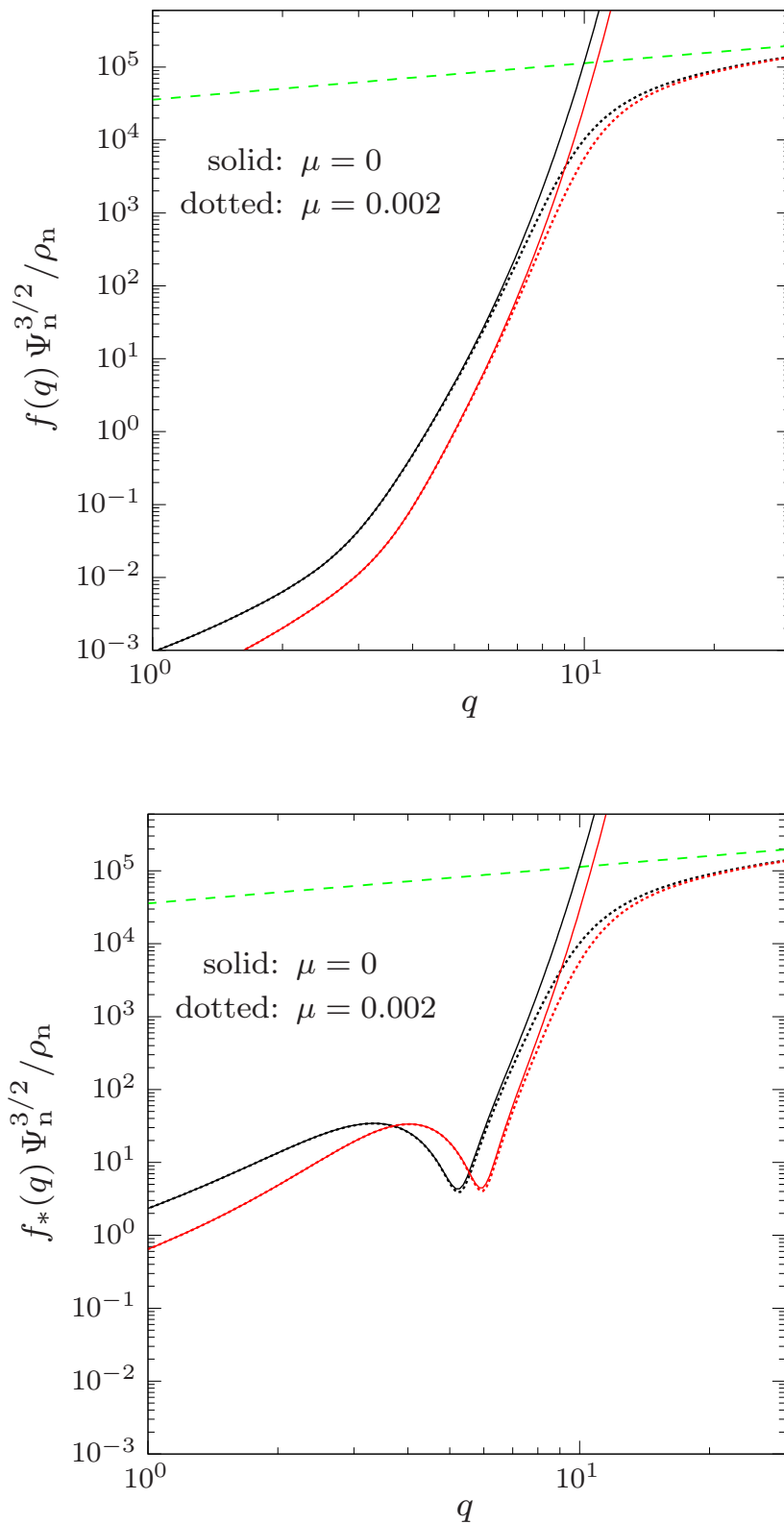
Figure 3.2. The DF of the stellar component for a minimum halo galaxy model with $\mathcal{R} = \xi = 10$ (black lines) and $\mathcal{R} = \xi = 20$ (red lines), in the isotropic (top panel) and anisotropic (bottom panel, $s_a = 0.02$) cases. The DFs are shown with and without (dotted and solid lines, respectively) the effect of the central BH (with $\mu = 0.002$). The green dashed line shows the DF of the Jaffe model in the BH dominated case.

$$U(q) \equiv \int_s^\infty \frac{d}{dx}\left[\frac{d\tilde{\rho}_*}{dx}\frac{x^2}{\mathcal{R}\ln(1+x/\xi)+\mu}\right]\frac{dx}{\sqrt{\psi(s)-\psi(x)}}\,, \tag{3.39}$$

and

$$V(q) \equiv \int_s^\infty \frac{d}{dx}\left[\frac{d(x^2\tilde{\rho}_*)}{dx}\frac{x^2}{\mathcal{R}\ln(1+x/\xi)+\mu}\right]\frac{dx}{\sqrt{\psi(s)-\psi(x)}}\,. \tag{3.40}$$

By virtue of these definitions, and remembering eq. (3.34), the DF of the stellar component can be written as

$$f_*(q) = \frac{\rho_n}{\sqrt{8}\pi^2\Psi_n^{3/2}}\left[U(q)+\frac{V(q)}{s_a^2}\right]. \tag{3.41}$$

Now, a direct inspection of the functions $U(q)$ and $V(q)$ lead us to determine numerically the lower limit on s_a for consistency: in particular, the investigation of the phase-space consistency leads to consider an inequality of the type eq. (3.14). First, note that in absence of the central BH, the variable q can be further scaled as $\tilde{q} \equiv q/\mathcal{R}$, and the quantity $\mathcal{R}^{-3/2}$ can be explicitily factored out in the functions $U(q)$ and $V(q)$, i.e.,

$$U(q) = \frac{U(\tilde{q})}{\mathcal{R}^{3/2}}, \qquad\qquad V(q) = \frac{V(\tilde{q})}{\mathcal{R}^{3/2}}. \tag{3.42}$$

In particular, for models with $\mu = 0$, the position of the maximum in eq. (3.15) depends on $\tilde{q}$, and the value of s_a^- is *independent* of the galaxy-to-stellar density ratio $\mathcal{R}$. A numerical exploration of eq. (3.39) shows that $U(q) \geq 0$, thus eq. (3.15) applies and only s_a^- exists: in Fig. 3.1 the black solid line shows the corresponding $s_a^-(\xi)$. At fixed ξ, anisotropy values $s_a \geq s_a^-(\xi)$ correspond to a non-negative DF; for a J3 galaxy model with $\xi = 13$, the approximate value of the minimum anisotropy radius is $r_a^- \simeq 0.0143\, r_*$ (see black circle in Fig 3.1). Moreover, it is also apparent how *the effect of a concentrated* DM *halo reduces the ability of the stellar component to sustain radial orbits*, a common property of the OM models, confirming the trend obtained from the WSC. Here we mention a point of little practical interest, but quite relevant conceptually. Indeed, in CZ18 was shown that for the single component Jaffe model the OM DF requires, for consistency, $s_a^- \simeq 0.02205$, and so one could argue that the purely radial Jaffe model does not exist. Nevertheless, the analytical DF for this particular model is positive, thus showing that the purely radial case is a singular limit for the OM DF: indeed, the results obtained in CZ18 show that *the Jaffe stellar component of* J3 *models can be supported by radial orbits only*. In any case this situation has not practical interest, as illustrated in Section 5.2.

In Fig. 3.2 we show the numerically recovered DF of the stellar component of two particular J3 galaxy models, namely the minimum halo models with $\xi = 10$ (black lines) and $\xi = 20$ (red lines), in the isotropic (top panel) and anisotropic (bottom panel, $s_a = 0.02$) cases; the DFs are depicted with and without the effect of the central BH. In addition, also the BH dominated DF (green dashed line) is shown. At least two things are important to note:

- At high relative energies the DF of the J3 models with a central BH is matched by the BH dominated DF, and the values of the isotropic and anisotropic DFs become coincident;

- The DFs for models with the central BH are lower at high relative energies than in the analogous models without the central BH, and the same happens at low relative energies for models with heavier and extended halos.

The physical reason of these behaviors is due to the fact that, qualitatively, the phase-space DF is inversely proportional to the cube of velocity dispersion (see Chapter 4), so that high velocity dispersions are expected to correspond to low values of the DF (see Fig. 4.5). Furthermore, we also notice that the curves relative to DFs in the strongly anisotropic cases behave (qualitatively) as the DFs of other OM models discussed in Ciotti & Lanzoni 1997 (Fig. 2), Ciotti 1999 (Figs. 2 and 3), CMZ09 (Fig. 3), and CZ18 (Fig. 3). In practice, *in* OM *models small values of* $s_{\rm a}$ *lead to a depression of the* DF *at intermediate energies, where model inconsistency finally sets in when the anisotropy radius drops below the consistency limit.*

CHAPTER 4

THE JEANS EQUATIONS WITH OM ANISOTROPY

IN this Chapter the analytical solution of the Jeans equations with OM anisotropy is presented. The Chapter is organized as follows.

In Section 4.1 the general solution is presented for generic values of the model parameters, and four fundamental functions are defined.

In Section 4.2 the stellar velocity dispersion profile of J3 models is derived, together with its asymptotic expansions near the center and in the outer regions.

In Section 4.3 the radial trend of the projected stellar velocity distribution is discussed. Since this quantity is related to an integral that, unsurprisingly, cannot be evaluated in terms of elementary functions for J3 models, an original integral formula, valid for OM systems, is derived in order to simplify the numerical inspection. Finally, the asymptotic behaviours of the projected velocity profile at small and large radii are presented.

4.1   The case of J3 models

For a given choice of the functions $\rho_*(r)$, $\Psi_T(r)$ and $\beta(r)$ in eq. (B19), the result of the integration is the velocity dispersion profile $\sigma_r(r)$. The natural boundary condition for eq. (B19) is

$$\rho_*(r_t)\sigma_r^2(r_t) = 0, \tag{4.1}$$

where r_t is the so-called *truncation radius*, for which $\rho_*(r) = 0$ if $r \geq r_t$. In applying the condition above, and setting $r_t = \infty$, the solution of the first order nonhomogeneous linear ordinary differential equation in eq. (B19) reads

$$\rho_*(r)\sigma_r^2(r) = -\int_r^\infty \rho_*(x)\frac{d\Psi_T(x)}{dx}\exp\left[2\int_r^x \frac{\beta(y)}{y}\,dy\right]dx. \tag{4.2}$$

In case of OM systems, the foregoing equation becomes

$$\rho_*(r)\sigma_r^2(r) = \frac{G}{r^2 + r_a^2}\int_r^\infty \rho_*(x)M_T(x)\left(1 + \frac{r_a^2}{x^2}\right)dx, \tag{4.3}$$

or, alternatively,

$$\rho_*(r)\sigma_r^2(r) = \frac{A(r) + r_a^2\,I(r)}{r^2 + r_a^2}, \tag{4.4}$$

where

$$A(r) \equiv G\int_r^\infty \rho_*(x)M_T(x)dx, \qquad I(r) \equiv G\int_r^\infty \rho_*(x)\frac{M_T(x)}{x^2}\,dx. \tag{4.5}$$

By inserting in these two integrals the expressions for the stellar density and total mass distributions, and using the substitution $y \equiv x/r_*$, we obtain

$$A(r) = r_*^2\rho_n\Psi_n\mathcal{A}(s), \qquad I(r) = \rho_n\Psi_n\mathcal{I}(s), \tag{4.6}$$

in which

$$\mathcal{A}(s) \equiv \int_s^\infty \frac{\mathcal{R}\ln(1 + y/\xi) + \mu}{y^2(1+y)^2}\,dy, \qquad \mathcal{I}(s) \equiv \int_s^\infty \frac{\mathcal{R}\ln(1 + y/\xi) + \mu}{y^4(1+y)^2}\,dy. \tag{4.7}$$

By virtue of these definitions, the right-hand side of eq. (4.4) can be normalized as follows:

$$\rho_*(r)\sigma_r^2(r) = \rho_n\Psi_n\frac{\mathcal{A}(s) + s_a^2\,\mathcal{I}(s)}{s^2 + s_a^2}. \tag{4.8}$$

Finally, in order to separate the contributions of the galaxy and the BH to the stellar velocity dispersion profile, we rewrite the functions in eq. (4.7) as

$$\mathcal{A}(s) = \mathcal{R}\,\mathcal{A}_g(s) + \mu\,\mathcal{A}_{BH}(s), \qquad \mathcal{I}(s) = \mathcal{R}\,\mathcal{I}_g(s) + \mu\,\mathcal{I}_{BH}(s), \tag{4.9}$$

for which the following definitions apply:

$$\mathcal{A}_{\mathrm{g}}(s) \equiv \int_s^\infty \ln\left(1 + \frac{y}{\xi}\right) \frac{dy}{y^2(1+y)^2}, \qquad \mathcal{A}_{\mathrm{BH}}(s) \equiv \int_s^\infty \frac{dy}{y^2(1+y)^2},$$

$$\mathcal{I}_{\mathrm{g}}(s) \equiv \int_s^\infty \ln\left(1 + \frac{y}{\xi}\right) \frac{dy}{y^4(1+y)^2}, \qquad \mathcal{I}_{\mathrm{BH}}(s) \equiv \int_s^\infty \frac{dy}{y^4(1+y)^2}. \tag{4.10}$$

For $r_{\mathrm{a}} = 0$ we have the solution of the purely radial case $[\rho_*(r)\sigma_{\mathrm{r}}^2(r)]_{\mathrm{rad}}$, while for $r_{\mathrm{a}} = \infty$ the fully isotropic case $[\rho_*(r)\sigma_{\mathrm{r}}^2(r)]_{\mathrm{iso}}$ is obtained. From eq. (4.8), these two solutions read

$$[\rho_*(r)\sigma_{\mathrm{r}}^2(r)]_{\mathrm{rad}} = \rho_{\mathrm{n}}\Psi_{\mathrm{n}}\frac{\mathcal{A}(s)}{s^2}, \qquad [\rho_*(r)\sigma_{\mathrm{r}}^2(r)]_{\mathrm{iso}} = \rho_{\mathrm{n}}\Psi_{\mathrm{n}}\mathcal{I}(s). \tag{4.11}$$

4.2 The velocity dispersion profile

To derive the velocity dispersion profile $\sigma_{\mathrm{r}}(r)$, we shall now solve the four integrals in eq. (4.10). Let us start from the BH contribution. By applying Hermite's method (see Hermite 1872, see also Goursat 1904), we find that the integrand for $\mathcal{A}_{\mathrm{BH}}(s)$ can be rewritten as

$$\frac{1}{y^2(1+y)^2} = 2\left(\frac{1}{1+y} - \frac{1}{y}\right) - \frac{d}{dy}\left[\frac{2y+1}{y(1+y)}\right]. \tag{4.12}$$

Therefore, performing the integration we obtain

$$\mathcal{A}_{\mathrm{BH}}(s) = 2\ln\frac{s}{1+s} + \frac{2s+1}{s(1+s)} \sim \begin{cases} \dfrac{1}{s}, & s \to 0, \\[2mm] \dfrac{1}{3s^3}, & s \to \infty. \end{cases} \tag{4.13}$$

Similarly, the integrand for $\mathcal{I}_{\mathrm{BH}}(s)$ is nothing else than

$$\frac{1}{y^4(1+y)^2} = 4\left(\frac{1}{1+y} - \frac{1}{y}\right) - \frac{d}{dy}\left[\frac{12y^3 + 6y^2 - 2y + 1}{3y^3(1+y)}\right], \tag{4.14}$$

whence,

$$\mathcal{I}_{\mathrm{BH}}(s) = 4\ln\frac{s}{1+s} + \frac{12s^3 + 6s^2 - 2s + 1}{3s^3(1+s)} \sim \begin{cases} \dfrac{1}{3s^3}, & s \to 0, \\[2mm] \dfrac{1}{5s^5}, & s \to \infty. \end{cases} \tag{4.15}$$

For what concerns the contribution to $\sigma_{\mathrm{r}}(r)$ due to the galaxy, remembering the definitions of $\mathcal{A}_{\mathrm{BH}}(s)$ and $\mathcal{I}_{\mathrm{BH}}(s)$ given in eq. (4.10), we have

$$\mathcal{A}_{\mathrm{g}}(s) = -\int_s^\infty \ln\left(1 + \frac{y}{\xi}\right) \frac{d\mathcal{A}_{\mathrm{BH}}(y)}{dy}\,dy, \qquad \mathcal{I}_{\mathrm{g}}(s) = -\int_s^\infty \ln\left(1 + \frac{y}{\xi}\right) \frac{d\mathcal{I}_{\mathrm{BH}}(y)}{dy}\,dy. \tag{4.16}$$

Thus, by an integration by parts we obtain

$$\mathcal{A}_{\mathrm{g}}(s) = \mathcal{A}_{\mathrm{BH}}(s) \ln \frac{\xi + s}{\xi} + \mathcal{F}_{\mathrm{rad}}(s), \qquad \mathcal{I}_{\mathrm{g}}(s) = \mathcal{I}_{\mathrm{BH}}(s) \ln \frac{\xi + s}{\xi} + \mathcal{F}_{\mathrm{iso}}(s), \qquad (4.17)$$

where we have defined

$$\mathcal{F}_{\mathrm{rad}}(s) \equiv \int_s^\infty \frac{\mathcal{A}_{\mathrm{BH}}(y)}{\xi + y} \, dy, \qquad \mathcal{F}_{\mathrm{iso}}(s) \equiv \int_s^\infty \frac{\mathcal{I}_{\mathrm{BH}}(y)}{\xi + y} \, dy. \qquad (4.18)$$

The solution of these two integrals presents no formal difficulty. Indeed, breaking up the integrand for $\mathcal{F}_{\mathrm{rad}}(s)$ into partial fraction, we find

$$\frac{\mathcal{A}_{\mathrm{BH}}(y)}{\xi + y} = \begin{cases} \dfrac{1}{\xi}\left(\dfrac{1}{y} - \dfrac{1}{\xi + y}\right) + \dfrac{1}{\xi - 1}\left(\dfrac{1}{1 + y} - \dfrac{1}{\xi + y}\right) - 2\dfrac{\ln(1 + 1/y)}{\xi + y}, & \xi \neq 1, \\[4mm] \dfrac{1}{y} - \dfrac{1}{1 + y} + \dfrac{1}{(1 + y)^2} - 2\dfrac{\ln(1 + 1/y)}{1 + y}, & \xi = 1. \end{cases} \qquad (4.19)$$

Therefore, by computing the integral in eq. (4.18) we obtain

$$\mathcal{F}_{\mathrm{rad}}(s) = \begin{cases} \dfrac{1}{\xi} \ln \dfrac{\xi + s}{s} + \dfrac{1}{\xi - 1} \ln \dfrac{\xi + s}{1 + s} - 2\,\mathcal{H}(\xi, s), & \xi \neq 1, \\[4mm] \ln \dfrac{1 + s}{s} + \dfrac{1}{1 + s} - 2\,\mathcal{H}(1, s), & \xi = 1, \end{cases} \qquad (4.20)$$

where $\mathcal{H}(\xi, s)$ is a function described in Appendix C. Similarly, the application of Hermite's method to the integrand for $\mathcal{F}_{\mathrm{iso}}(s)$ leads to

$$\frac{\mathcal{I}_{\mathrm{BH}}(y)}{\xi + y} = \begin{cases} \dfrac{9\xi^2 + 3\xi + 1}{3\xi^3}\left(\dfrac{1}{y} - \dfrac{1}{\xi + y}\right) + \dfrac{1}{\xi - 1}\left(\dfrac{1}{1 + y} - \dfrac{1}{\xi + y}\right) + \\[4mm] + \dfrac{d}{dy}\left[\dfrac{2(1 + 3\xi)y - \xi}{6\xi^2 y^2}\right] - 4\dfrac{\ln(1 + 1/y)}{\xi + y}, & \xi \neq 1, \\[4mm] \dfrac{13}{3}\left(\dfrac{1}{y} - \dfrac{1}{1 + y}\right) + \dfrac{d}{dy}\left[\dfrac{2y^2 + 7y - 1}{6y^2(1 + y)}\right] - 4\dfrac{\ln(1 + 1/y)}{1 + y}, & \xi = 1, \end{cases} \qquad (4.21)$$

whence, performing the integration in eq. (4.18),

$$\mathcal{F}_{\mathrm{iso}}(s) = \begin{cases} \dfrac{9\xi^2 + 3\xi + 1}{3\xi^3} \ln \dfrac{\xi + s}{s} + \dfrac{1}{\xi - 1} \ln \dfrac{\xi + s}{1 + s} - \dfrac{2(1 + 3\xi)s - \xi}{6\xi^2 s^2} - 4\,\mathcal{H}(\xi, s), & \xi \neq 1, \\[4mm] \dfrac{13}{3} \ln \dfrac{1 + s}{s} - \dfrac{2s^2 + 7s - 1}{6s^2(1 + s)} - 4\,\mathcal{H}(1, s), & \xi = 1. \end{cases}$$
$$(4.22)$$

Note that the expressions in eqs. (4.20) and (4.22) for $\xi = 1$ may be formally obtained by considering the limit for $\xi \to 1$ of the corresponding expressions for $\xi \neq 1$. In the limit $\xi \to 0$, instead, the functions $\mathcal{A}_g(s)$ and $\mathcal{I}_g(s)$ do *not* reduce to $\mathcal{A}_{BH}(s)$ and $\mathcal{I}_{BH}(s)$, respectively: indeed, the galaxy potential $\Psi_g(r)$, for fixed r and $r_g \to 0$, does *not* become the potential of a point mass.

On expanding the functions $\mathcal{A}_g(s)$ and $\mathcal{I}_g(s)$ at small and large radii, and making use of the results in Appendix C, we find

$$
\mathcal{A}_g(s) \sim
\begin{cases}
-\dfrac{\ln s}{\xi}, & s \to 0, \\[2ex]
\dfrac{\ln s}{3s^3}, & s \to \infty,
\end{cases}
\qquad\qquad
\mathcal{I}_g(s) \sim
\begin{cases}
\dfrac{1}{2\xi s^2}, & s \to 0, \\[2ex]
\dfrac{\ln s}{5s^5}, & s \to \infty.
\end{cases}
\tag{4.23}
$$

Note that by repeating the expansion directly on the integrands in eq. (4.10), and then performing the integrations, we would obtain the same formulae above.

4.2.1 The central region

For $s \to 0$, the asymptotic behaviours of the functions $\mathcal{A}_g(s)$, $\mathcal{A}_{BH}(s)$, $\mathcal{I}_g(s)$ and $\mathcal{I}_{BH}(s)$ introduced in this Chapter are given by

$$
\mathcal{A}_g(s) \sim -\frac{\ln s}{\xi}, \qquad \mathcal{A}_{BH}(s) \sim \frac{1}{s}, \qquad \mathcal{I}_g(s) \sim \frac{1}{2\xi s^2}, \qquad \mathcal{I}_{BH}(s) \sim \frac{1}{3s^3}. \tag{4.24}
$$

Therefore, in *presence* of the central BH the velocity dispersion profile is dominated by its contribution. In other words,

$$
\mathcal{A}(s) \sim \frac{\mu}{s}, \qquad\qquad \mathcal{I}(s) \sim \frac{\mu}{3s^3}. \tag{4.25}
$$

Hence, from eqs. (4.8) and (2.1) we obtain

$$
\sigma_r^2(r) \sim \frac{\Psi_n \mu}{s} \times
\begin{cases}
1, & s_a = 0, \\[2ex]
\dfrac{1}{3}, & 0 < s_a \leq \infty.
\end{cases}
\tag{4.26}
$$

In words: *in presence* of the central BH, *at small radii $\sigma_r^2(r) \propto r^{-1}$ for generic values of the anisotropy radius r_a*. In particular, it diverges as r^{-1} with a factor of 3 of difference between the fully radially anisotropic case, and all the other cases with $s_a > 0$, including $s_a = \infty$. Figure 4.1 shows the behaviour of $\sigma_r(r)$ for two different minimum halo models with $\xi = 10$ and $\xi = 20$ (see Section 2.3.3 for this particular choice), in the isotropic and quite anisotropic case. The case $s_a = 0$ is depicted in Fig. 4.2, together with a selection of cases with positive s_a, for a minimum halo model with $\xi = 13$.

In *absence* of the central BH, instead, $\mathcal{A}(s) = \mathcal{R}\,\mathcal{A}_g(s)$ and $\mathcal{I}(s) = \mathcal{R}\,\mathcal{I}_g(s)$. Therefore, from eqs. (4.8) and (2.1) it follows

$$
\sigma_r^2(r) \sim \frac{\Psi_n \mathcal{R}}{\xi} \times
\begin{cases}
-\ln s, & s_a = 0, \\[2ex]
\dfrac{1}{2}, & 0 < s_a \leq \infty.
\end{cases}
\tag{4.27}
$$
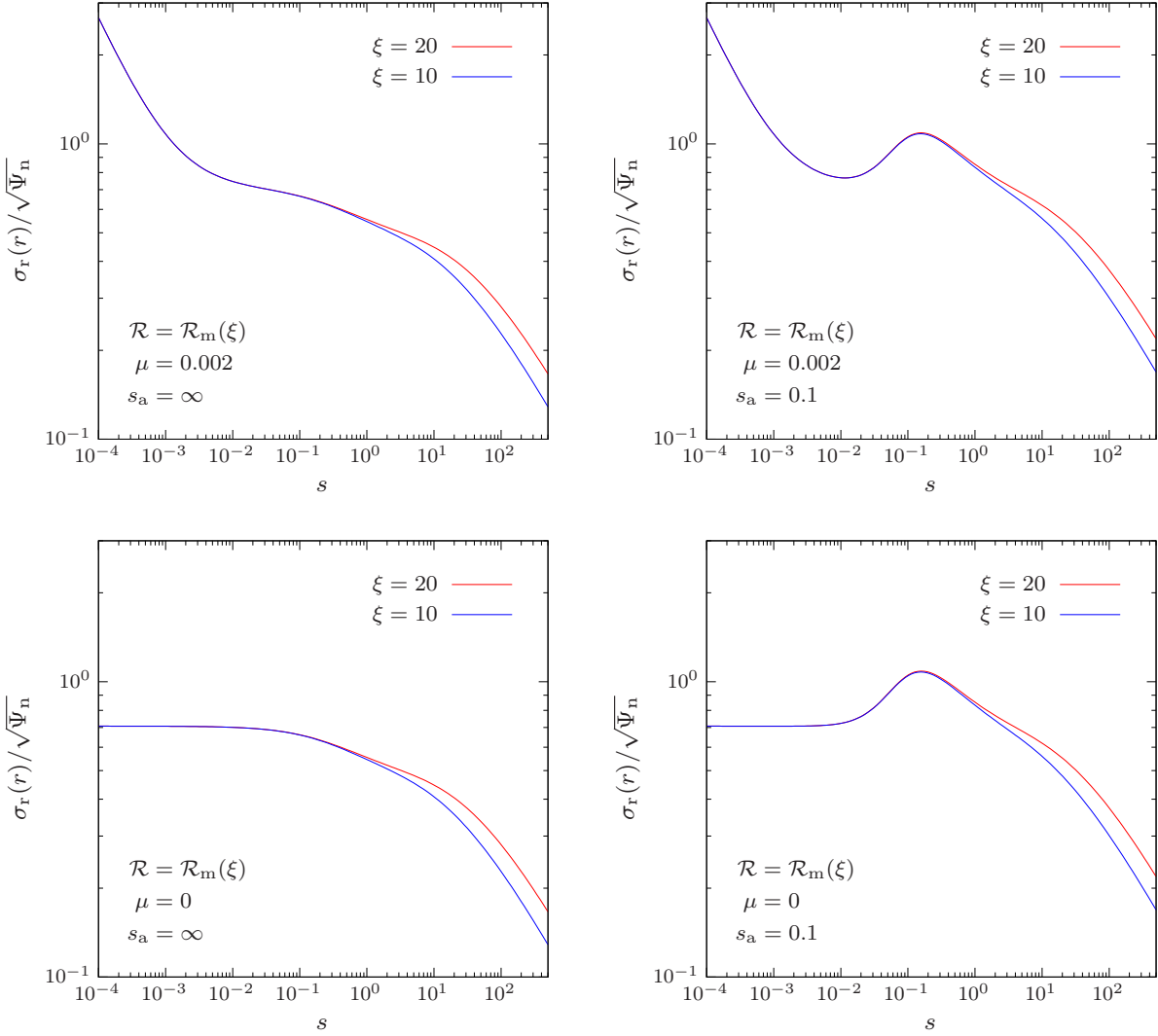
Figure 4.1. Top panels: radial trend of the stellar velocity dispersion σ_r for two representative *minimum halo* models, in presence of the central BH, in the isotropic (left) and anisotropic (right, $s_\mathrm{a} = 0.1$) cases; according to eq. (4.26), at small radii $\sigma_\mathrm{r}(r) \propto r^{-1}$ independently on ξ. Bottom panels: radial trend of σ_r for the same models in the top panels, in absence of the central BH; according to eq. (4.28), $\sigma_\mathrm{r}(0) \simeq 0.71\sqrt{\Psi_\mathrm{n}}$. In both panels, $\sigma_\mathrm{r}^2(r) \propto (\ln s)/s$ at large radii, as shown in eq. (4.31), with a different proportionality constant depending on ξ and the degree of anisotropy.

In particular, if $s_\mathrm{a} = 0$, the central velocity dispersion diverges logarithmically, while for all values $s_\mathrm{a} > 0$, the central velocity dispersion converges to a finite value, coincident with that of the isotropic case, i.e.,

$$\sigma_\mathrm{r}^2(0) = \frac{\Psi_\mathrm{n}\mathcal{R}}{2\xi}. \tag{4.28}$$

Notice that, according to eq. (2.27), *in the minimum halo model with $\xi \geq 1/2$, the value of the central velocity dispersion is independent of ξ*, and it takes the value $\sigma_\mathrm{r}^2(0) = \Psi_\mathrm{n}/2$ (see Fig. 4.1).
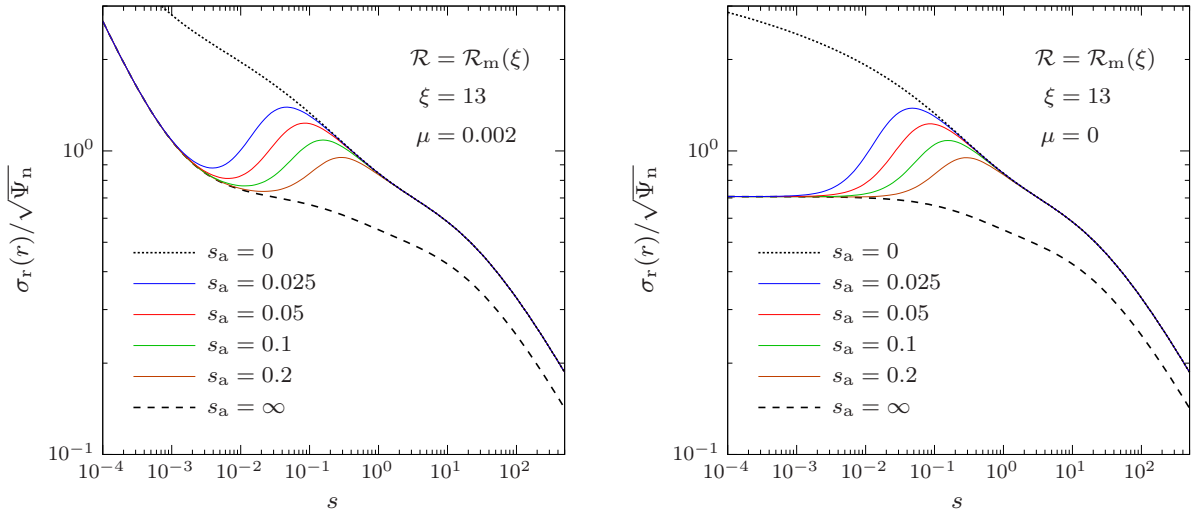
Figure 4.2. Left panel: radial trend of σ_r of the stellar component for a minimum halo model with $\mathcal{R} = \xi = 13$, in presence of the central BH, for different values of s_a; in the central region, according to eq. (4.26), $\sigma_r^2(r) \propto r^{-1}$, with only a factor of 3 of difference between the fully radially anisotropic case, and all the other cases with $s_a > 0$. Right panel: radial trend of the stellar velocity dispersion for the same model in the left panel, in absence of the central BH, for different values of s_a; at small radii, in accordance with eq. (4.27), $\sigma_r^2(r)$ diverges as $-\ln s$ in the purely radial case, while it reduces to a constant for all positive values of s_a (including $s_a = \infty$). In both panels, $\sigma_r^2(r) \propto (\ln s)/s$ at large radii, as shown in eq. (4.31), with a different proportionality constant depending on whether $s_a < \infty$ or $s_a = \infty$; note how a generic profile, once a finite positive value of s_a is fixed, lies between the fully isotropic and the purely radial cases.

4.2.2 The external regions

For $s \to \infty$ we have the following set of trends:

$$\mathcal{A}_g(s) \sim \frac{\ln s}{3s^3}, \qquad \mathcal{A}_{BH}(s) \sim \frac{1}{3s^3}, \qquad \mathcal{I}_g(s) \sim \frac{\ln s}{5s^5}, \qquad \mathcal{I}_{BH}(s) \sim \frac{1}{5s^5}. \qquad (4.29)$$

Therefore, at the leading order,

$$\mathcal{A}(s) \sim \frac{\mathcal{R}\ln s}{3s^3}, \qquad \mathcal{I}(s) \sim \frac{\mathcal{R}\ln s}{5s^5}, \qquad (4.30)$$

whence, from eqs. (4.8) and (2.1),

$$\sigma_r^2(r) \sim \Psi_n \mathcal{R} \frac{\ln s}{s} \times \begin{cases} \dfrac{1}{3}, & 0 \le s_a < \infty, \\[2mm] \dfrac{1}{5}, & s_a = \infty. \end{cases} \qquad (4.31)$$

In words: *in presence or in absence of the central* BH, *at large radii* $\sigma_r^2(r) \propto (\ln s)/s$ *for generic values of* $\mathcal{R}$ *and* s_a. The velocity dispersion profile goes to zero as $(\ln s)/s$ with a different proportionality constant depending on the galaxy-to-stellar density ratio $\mathcal{R}$, and whether $s_a < \infty$ or $s_a = \infty$. In particular, for a chosen $\mathcal{R}$ and fixed r, the radially anisotropic $\sigma_r(r)$ are above those in the corresponding isotropic cases (see Fig. 4.2), a well known consequence of the OM parametrization; for a chosen s_a and fixed r, instead, $\sigma_r(r)$ increases for increasing $\mathcal{R}$ (see Fig. 4.1).

4.3   The projected velocity dispersion

The projected velocity dispersion profile associated with a general anisotropy function $\beta(r)$ is given by

$$\Sigma_*(R)\sigma_{\mathrm{p}}^2(R) = 2\int_R^\infty \left[1 - \beta(r)\frac{R^2}{r^2}\right]\frac{\rho_*(r)\sigma_{\mathrm{r}}^2(r)rdr}{\sqrt{r^2 - R^2}}, \tag{4.32}$$

(see, e.g., Binney & Tremaine 2008), where, in the case of OM anisotropy, $\beta(r)$ is defined in eq. (3.6). The projection integral in eq. (4.32) cannot be evaluated analytically for J3 models in terms of elementary functions. Nevertheless, by using eq. (4.3), and changing the order of integration, we find that eq. (4.32) can be rewritten as

$$\Sigma_*(R)\sigma_{\mathrm{p}}^2(R) = G\int_R^\infty \mathcal{K}(r,R)\rho_*(r)M_{\mathrm{T}}(r)\left(1 + \frac{r_{\mathrm{a}}^2}{r^2}\right)dr, \tag{4.33}$$

where

$$\mathcal{K}(r,R) \equiv 2\int_R^r \left(1 - \frac{R^2}{x^2 + r_{\mathrm{a}}^2}\right)\frac{xdx}{(x^2 + r_{\mathrm{a}}^2)\sqrt{x^2 - R^2}}. \tag{4.34}$$

The integral in the equation above can be solved without any difficulty. Indeed, by the change of variable $y^2 \equiv (x^2 - R^2)/(r_{\mathrm{a}}^2 + R^2)$, eq. (4.34) becomes

$$\mathcal{K}(r,R) = 2\frac{(r_{\mathrm{a}}^2 + R^2)\mathcal{J}_1(r,R) - R^2\mathcal{J}_2(r,R)}{(r_{\mathrm{a}}^2 + R^2)^{3/2}}, \qquad \mathcal{J}_n(r,R) \equiv \int_0^b \frac{dy}{(1 + y^2)^n}, \tag{4.35}$$

in which $b \equiv \sqrt{(r^2 - R^2)/(r_{\mathrm{a}}^2 + R^2)}$. Now, for $r_{\mathrm{a}} \neq 0$ and $R \neq 0$, by elementary calculations it follows that

$$\mathcal{K}(r,R) = \frac{2r_{\mathrm{a}}^2 + R^2}{(r_{\mathrm{a}}^2 + R^2)^{3/2}}\tan^{-1}\sqrt{\frac{r^2 - R^2}{r_{\mathrm{a}}^2 + R^2}} - \frac{R^2\sqrt{r^2 - R^2}}{(r_{\mathrm{a}}^2 + R^2)(r_{\mathrm{a}}^2 + r^2)}. \tag{4.36}$$

The special case for $r_{\mathrm{a}} = 0$ and $R = 0$ can be treated directly in eq. (4.32); simple algebra shows that, for this particular choice of r_{a} and R, the right-hand side of eq. (4.32) diverges. A more detailed discussion of a J3 galaxy model supported by pure radial orbits in the central region will be made in the next Section. Equations (4.33) and (4.36), although seem rather complicated, actually reduce the dimensionality of the integral in eq. (4.32). This is a useful property in numerical works, avoiding the task of the computation of the two-dimensional integral in eq. (4.32).

4.3.1   The central region

At small radii, both the integrals defining $\Sigma_*(R)\sigma_{\mathrm{p}}^2(R)$ (see eq. [4.32]) and $\Sigma_*(R)$ (see eq. [2.5]) are asymptotically dominated by their integrands for $r \to 0$. Therefore, in this region $\sigma_{\mathrm{p}}(R)$ can be properly defined only as the limit for $R \to 0$ of the ratio of two diverging quantities. In order to find the asymptotic behaviour of $\sigma_{\mathrm{p}}(R)$ close to the center, we shall adopt the following strategy. Let the integrand in eq. (4.32) be $\Lambda(R,r)$, and ε a positive quantity. Now we rewrite eq. (4.32) as

$$\Sigma_*(R)\sigma_{\mathrm{p}}^2(R) = \int_R^\varepsilon \Lambda(R,r)dr + \int_\varepsilon^\infty \Lambda(R,r)dr, \tag{4.37}$$
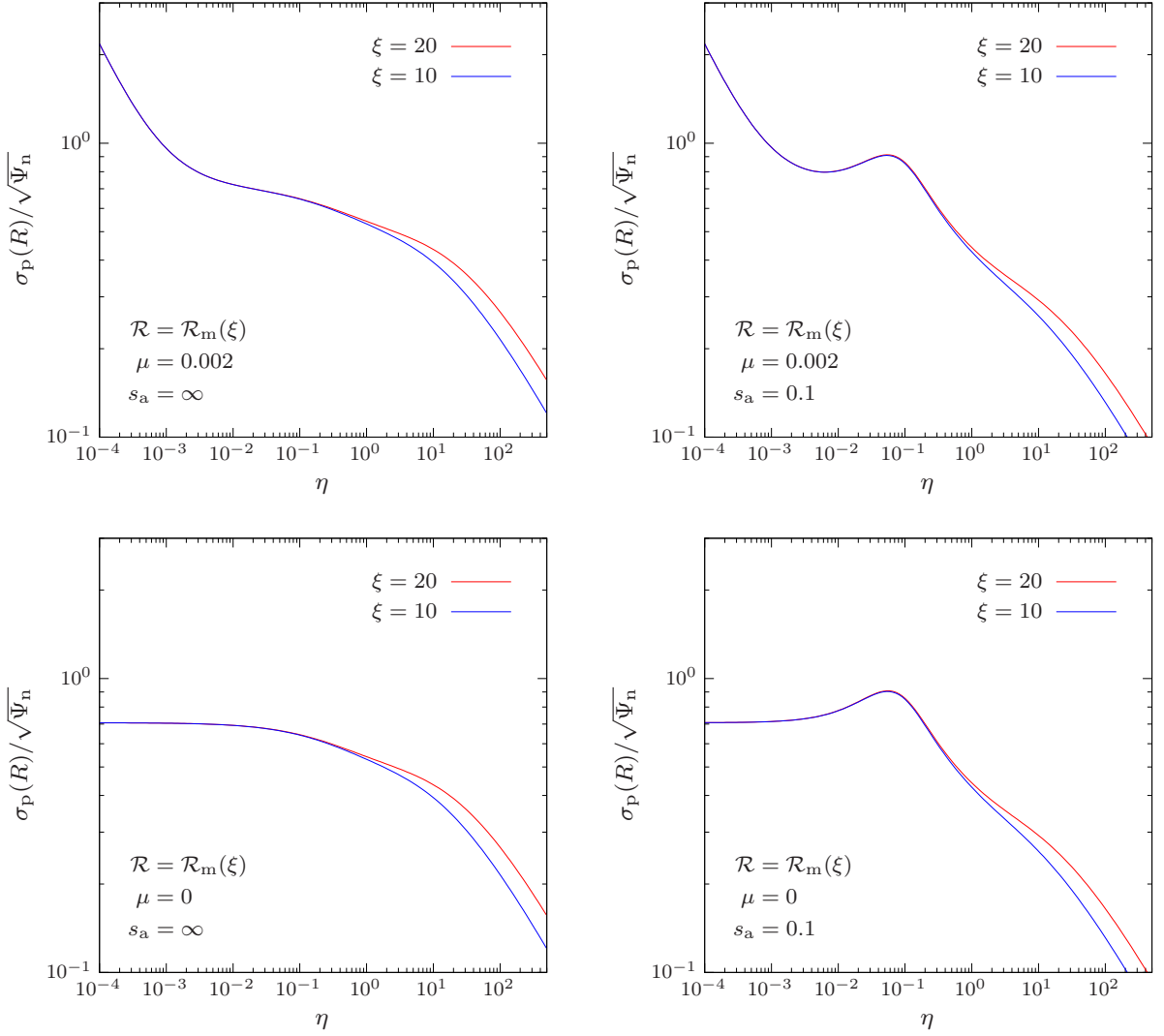
Figure 4.3. Top panels: radial trend of the projected stellar velocity dispersion σ_p for two representative *minimum halo* models, in presence of the central BH, in the isotropic (left) and anisotropic (right, $s_\mathrm{a} = 0.1$) cases; according to eq. (4.46), at small radii $\sigma_\mathrm{p}(R) \propto R^{-1}$ independently on ξ. Bottom panels: radial trend of σ_p for the same models in the top panels, in absence of the central BH; according to eq. (4.46), $\sigma_\mathrm{p}(0) \simeq 0.71 \sqrt{\Psi_\mathrm{n}}$. In both panels, $\sigma_\mathrm{r}^2(R) \propto (\ln \eta)/\eta$ at large radii, as shown in eq. (4.54), with a different proportionality constant depending on ξ, and whether $s_\mathrm{a} < \infty$ or $s_\mathrm{a} = \infty$.

and treat ε as a small quantity. Since the second integral on the right-hand side of the foregoing equation converges when R tends to zero, the required asymptotic behaviour is given by the leading order term of the first integral as $R \to 0$.

In *presence* of the central BH, $\sigma_\mathrm{r}(r)$ is dominated by the BH contribution, and its behaviour is given in eq. (4.26). Hence, in order to derive $\sigma_\mathrm{p}(R)$, we have to distinguish two cases: the case $s_\mathrm{a} = 0$, and the case $0 < s_\mathrm{a} \leq \infty$. In the pure purely radial case, $\beta(r) = 1$; then, by inserting eq. (4.26) in eq. (4.32), and applying the strategy explained above, we have

$$\Sigma_*(R)\sigma_\mathrm{p}^2(R) \sim 2\,\Sigma_\mathrm{n}\Psi_\mathrm{n}\mu \int_\eta^{\tilde{\varepsilon}} \frac{\sqrt{s^2 - \eta^2}}{s^4}\,ds, \tag{4.38}$$
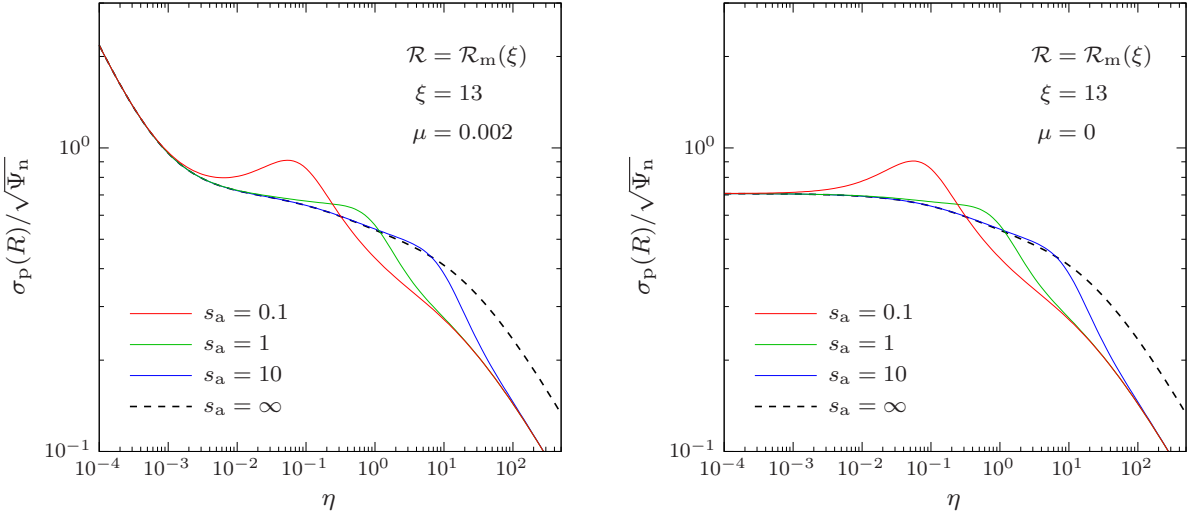
Figure 4.4. Left panel: radial trend of $\sigma_{\rm p}$ of the stellar component for a minimum halo model with $\mathcal{R} = \xi = 13$, in presence of the central BH, for different values of $s_{\rm a}$; in the central region, according to eq. (4.41), $\sigma_{\rm p}^2(R) \propto R^{-1}$ independently on $s_{\rm a}$. Right panel: radial trend of the projected stellar velocity dispersion for the same model in the left panel, in absence of the central BH, for different values of $s_{\rm a}$; at small radii, in accordance with eq. (4.46), $\sigma_{\rm p}(R)$ reduces to a constant for all positive values of $s_{\rm a}$ (including $s_{\rm a} = \infty$). In both panels, $\sigma_{\rm p}^2(R) \propto (\ln \eta)/\eta$ at large radii, as shown in eq. (4.54), with a different proportionality constant depending on whether $s_{\rm a} < \infty$ or $s_{\rm a} = \infty$.

where $\tilde{\varepsilon} \equiv \varepsilon/r_*$. With the substitution $\eta/s \equiv y$ we readily find

$$\Sigma_*(R)\sigma_{\rm p}^2(R) \sim \frac{2\,\Sigma_{\rm n}\Psi_{\rm n}\mu}{3\eta^2}. \tag{4.39}$$

For what concerns the other case, we know that $\beta(r) = 0$ for $s_{\rm a} = \infty$; moreover, for finite values of $s_{\rm a}$, the velocity dispersion tensor becomes isotropic in the limit $r \to 0$. Hence, for $0 < s_{\rm a} \leq \infty$ we obtain

$$\Sigma_*(R)\sigma_{\rm p}^2(R) \sim \frac{2\,\Sigma_{\rm n}\Psi_{\rm n}\mu}{3} \int_\eta^{\tilde{\varepsilon}} \frac{ds}{s^2\sqrt{s^2 - \eta^2}}, \tag{4.40}$$

which gives, after some minor reductions, the same result as in eq. (4.39). Finally, by using eq. (2.5), we conclude that, *independently of the value of $s_{\rm a}$*, it is found

$$\sigma_{\rm p}^2(R) \sim \frac{2\Psi_{\rm n}\mu}{3\pi\eta}. \tag{4.41}$$

In words: *in presence of the central* BH, *at small radii $\sigma_{\rm p}^2(R) \propto R^{-1}$ for generic values of the anisotropy radius $r_{\rm a}$*. The situation is shown in Fig. 4.4, in which, for different values of the anisotropy parameter, a minimum halo model with $\xi = 13$ is considered. Moreover, as expected, close to center $\sigma_{\rm p}(R)$ is reasonably *independent* on the galaxy-to-stellar scale lenght ratio ξ. In analogy with Fig. 4.1, in Fig. 4.3 we show the behaviour of $\sigma_{\rm p}(R)$ for two different minimum halo models with $\xi = 10$ and $\xi = 20$, in the isotropic and quite anisotropic case.

On the other hand, in *absence* of the central BH the stellar velocity dispersion is given by eq. (4.27). If the galaxy is supported by pure radial orbits, $\sigma_{\rm p}(R)$ diverges at the center; indeed, by inserting eq. (4.27) in eq. (4.32) we find

$$\Sigma_*(R)\sigma_{\rm p}^2(R) \sim -\frac{2\,\Sigma_{\rm n}\Psi_{\rm n}\mathcal{R}}{\xi} \int_\eta^{\tilde{\varepsilon}} \frac{\sqrt{s^2-\eta^2}\,\ln s}{s^3}\,ds, \tag{4.42}$$

whence, by retaining the leading order term,

$$\Sigma_*(R)\sigma_{\rm p}^2(R) \sim -\frac{\pi\Sigma_{\rm n}\Psi_{\rm n}\mathcal{R}}{2\xi} \times \frac{\ln\eta}{\eta}. \tag{4.43}$$

For $0 < s_{\rm a} \leq \infty$, instead, by the same arguments used after eq. (4.39), we have

$$\Sigma_*(R)\sigma_{\rm p}^2(R) \sim \frac{\Sigma_{\rm n}\Psi_{\rm n}\mathcal{R}}{\xi} \int_\eta^{\tilde{\varepsilon}} \frac{ds}{s\sqrt{s^2-\eta^2}}, \tag{4.44}$$

or, after performing the integration,

$$\Sigma_*(R)\sigma_{\rm p}^2(R) \sim \frac{\pi\Sigma_{\rm n}\Psi_{\rm n}\mathcal{R}}{2\xi\eta}. \tag{4.45}$$

By comparison with eq. (4.43), and using eq. (2.5), we finally obtain

$$\sigma_{\rm p}^2(R) \sim \frac{\Psi_{\rm n}\mathcal{R}}{2\xi} \times \begin{cases} -\ln\eta, & s_{\rm a} = 0, \\[2mm] 1, & 0 < s_{\rm a} \leq \infty. \end{cases} \tag{4.46}$$

Therefore, in the central region, the projected velocity dispersion reduces to the *same* constant value as in eq. (4.28), i.e.:

$$\sigma_{\rm r}(0) = \sigma_{\rm p}(0) \quad \text{for} \quad 0 < s_{\rm a} \leq \infty. \tag{4.47}$$

In words: *in absence of the central* BH, *at small radii the projected velocity dispersion coincides with the radial component of the isotropic velocity dispersion, independently of the value of $s_{\rm a} > 0$* (see Fig. 4.4).

4.3.2 The external regions

The behaviour of $\sigma_{\rm p}(R)$ at large radii can be described by considering the leading term of the asymptotic expansion of the integral in eq. (4.32) for $R \to \infty$. As for the central region, there is no formal difficulty; the only care required is to take into account the effect of the radial anisotropy, and to distinguish two different cases: the isotropic case and any other model with finite $s_{\rm a}$.

For finite values of the anisotropy radius, $\beta(r) \sim 1$ for $r \to \infty$, therefore the projection integral, by virtue of eq. (4.31), becomes

$$\Sigma_*(R)\sigma_{\rm p}^2(R) \sim \frac{2\,\Sigma_{\rm n}\Psi_{\rm n}\mathcal{R}}{3} \int_\eta^\infty \frac{\sqrt{s^2-\eta^2}\,\ln s}{s^6}\,ds. \tag{4.48}$$

Hence, with the substitution $\eta/s \equiv y$, and by retaining the leading order term, we obtain

$$\Sigma_*(R)\sigma_{\rm p}^2(R) \sim \frac{2\,\Sigma_{\rm n}\Psi_{\rm n}\mathcal{R}\ln\eta}{3\eta^4} \int_0^1 y^3\sqrt{1-y^2}\,dy, \tag{4.49}$$

or, after some reductions,
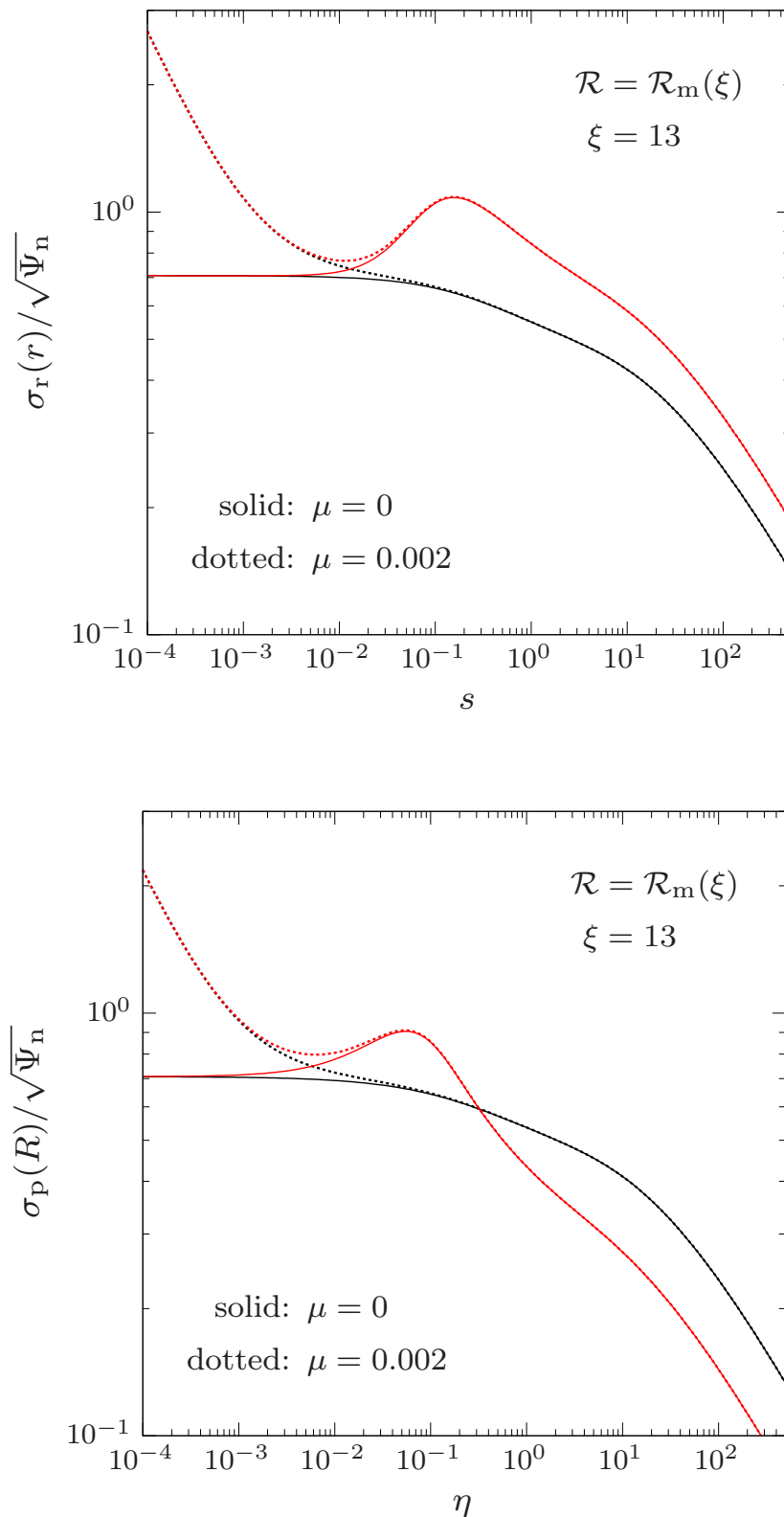
Figure 4.5. Top panel: radial trend of the stellar velocity dispersion for a minimum halo galaxy model with $\mathcal{R} = \xi = 13$; black lines refer to the isotropic case, red lines show the quite anisotropic case with $s_\mathrm{a} = 0.1$. Bottom panel: radial trend of the projected stellar velocity dispersion for the same model in the top panel. In both panels, the radial trends are shown with and without (dotted and solid lines, respectively) the effect of the central BH.

$$\Sigma_*(R)\sigma_{\rm p}^2(R) \sim \frac{4\,\Sigma_{\rm n}\Psi_{\rm n}\mathcal{R}}{45} \times \frac{\ln\eta}{\eta^4}. \tag{4.50}$$

In the fully isotropic case, by setting $\beta(r) = 0$ and inserting eq. (4.31) in eq. (4.32) we find

$$\Sigma_*(R)\sigma_{\rm p}^2(R) \sim \frac{2\,\Sigma_{\rm n}\Psi_{\rm n}\mathcal{R}}{5} \int_\eta^\infty \frac{\ln s}{s^4\sqrt{s^2 - \eta^2}}\,ds. \tag{4.51}$$

Thus, following the same approach adopted in the case of finite $s_{\rm a}$, we obtain

$$\Sigma_*(R)\sigma_{\rm p}^2(R) \sim \frac{2\,\Sigma_{\rm n}\Psi_{\rm n}\mathcal{R}\ln\eta}{5\eta^4} \int_0^1 \frac{y^3 dy}{\sqrt{1 - y^2}} \tag{4.52}$$

or, after performing the required integration,

$$\Sigma_*(R)\sigma_{\rm p}^2(R) \sim \frac{4\,\Sigma_{\rm n}\Psi_{\rm n}\mathcal{R}}{15} \times \frac{\ln\eta}{\eta^4}. \tag{4.53}$$

Finally, eqs. (4.50) and (4.53) can be combined to give

$$\sigma_{\rm p}^2(R) \sim \frac{8\Psi_{\rm n}\mathcal{R}\ln\eta}{15\pi\eta} \times
\begin{cases}
\dfrac{1}{3}, & 0 \leq s_{\rm a} < \infty, \\[2ex]
1, & s_{\rm a} = \infty,
\end{cases} \tag{4.54}$$

or, in words: *at large radii $\sigma_{\rm p}^2(R) \propto (\ln\eta)/\eta$ for generic values of the anisotropy radius $r_{\rm a}$.* In particular, for fixed galaxy-to-stellar density ratio $\mathcal{R}$, $\sigma_{\rm p}^2(R)$ goes to zero as $(\ln\eta)/\eta$ with a factor of 3 of difference between the fully isotropic case, and all the other cases with $s_{\rm a} < \infty$, including $s_{\rm a} = 0$. This important property involving the outer regions is nothing else than a natural result due to the projection effect on the radial orbit population: as shown in Fig. 4.4, indeed, the radially anisotropic $\sigma_{\rm p}(R)$'s are below those in the corresponding isotropic case.

All the relevant properties of $\sigma_{\rm r}(r)$ and $\sigma_{\rm p}(R)$ are illustrated in Fig. 4.5, where we consider a minimum halo model with $\xi = 13$, with and without the effect of the central BH, in the isotropic and anisotropic cases.

CHAPTER 5

THE ENERGETICS OF THE MODELS

IN this Chapter the application of the Virial theorem to J3 models is presented. The Chapter is organized as follows.

In Section 5.1 the analytical expressions of the relevant quantities entering the Virial theorem, such as the stellar kinetic energy, the interaction energy, and the potential energy, are derived as functions of the model parameters.

In Section 5.2 the fiducial anisotropy limit required to prevent the onset of Radial Orbit Instability is determined as a function of the galaxy parameters.

5.1   Kinetic, interaction, and potential energies

As is well known, the *scalar virial theorem* for the stellar component of a multi-component stellar system reads

$$2K_* = -W_*, \tag{5.1}$$

(see Binney & Tremaine 2008, Ciotti 2000; see also Ogorodnikov 1965, Saslaw 1985), where K_* is the *total kinetic energy*, and W_* is the *total interaction energy*.

In case of spherical systems the energy K_* is given by

$$K_* = 2\pi \int_0^\infty \rho_*(r)[\sigma_\mathrm{r}^2(r) + \sigma_\mathrm{t}^2(r)]r^2 dr, \tag{5.2}$$

which can be conveniently rewritten as $K_* = K_{*\mathrm{r}} + K_{*\mathrm{t}}$ once the following definitions are applied:

$$K_{*\mathrm{r}} \equiv 2\pi \int_0^\infty \rho_*(r)\sigma_\mathrm{r}^2(r)r^2 dr, \qquad K_{*\mathrm{t}} \equiv 2\pi \int_0^\infty \rho_*(r)\sigma_\mathrm{t}^2(r)r^2 dr. \tag{5.3}$$

These two quantities have a natural physical interpretation: they are the total kinetic energy of stars associated with the radial and tangential components of the velocity dispersion tensor, respectively. Therefore, in principle, to evaluate K_* we should first solve the Jeans equations.

For what concerns the quantity W_*, instead, it represents the cumulative interaction energy of the stars with the gravitational field of any other component of the system, and is therefore obtained by adding the contributions produced by all components. Let $M_k(r)$ be the mass distribution of the k-th component; then, the interaction energy of the stars with the gravitational field of this component is given by

$$W_{*k} = -4\pi G \int_0^\infty \rho_*(r)M_k(r)rdr. \tag{5.4}$$

Hence, since for J3 models the stars interact with the gravitational fields produced by the galaxy and the central BH, eq. (5.1) becomes

$$2K_* = -(W_{*\mathrm{g}} + W_{*\mathrm{BH}}), \tag{5.5}$$

where

$$W_{*\mathrm{g}} = -4\pi G \int_0^\infty \rho_*(r)M_\mathrm{g}(r)rdr, \qquad W_{*\mathrm{BH}} = -4\pi G M_\mathrm{BH} \int_0^\infty \rho_*(r)rdr. \tag{5.6}$$

From the virial theorem, in practice, K_* *is independent of the specific orbital anisotropy considered*, and can be obtained without using the explicit solution of the Jeans equations. Indeed, as shown in eq. (5.6), to derive K_* it is enough to know the mass distribution of the components with which the stars interact. In addition, simple algebra shows that the quantity $W_{*\mathrm{BH}}$ in eq. (5.6) diverges; then, since the total kinetic energy of the stars can be decomposed into the two contributions due to the galaxy and the BH, i.e., $K_* = K_{*\mathrm{g}} + K_{*\mathrm{BH}}$, the virial theorem implies that also $K_{*\mathrm{BH}}$ diverges. The contribution of the total galaxy potential to $W_{*\mathrm{g}}$, instead, is finite. Indeed, after an integration by parts, it can be rewritten as

$$W_{*\mathrm{g}} = -\Psi_\mathrm{n} M_* \mathcal{R} \int_0^\infty \frac{\mathcal{N}(y)}{\xi + y} dy, \qquad \mathcal{N}(y) \equiv \ln \frac{1+y}{y} - \frac{1}{1+y}. \tag{5.7}$$

Splitting the integrand for $W_{*\mathrm{g}}$ into partial fractions we find

$$\frac{\mathcal{N}(y)}{\xi + y} = \begin{cases} \dfrac{\ln(1 + 1/y)}{\xi + y} - \dfrac{1}{\xi - 1}\left(\dfrac{1}{1 + y} - \dfrac{1}{\xi + y}\right), & \xi \neq 1, \\[3mm] \dfrac{\ln(1 + 1/y)}{1 + y} - \dfrac{1}{(1 + y)^2}, & \xi = 1, \end{cases} \tag{5.8}$$

whence, making use of the results in Appendix C,

$$W_{*\mathrm{g}} = -\Psi_{\mathrm{n}} M_* \mathcal{R} \times \begin{cases} \mathcal{H}(\xi, 0) - \dfrac{\ln \xi}{\xi - 1}, & \xi \neq 1, \\[3mm] \dfrac{\pi^2}{6} - 1, & \xi = 1. \end{cases} \tag{5.9}$$

A useful consequence of the finite value of $W_{*\mathrm{g}}$ is the possibility to define the 3-dimensional stellar *virial velocity dispersion* as $\sigma_{\mathrm{V}}^2 \equiv |W_{*\mathrm{g}}|/M_*$: in particular, for a minimum halo model with $\xi = 13$ we obtain $\sigma_{\mathrm{V}}^2 \simeq 0.91\, \Psi_{\mathrm{n}}$. In Fig. 5.1 the behaviour of $|W_{*\mathrm{g}}|$ as a function of ξ is shown in the case of a minimum halo galaxy model. For realistic values of ξ (i.e., $\xi \geq 1$), the absolute value of $W_{*\mathrm{g}}$ increases for increasing ξ, tending to $\Psi_{\mathrm{n}} M_*$ as ξ tends to infinity; consequently, in these cases we have always $\sigma_{\mathrm{V}}^2 < \Psi_{\mathrm{n}}$. Moreover, from eq. (5.4) we find

$$W_{**} = -4\pi G \int_0^\infty \rho_*(r) M_*(r) r\, dr, \tag{5.10}$$

or, performing the integration,

$$W_{**} = -\frac{\Psi_{\mathrm{n}} M_*}{2}. \tag{5.11}$$

Therefore, *the energy of the stars due to the self-interaction of the stellar distribution is a constant value, independent on $\mathcal{R}$ and ξ*. Finally, since $M_{\mathrm{DM}}(r) = M_{\mathrm{g}}(r) - M_*(r)$, from eq. (5.4) we can compute $W_{*\mathrm{DM}} = W_{*\mathrm{g}} - W_{**}$ without performing additional integrations.

We shall now calculate the different contributions to the *potential energy* U_* of the stellar component[1]. As for the other energies we have introduced, also for the potential energy U_* holds the decomposition

$$U_* = U_{*\mathrm{g}} + U_{*\mathrm{BH}}, \qquad \text{with} \qquad U_{*\mathrm{g}} = U_{**} + U_{*\mathrm{DM}}. \tag{5.12}$$

The self-gravitational energy U_{**} and the potential energy $U_{*\mathrm{DM}}$ due to the effect of the DM halo are given by, respectively,

$$U_{**} = -2\pi \int_0^\infty \rho_*(r)\Psi_*(r) r^2\, dr, \qquad U_{*\mathrm{DM}} = -4\pi \int_0^\infty \rho_*(r)\Psi_{\mathrm{DM}}(r) r^2\, dr, \tag{5.13}$$

while the contribution of the central BH, as well known, diverges as $W_{*\mathrm{BH}}$:

---

[1] As well known, in multi component systems the energy W of a given component is *not* the potential energy of the component itself in the total potential.
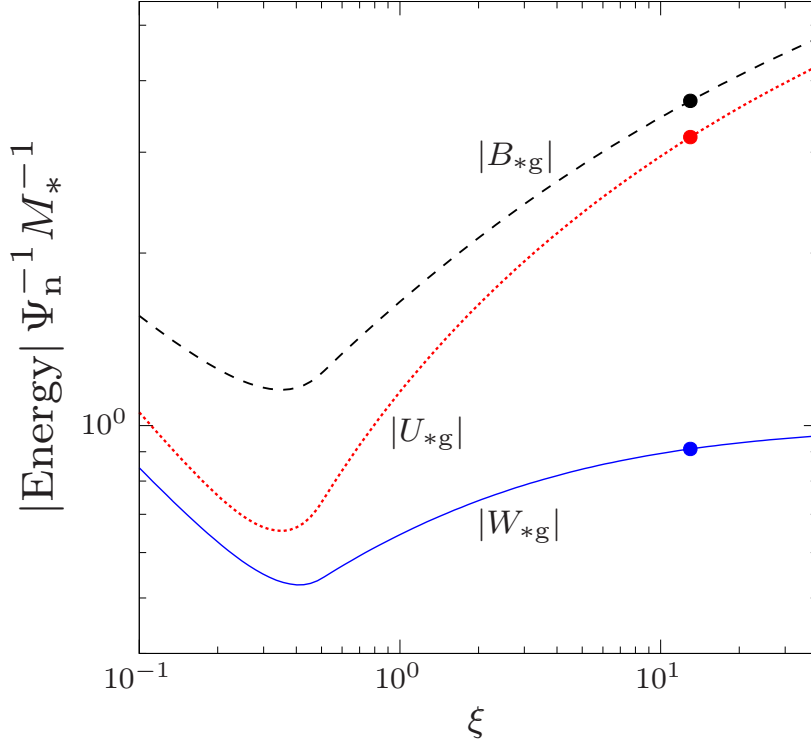
Figure 5.1. Absolute values of the normalized gravitational energies for the stellar component, as a function of ξ, in case of minimum halo and absence of a central BH. In the limit $\xi \to \infty$, while both $|B_{*\mathrm{g}}|$ and $|U_{*\mathrm{g}}|$ tends to infinity, $|W_{*\mathrm{g}}|$ reduces to the constant value $\Psi_\mathrm{n} M_*$. The circles show the corresponding values for a minimum halo case with $\mathcal{R} = \xi = 13$: $|W_{*\mathrm{g}}| \simeq 0.91\,\Psi_\mathrm{n} M_*$ (blue circle, see eq. [5.9]), $|U_{*\mathrm{g}}| \simeq 3.19\,\Psi_\mathrm{n} M_*$ (red circle, see eq. [5.21]), and $|B_{*\mathrm{g}}| \simeq 3.69\,\Psi_\mathrm{n} M_*$ (black circle, see eq. [5.19]).

$$U_{*\mathrm{BH}} = -\,4\pi G M_{\mathrm{BH}} \int_0^\infty \rho_*(r) r\,dr = W_{*\mathrm{BH}}. \tag{5.14}$$

Let us calculate the self-gravitational energy U_{**}. By substituing the expressions for $\rho_*(r)$ and $M_*(r)$ in eq. (5.13) we have

$$U_{**} = -\,\frac{\Psi_\mathrm{n} M_*}{2} \int_0^\infty \ln\!\left(1 + \frac{1}{y}\right) \frac{dy}{(1+y)^2}, \tag{5.15}$$

whence, by integrating by parts we find, after elementary calculations,

$$U_{**} = -\,\frac{\Psi_\mathrm{n} M_*}{2} = W_{**}. \tag{5.16}$$

This result does not surprise us, inasmuch as the self-gravitational and self-interaction energies of each density component of a multicomponent system coincide. In order to derive $U_{*\mathrm{g}}$ and $U_{*\mathrm{DM}}$, instead, we shall adopt a different strategy. Let us consider another form of energy, which we define as

$$B_{*\mathrm{g}} \equiv -\,4\pi \int_0^\infty \rho_*(r) \Psi_\mathrm{g}(r) r^2\,dr. \tag{5.17}$$

This energy is *not* the gravitational energy of the stars in the galaxy total potential. Yet, it is not just a mathematical expression, since it is useful in the theory of galactic winds and studies of the origin of the X-ray emission of early-type galaxies. Indeed, it measures the energy per unit time ($L_{\rm grav}$) to be provided to the ISM of early-type galaxies (via, e.g., supernova explosions, or thermalization of the velocity of stellar winds, or AGN feedback) in order to steadily extract the mass input injected over the galaxy body from evolving stars: it is found that $L_{\rm grav} \propto |B_{*\rm g}|$ (see Pellegrini 2011, Posacki et al. 2013). A nice feature of J3 models is that $B_{*\rm g}$ is finite, although its expression cannot be obtained via elementary functions. Indeed, inserting the expressions for $\rho_*(r)$ and $\Psi_{\rm g}(r)$ in the foregoing equation, we find

$$B_{*\rm g} = W_{*\rm g} - \frac{\Psi_{\rm n} M_* \mathcal{R}}{\xi} \int_0^\infty \ln\left(1 + \frac{\xi}{y}\right) \frac{dy}{(1+y)^2}. \tag{5.18}$$

By an integration by parts, and after some reductions, for all positive values of ξ we obtain

$$B_{*\rm g} = -\,\Psi_{\rm n} M_* \mathcal{R} \mathcal{H}(\xi, 0). \tag{5.19}$$

Figure 5.1 shows the trend of $|B_{*\rm g}|$, as a function of ξ, in the minimum halo case. For $\xi \geq 1$ the absolute value of $W_{*\rm g}$ increases for increasing ξ, and it diverges in the limit $\xi \to \infty$. In particular, for a minimum halo galaxy model with $\xi = 13$, as marked by the black circle in Fig. 5.1, we find that $|B_{*\rm g}| \simeq 3.69\,\Psi_{\rm n} M_*$. Now, remembering that $\Psi_{\rm DM}(r) = \Psi_{\rm g}(r) - \Psi_*(r)$, from eqs. (5.13) and (5.12) it is found that

$$U_{*\rm DM} = B_{*\rm g} - 2U_{**}, \qquad U_{*\rm g} = B_{*\rm g} - U_{**}. \tag{5.20}$$

Hence, without performing additional integrals, we are able to derive $U_{*\rm DM}$ and $U_{*\rm g}$ just combining the energies $B_{*\rm g}$ and U_{**}. By inserting eqs. (5.16) and (5.19) in eq. (5.20) we therefore obtain

$$U_{*\rm DM} = -\,\Psi_{\rm n} M_* \times [\mathcal{R} \mathcal{H}(\xi, 0) - 1], \qquad U_{*\rm g} = -\,\Psi_{\rm n} M_* \times \left[\mathcal{R} \mathcal{H}(\xi, 0) - \frac{1}{2}\right]. \tag{5.21}$$

As for $|B_{*\rm g}|$ and $|W_{*\rm g}|$, also the behaviour of $|U_{*\rm g}|$ as a function of ξ is depicted in Fig. 5.1, in the minimum halo case. For $\xi = 13$, by virtue of eq. (5.21), we obtain the approximate value $|U_{*\rm g}| \simeq 3.19\,\Psi_{\rm n} M_*$ (see the red circle in Fig. 5.1).

5.2 Orbital Stability

We shall now investigate a particularly relevant application of the virial theorem: the determination of the conditions required to prevent the onset of the Radial Orbit Instability (hereafter, ROI). Indeed, stellar systems supported by a large amount of radial orbits are in general unstable (see Fridman & Polyachenko 1984). Since the stability, in general, depends on the value of the global anisotropy of the system, we introduce the so-called "stability indicator" Ξ for the stellar component. This quantity is defined as

$$\Xi \equiv \frac{2K_{*\rm r}}{K_{*\rm t}}, \tag{5.22}$$

and measures the ratio of the radial kinetic energy to the tangential one. Therefore, from its

definition, $\Xi \to 1$ in the limit $r_{\mathrm{a}} \to \infty$, while $\Xi \to \infty$ for $r_{\mathrm{a}} \to 0$. Numerous investigations of *one-component* systems have confirmed that the onset of ROI is in general prevented by the empirical requirement that $\Xi < \Xi_{\mathrm{c}}$, where $\Xi_{\mathrm{c}} = 1.70 \pm 0.25$. Note that the interval of values Ξ_{c} is rather narrow, though the exact critical value Ξ_{c} depends on the particular model (see Merritt & Aguilar 1985, Bertin & Stiavelli 1989, Bertin et al. 1994, Meza & Zamorano 1997, Nipoti et al. 2002). Nevertheless, N-body simulations have shown that the presence of a DM halo does not change very much the situation with respect to the one-component systems (see Stiavelli & Sparke 1991, Nipoti et al. 2002). For this reason, although we are considering *two-component* systems, we shall assume 1.7 as a fiducial *maximum* value of Ξ for stability, and discuss the "fiducial stability condition" $\Xi = 1.7$. For, we rewrite eq. (5.22) in a more useful way.

Since the kinetic energy $K_{*\mathrm{BH}}$ diverges, we *exclude* the effect of the central BH; then, by virtue of eq. (5.1), we have $2K_* = |W_{*\mathrm{g}}|$. Therefore, as $K_{*\mathrm{t}} = K_* - K_{*\mathrm{r}}$, eq. (5.22) becomes

$$\Xi = \frac{4}{|W_{*\mathrm{g}}|/K_{*\mathrm{r}} - 2}. \tag{5.23}$$

By using eq. (4.3), and changing the order of integration in the integral defining $K_{*\mathrm{r}}$ (see eq. [5.3]), we obtain

$$K_{*\mathrm{r}} = 2\pi G \int_0^\infty \mathcal{L}_{\mathrm{r}}(r) \rho_*(r) M_{\mathrm{g}}(r) \left(1 + \frac{r_{\mathrm{a}}^2}{r^2}\right) dr, \qquad \mathcal{L}_{\mathrm{r}}(r) \equiv \int_0^r \frac{x^2 dx}{x^2 + r_{\mathrm{a}}^2}, \tag{5.24}$$

whence, after an elementary integration,

$$\mathcal{L}_{\mathrm{r}}(r) = r - r_{\mathrm{a}} \tan^{-1} \frac{r}{r_{\mathrm{a}}}. \tag{5.25}$$

First note that, as eqs. (4.33) and (4.36) reduce the dimensionality of the integral defining $\Sigma_*(R) \sigma_{\mathrm{p}}^2(R)$ (see Section 4.3), eqs. (5.24) and (5.25) actually reduce the dimensionality of the integral defining $K_{*\mathrm{r}}$ from two to one, an useful property in numerical works if one wanted to prevent the task of the computation of the two-dimensional integral defining the energy $K_{*\mathrm{r}}$. Second, from eqs. (5.6) and (5.24), and remembering the expression of $M_{\mathrm{g}}(r)$ given in eq. (2.12), it follows that the ratio $|W_{*\mathrm{g}}|/K_{*\mathrm{r}}$ does *not* depend on $\mathcal{R}$, while it depends on ξ and s_{a}. In other words: *in absence of the central* BH, *the stability indicator* Ξ *depends only on the galaxy-to-stellar scale lenght ratio* ξ *and the anisotropy radius* s_{a}. Thus, in order to investigate the problem of the ROI, we have to discuss the condition $\Xi(\xi, s_{\mathrm{a}}) = 1.7$. At variance with $W_{*\mathrm{g}}$, the energy $K_{*\mathrm{r}}$ cannot be expressed in terms of elementary functions, and so a numerical exploration is required. Figure 5.2 shows the resulting lower bound $s_{\mathrm{a}}(\xi)$. It is evident that the critical value of s_{a} increases with ξ: indeed, a spatially extended DM halo increases the contribution to the kinetic energy of the velocity dispersion in the external regions, which are radially anisotropic in the OM case; hence, to guarantee stability in presence of an extended DM halo, the amount of radial orbits must be correspondingly reduced, and so larger values of s_{a} are nedeed. Conversely, when the DM halo is more concentrated than the stellar component, the velocity dispersion is increased preferentially in the central region, which is in practice isotropic in the OM case, thus a larger amount of radial orbits can be supported.

With an analogous treatment to that adopted to derive eq. (5.22), we shall now focus on $K_{*\mathrm{t}}$. Again, we exclude the effect of the central BH, to avoid the divergence of the energy $K_{*\mathrm{BH}}$. Now, since $K_{*\mathrm{r}} = K_* - K_{*\mathrm{t}}$, the stability indicator Ξ in eq. (5.22) can be rewritten in the following equivalent manner:

$$\Xi = \frac{|W_{*\mathrm{g}}|}{K_{*\mathrm{t}}} - 2. \tag{5.26}$$
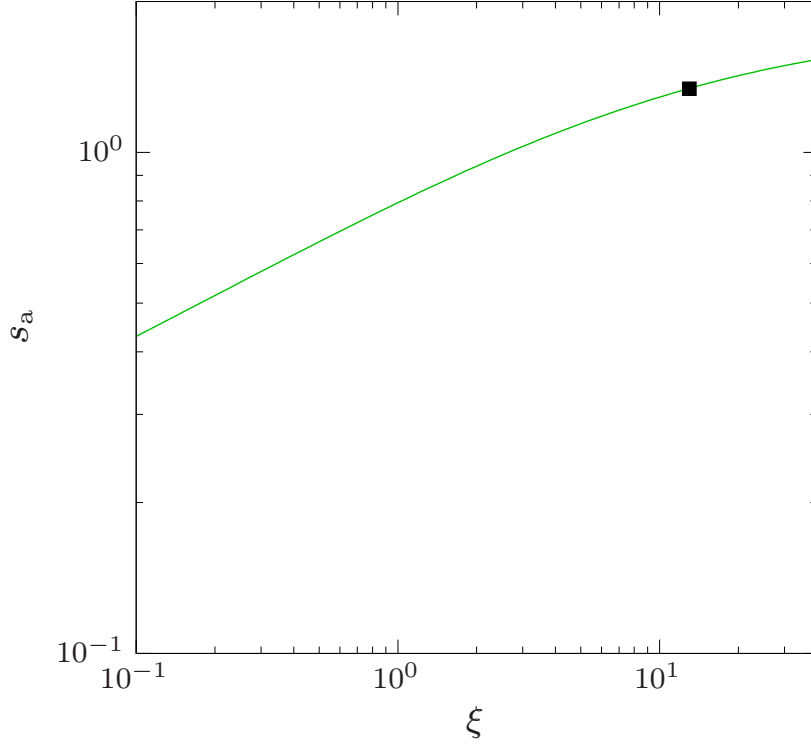
Figure 5.2. The fiducial stability condition $\Xi(\xi, s_\mathrm{a}) = 1.7$. The critical value of s_a increases for increasing ξ. The physical reason for this is that a spatially extended DM halo increases the contribution to the kinetic energy of the velocity dispersion at large radii, where $\beta(r) \sim 1$ for fixed s_a; then, in order to guarantee stability, larger values of s_a are nedeed. On the other hand, when the DM halo is more concentrated than the stellar component, the velocity dispersion is increased preferentially in the central region, which is in practice isotropic; thus, a larger amount of radial orbits can be supported. The black square correspond to the minimum halo case with $\xi = 13$, for which we find $s_\mathrm{a} \simeq 1.34$.

Moreover, by comparing the definition of $\beta(r)$ in eq. (B19) with eq. (3.6), we readily find

$$\rho_*(r)\sigma_\mathrm{t}^2(r) = \frac{2r_\mathrm{a}^2}{r^2 + r_\mathrm{a}^2}\, \rho_*(r)\sigma_\mathrm{r}^2(r). \tag{5.27}$$

Therefore, in analogy with eq. (5.24), by inserting eq. (5.27) in the integral defining $K_{*\mathrm{t}}$ (see eq. [5.3]), using eq. (4.3), and changing the order of integration, it is found that

$$K_{*\mathrm{t}} = 2\pi G \int_0^\infty \mathcal{L}_\mathrm{t}(r)\rho_*(r)M_\mathrm{g}(r)\left(1 + \frac{r_\mathrm{a}^2}{r^2}\right)dr, \qquad \mathcal{L}_\mathrm{t}(r) \equiv 2r_\mathrm{a}^2 \int_0^r \frac{x^2 dx}{(x^2 + r_\mathrm{a}^2)^2}. \tag{5.28}$$

Elementary calculations show that the function $\mathcal{L}_\mathrm{t}(r)$ is given by

$$\mathcal{L}_\mathrm{t}(r) = r_\mathrm{a}\tan^{-1}\frac{r}{r_\mathrm{a}} - r\,\frac{r_\mathrm{a}^2}{r^2 + r_\mathrm{a}^2}, \tag{5.29}$$

which is related to $\mathcal{L}_\mathrm{r}(r)$ by the following relation:

$$\mathcal{L}_\mathrm{r}(r) + \mathcal{L}_\mathrm{t}(r) = r\beta(r). \tag{5.30}$$

Again, by the same arguments used after eq. (5.25), the ratio $|W_{*\mathrm{g}}|/K_{*\mathrm{t}}$ in eq. (5.26) does depend only on ξ and s_a. Moreover, also in this case a numerical inspection of the condition $\Xi(\xi, s_\mathrm{a}) = 1.7$ is nedeed; however, since the comparison of eqs. (5.23) and (5.26) yield the virial theorem (5.1), the numerical result does not change with respect to the discussion below eq. (5.25).

CHAPTER 6

CONCLUSIONS

A new family of two-component spherical galaxy models is presented. These models, called J3 models, have a *stellar* density component $\rho_*(r)$ described by Jaffe's profile, and a *galaxy* density component $\rho_{\mathrm{g}}(r)$ such that the resulting dark matter (DM) halo density $\rho_{\mathrm{DM}}(r)$, defined as the difference between the galaxy and the stellar density distributions, can be made asymptotically identical to a Navarro-Frenk-White (NFW) profile, both at the center and in the external regions. A black hole (BH) is also added at the center of the system, and the orbital structure of the stellar component follows the Osipkov-Merritt (OM) anisotropy profile. A J3 galaxy model is fully determined once six parameters are fixed:

1. the total stellar mass M_*;

2. the stellar scale lenght r_*;

3. the galaxy-to-stellar density ratio $\mathcal{R}$;

4. the galaxy-to-stellar scale length ratio ξ;

5. the BH-to-stellar mass ratio μ;

6. the anisotropy radius r_{a}.

Remarkably, the J3 models allow for an almost complete analytical treatment with quite simple explicit expressions of several quantities of interest in observational and theoretical works. The main results of this thesis work can be summarized as follows.

- We derive analytical constraints on $\mathcal{R}$ and ξ to assure the positivity and monotonicity of the DM halo density distribution. For a given ξ, the model corresponding to the minimum value allowed for $\mathcal{R}$ is called *minimum halo model*. In particular, for $\xi \geq 1/2$ the positivity and monotonicity conditions coincide, requiring $\mathcal{R} \geq \xi$. For arbitrary choices of $\mathcal{R}$ and ξ, in the central region the DM density profile diverges as $\rho_{\mathrm{DM}}(r) \propto r^{-2}$, but in the minimum halo case with $\xi > 1/2$ the models are centrally "baryon dominated", with $\rho_{\mathrm{DM}}(r) \propto r^{-1}$, as for the NFW profile. Moreover, at large radii $\rho_{\mathrm{DM}}(r)$ is, by construction, always proportional to r^{-3}, again following the NFW profile. Two simple formulae determine the parameters of the NFW model *identical* to $\rho_{\mathrm{DM}}(r)$ close to the center and at large radii; remarkably, the NFW profile so obtained stays close to $\rho_{\mathrm{DM}}(r)$ *also* in the intermediate region.

- The minimum value of the OM anisotropy radius r_a, corresponding to a dynamically consistent stellar component, is first estimated using the necessary and weak sufficient conditions (NC and WSC, respectively) given in CP92. The consistency analysis is then performed for the isotropic DM halo and in presence of a central BH; we found that for $\xi \geq 1$, once positivity *only* of $\rho_\mathrm{DM}(r)$ is assured, i.e. $\mathcal{R} \geq \xi$, $\rho_\mathrm{DM}(r)$ automatically satisfies the NC and WSC for consistency, and so it can be supported by a nowhere negative phase-space distribution function (DF).

- The DF is recovered numerically, and its behavior is shown for a few representative cases, for different choices of $\mathcal{R}$, ξ, and r_a. Then we determined the (minimum) critical value of r_a, as a function of the model parameters, finding a curve that nicely parallels that given by the WSC. We showed that in absence of the central BH, the minimum value of r_a depends only on ξ, and it is independent of $\mathcal{R}$. For reference, for J3 models with $\xi = 13$ and no BH, the non-negativity of the DF requires $r_\mathrm{a} \gtrsim 0.0143\, r_*$. In particular, r_a decreases for increasing ξ, i.e., *a* DM *halo more extended than the stellar distribution increases the ability of the stellar component to sustain radial anisotropy. Conversely, more concentrated* DM *halos require a more isotropic orbital distribution.*

- The Jeans equations for the stellar component are solved analytically for generic values of the model parameters. Then, we determine the asymptotic behaviours of the velocity dispersion $\sigma_\mathrm{r}(r)$ and projected velocity dispersion $\sigma_\mathrm{p}(R)$, at small and large radii. In absence of the central BH, $\sigma_\mathrm{p}^2(0) = \sigma_\mathrm{r}^2(0) = \Psi_\mathrm{n}\mathcal{R}/(2\xi)$ for all values of $r_\mathrm{a} > 0$ (isotropic case included). In presence of the BH, in the central regions $\sigma_\mathrm{r}^2(r) \propto r^{-1}$, and $\sigma_\mathrm{p}^2(R) \propto R^{-1}$, *independently of the anisotropy radius.*

- Finally, the analytical expressions for the quantities entering the Virial theorem, such as the stellar kinetic energy, the interaction energy, and the potential energies, are derived as functions of the model parameters. We also evaluated numerically the minimum value of r_a corresponding to the fiducial value of $\simeq 1.7$ for the Fridman-Polyachenko instability indicator, so that more anisotropic models are prone to the onset of Radial Orbit Instability. It is found that *the minimum r_a for stability increases for increasing ξ; further, in absence of the central* BH, *its value depends only on ξ.*

We conclude by noting that J3 models can be a useful starting point for more advanced modeling of the dynamics of elliptical galaxies, and can be easily implemented in numerical simulations. In addition, it can be shown that J3 models allow for a fully analytical treatment of Bondi accretion along the lines discussed elsewhere (Ciotti & Pellegrini 2017, 2018).

APPENDIX A

PROJECTED DENSITIES

IN Chapter 2 we have seen that the projected mass density profiles $\Sigma_*(R)$ and $\Sigma_{\mathrm{g}}(R)$, and the projected mass profiles $M_{\mathrm{p}*}(R)$ and $M_{\mathrm{pg}}(R)$, can be expressed in terms of some dimensionless functions. Those related to the stellar component are well-known in literature (see, e.g., Binney & Tremaine 2008, see also Jaffe 1983), thus we report them without any further dicussion about their derivation; the projected stellar density distribution $\Sigma_*(R)$, remembering the definition of Σ_{n} given after eq. (2.5), reads

$$\Sigma_*(R) = \Sigma_{\mathrm{n}} \times g_*(\eta), \qquad g_*(\eta) = \begin{cases} \dfrac{\pi}{\eta} + 2\,\dfrac{\sqrt{1-\eta^2} - (2-\eta^2)\operatorname{sech}^{-1}\eta}{(1-\eta^2)^{3/2}}, & 0 < \eta < 1, \\[2ex] \pi - \dfrac{8}{3}, & \eta = 1, \\[2ex] \dfrac{\pi}{\eta} - 2\,\dfrac{\sqrt{\eta^2-1} + (\eta^2-2)\sec^{-1}\eta}{(\eta^2-1)^{3/2}}, & \eta > 1, \end{cases} \tag{A1}$$

while the projected stella mass $M_{\mathrm{p}*}(R)$ is given by

$$M_{\mathrm{p}*}(R) = M_* \times h_*(\eta), \qquad h_*(\eta) = \eta \times \begin{cases} \dfrac{\pi}{2} - \eta\,\dfrac{\operatorname{sech}^{-1}\eta}{\sqrt{1-\eta^2}}, & 0 < \eta < 1, \\[2ex] \dfrac{\pi}{2} - 1, & \eta = 1, \\[2ex] \dfrac{\pi}{2} - \eta\,\dfrac{\sec^{-1}\eta}{\sqrt{\eta^2-1}}, & \eta > 1. \end{cases} \tag{A2}$$

Let us now consider the galaxy contribution. In analogy with eq. (2.5), the galaxy projected density at radius R in the projection plane is given by

$$\Sigma_{\mathrm{g}}(R) = 2 \int_R^\infty \frac{\rho_{\mathrm{g}}(r)r\,dr}{\sqrt{r^2 - R^2}}, \tag{A3}$$

where $\rho_{\mathrm{g}}(r)$ is defined in eq. (2.11). First, making use of the substitution $x \equiv r/R$, we find

$$\Sigma_{\mathrm{g}}(R) = \frac{M_* \mathcal{R}}{2\pi\eta r_*^2} \int_1^\infty \frac{dx}{x(\xi + \eta x)\sqrt{x^2 - 1}}, \tag{A4}$$

or, after some minor reductions,

$$\Sigma_{\mathrm{g}}(R) = \frac{\Sigma_{\mathrm{n}} \mathcal{R}}{\xi} \left[\frac{\pi}{\eta} - 2\int_1^\infty \frac{dx}{(\xi + \eta x)\sqrt{x^2 - 1}} \right]. \tag{A5}$$

Now, with the second substitution $t \equiv 1/(\xi + \eta x)$, the projected density profile can be rewritten as

$$\Sigma_{\mathrm{g}}(R) = \frac{\Sigma_{\mathrm{n}} \mathcal{R}}{\xi} \left[\frac{\pi}{\eta} - 2\int_0^b \frac{dt}{\sqrt{(\xi^2 - \eta^2)t^2 - 2\xi t + 1}} \right], \tag{A6}$$

where $b \equiv 1/(\xi + \eta)$. The integral on the the right-hand side of the equation above presents no formal difficulty; the only care is to take into account the sign of $\xi^2 - \eta^2$. Then, in analogy with eq. (A1), computing this integral one finally has

$$\Sigma_{\mathrm{g}}(R) = \Sigma_{\mathrm{n}} \times \frac{\mathcal{R}}{\xi^2} g_{\mathrm{g}}(\zeta), \qquad g_{\mathrm{g}}(\zeta) = \begin{cases} \dfrac{\pi}{\zeta} - \dfrac{2\operatorname{sech}^{-1}\zeta}{\sqrt{1 - \zeta^2}}, & 0 < \zeta < 1, \\[2ex] \pi - 2, & \zeta = 1, \\[2ex] \dfrac{\pi}{\zeta} - \dfrac{2\sec^{-1}\zeta}{\sqrt{\zeta^2 - 1}}, & \zeta > 1. \end{cases} \tag{A7}$$

As specified in Section 2.3, the projected mass $M_{\mathrm{pg}}(R)$ cannot be obtained applying the eq. (2.9) to the profile $\rho_{\mathrm{g}}(r)$, inasmuch as the cumulative mass associated with the galaxy density profile is divergent; for this purpose we must necessarily integrate the projected density $\Sigma_{\mathrm{g}}(R)$ previously derived. Consider the quantity

$$\mathcal{J}(x, y) \equiv 2\pi \int_x^y \Sigma_{\mathrm{g}}(R')R'dR'. \tag{A8}$$

Now, since $\Sigma_{\mathrm{g}}(R)$ is given by a different analytical profile depending on whether ζ is less than, equal to, or greater than 1 (see eq. [A7]), the projected mass $M_{\mathrm{pg}}(R)$ can be calculate as

$$M_{\mathrm{pg}}(R) = \begin{cases} \mathcal{J}(0, R), & 0 < R < r_{\mathrm{g}}, \\[1.5ex] \mathcal{J}(0, r_{\mathrm{g}}), & R = r_{\mathrm{g}}, \\[1.5ex] \mathcal{J}(0, r_{\mathrm{g}}) + \mathcal{J}(r_{\mathrm{g}}, R), & R > r_{\mathrm{g}}. \end{cases} \tag{A9}$$

For $0 < R < r_{\mathrm{g}}$, the substitution $y \equiv R'/r_{\mathrm{g}}$ in $\mathcal{J}(0, R)$ yield

$$M_{\mathrm{pg}}(R) = M_* \mathcal{R} \times \left(\frac{\pi}{2}\zeta - \int_0^\zeta \frac{y\operatorname{sech}^{-1}y}{\sqrt{1 - y^2}}\, dy \right), \tag{A10}$$

whence, by an elementary integration,

$$M_{\mathrm{pg}}(R) = M_* \mathcal{R} \times \left(\frac{\pi}{2} \zeta - \ln \frac{2}{\zeta} + \sqrt{1 - \zeta^2} \operatorname{sech}^{-1} \zeta \right), \qquad (0 < R < r_{\mathrm{g}}). \qquad (\mathrm{A}11)$$

For $R = r_{\mathrm{g}}$, $M_{\mathrm{pg}}(R)$ is a constant value that can be obtained considering the limit of the foregoing expression for $\zeta \to 1$. This leads to the following result:

$$M_{\mathrm{pg}}(r_{\mathrm{g}}) = M_* \mathcal{R} \times \left(\frac{\pi}{2} - \ln 2 \right). \qquad (\mathrm{A}12)$$

When $R > r_{\mathrm{g}}$, with the usual change of variable $y \equiv R'/r_{\mathrm{g}}$, eq. (A9) becomes

$$M_{\mathrm{pg}}(R) = M_{\mathrm{pg}}(r_{\mathrm{g}}) + M_* \mathcal{R} \times \left[\frac{\pi}{2} (\zeta - 1) - \int_1^\zeta \frac{y \sec^{-1} y}{\sqrt{y^2 - 1}} \, dy \right], \qquad (\mathrm{A}13)$$

whence, by performing the integration,

$$M_{\mathrm{pg}}(R) = M_* \mathcal{R} \times \left(\frac{\pi}{2} \zeta - \ln \frac{2}{\zeta} - \sqrt{\zeta^2 - 1} \sec^{-1} \zeta \right), \qquad (R > r_{\mathrm{g}}). \qquad (\mathrm{A}14)$$

Summurizing, in analogy with eq. (A2), and introducing the dimensionless function $h_{\mathrm{g}}(\zeta)$, the project galaxy mass distribution can be written as

$$M_{\mathrm{pg}}(R) = M_* \mathcal{R} \times h_{\mathrm{g}}(\zeta), \qquad h_{\mathrm{g}}(\zeta) = \zeta \times \begin{cases} \dfrac{\pi}{2} - \dfrac{\ln(2/\zeta)}{\zeta} + \dfrac{\sqrt{1 - \zeta^2} \operatorname{sech}^{-1} \zeta}{\zeta}, & 0 < \zeta < 1, \\[2ex] \dfrac{\pi}{2} - \ln 2, & \zeta = 1, \\[2ex] \dfrac{\pi}{2} - \dfrac{\ln(2/\zeta)}{\zeta} - \dfrac{\sqrt{\zeta^2 - 1} \sec^{-1} \zeta}{\zeta}, & \zeta > 1. \end{cases}$$
$$(\mathrm{A}15)$$

APPENDIX B

THE COLLISIONLESS BOLTZMANN EQUATION

IN a general way it appears that the most convenient method of describing the state of motions in a stellar system is by specifying the mass $f_*(\mathbf{x}, \mathbf{v}, t)d^3\mathbf{x}d^3\mathbf{v}$ of stars having, at a certain instant of time t, position in the element of volume $d^3\mathbf{x}$ centered on $\mathbf{x}$, and velocities in the range $d^3\mathbf{v}$ centered on $\mathbf{v}$. The quantity $f_*(\mathbf{x}, \mathbf{v}, t)$ is called *distribution function* (DF) or *phase-space density*[1]; from its definition, it follows that

$$\int_{\mathbb{R}^3} f_*(\mathbf{x}, \mathbf{v}, t)d^3\mathbf{v} = \rho_*(\mathbf{x}, t). \tag{B1}$$

Let the coordinates in phase-space be $(\mathbf{x}, \mathbf{v}) \equiv \mathbf{w} \equiv (w_1, \ldots, w_6)$. Then it can be shown that the evolutionary equation for the phase-space DF is described by

$$\frac{Df_*(\mathbf{w}, t)}{Dt} = 0, \qquad \frac{D}{Dt} \equiv \frac{\partial}{\partial t} + \sum_{j=1}^{6} \dot{w}_j \frac{\partial}{\partial w_j}, \tag{B2}$$

(see, e.g., Chandrasekhar 1942, Ogorodnikov 1965, Saslaw 1987; see also Binney & Tremaine 2008), a linear homogeneous partial differential equation of the first order known as *Collisionless Boltzmann Equation* (hereafter, CBE). By extending the concept of the *lagrangian derivative* to six dimensions, it follows that the quantity $Df_*(\mathbf{w}, t)/Dt$ does represent the rate of change of the density of phase points as seen by an observer who moves through phase-space with a star at velocity $\dot{\mathbf{w}}$. This lead us to a simple physical meaning of the eq. (B2): *the flow of stellar phase points through phase space is incompressible, i.e., $f_*(\mathbf{w}, t)$ is constant along the trajectories of stellar phase points*. For this reason, eq. (B2) is often reffered to the "equation of continuity", though this must be carefully distinguished from the ordinary macroscopic equation of continuity of hydrodynamics. In the following discussion, we shall take the CBE as the basic equation.

Since eq. (B2) is true in *any* system of coordinates, we shall now consider spherical coordinates (r, θ, φ); in this case $f_* = f_*(r, \theta, \varphi, v_r, v_\theta, v_\varphi, t)$, then form eq. (B2) we readily have

$$\frac{\partial f_*}{\partial t} + \dot{r}\frac{\partial f_*}{\partial r} + \dot{\theta}\frac{\partial f_*}{\partial \theta} + \dot{\varphi}\frac{\partial f_*}{\partial \varphi} + \dot{v}_r\frac{\partial f_*}{\partial v_r} + \dot{v}_\theta\frac{\partial f_*}{\partial v_\theta} + \dot{v}_\varphi\frac{\partial f_*}{\partial v_\varphi} = 0, \tag{B3}$$

---

[1]We have inserted an asterisk in superscript to stress the fact that, in case of a multi-component stellar system, $f_*(\mathbf{x}, \mathbf{v}, t)$ represents the distribution function of the stellar component *only*.

where v_r, v_θ and v_φ are the components of the velocity **v**. Notice that the derivatives of the phase-space coordinates can be expressed in terms of the coordinates themselves. Indeed, to eliminate $\dot{r}$, $\dot{\theta}$, and $\dot{\varphi}$ we can use the following set of relations:

$$v_r = \dot{r}, \qquad v_\theta = r\dot{\theta}, \qquad v_\varphi = r\dot{\varphi}\sin\theta. \tag{B4}$$

To eliminate $\dot{v}_r$, $\dot{v}_\theta$, and $\dot{v}_\varphi$, instead, we use the Lagrangian equations of motion for a free particle in spherical coordinate, i.e.,

$$\dot{v}_r - \frac{v_\theta^2 + v_\varphi^2}{r} = \frac{\partial \Psi_T}{\partial r}, \quad \dot{v}_\theta - \frac{v_\varphi^2 \cot\theta - v_r v_\theta}{r} = \frac{1}{r}\frac{\partial \Psi_T}{\partial \theta}, \quad \dot{v}_\varphi + \frac{v_\varphi(v_r + v_\theta \cot\theta)}{r} = \frac{1}{r\sin\theta}\frac{\partial \Psi_T}{\partial \varphi}, \tag{B5}$$

where $\Psi_T = \Psi_T(r, \theta, \varphi, t)$ is the potential function under whose influence the stars move. Hence, by substituiting eqs. (B4) and (B5) in eq. (B3) we obtain the CBE in spherical coordinates:

$$\frac{\partial f_*}{\partial t} + v_r \frac{\partial f_*}{\partial r} + \frac{v_\theta}{r}\frac{\partial f_*}{\partial \theta} + \frac{v_\varphi}{r\sin\theta}\frac{\partial f_*}{\partial \varphi} + \left(\frac{v_\theta^2 + v_\varphi^2}{r} + \frac{\partial \Psi_T}{\partial r} \right)\frac{\partial f_*}{\partial v_r} + $$

$$\tag{B6}$$

$$+ \frac{1}{r}\left(v_\varphi^2 \cot\theta - v_r v_\theta + \frac{\partial \Psi_T}{\partial \theta} \right)\frac{\partial f_*}{\partial v_\theta} - \frac{1}{r}\left[v_\varphi(v_r + v_\theta \cot\theta) - \frac{1}{\sin\theta}\frac{\partial \Psi_T}{\partial \varphi} \right]\frac{\partial f_*}{\partial v_\varphi} = 0.$$

This equation, considered as an equation of f_*, is a partial differential equation[2] of the standard Lagrangian type in the seven variables r, θ, φ, v_r, v_θ, v_φ, and t. Hence, the general solution can be written in terms of six independent integrals of the *Lagrangian subsidiary equations*

$$dt = \frac{dr}{v_r} = \frac{d\theta}{\frac{v_\theta}{r}} = \frac{d\varphi}{\frac{v_\varphi}{r\sin\theta}} = \frac{dv_r}{\frac{v_\theta^2 + v_\varphi^2}{r} + \frac{\partial \Psi_T}{\partial r}}$$

$$\tag{B7}$$

$$= \frac{dv_\theta}{\frac{v_\varphi^2 \cot\theta - v_r v_\theta}{r} + \frac{1}{r}\frac{\partial \Psi_T}{\partial \theta}} = \frac{dv_\varphi}{-\frac{v_\varphi(v_r + v_\theta \cot\theta)}{r} + \frac{1}{r\sin\theta}\frac{\partial \Psi_T}{\partial \varphi}},$$

which are precisely the equations of motion (B5). Therefore, if

$$I_i = \text{constant}, \qquad (i = 1, \ldots, 6), \tag{B8}$$

represent six integrals corresponding to the most general solution of the equations of motion (B7), the general solution of the eq. (B6) (see, e.g., Goursat 1917) can be written as

$$f_* = f_*(I_1, \ldots, I_6). \tag{B9}$$

Unfortunately, eq. (B9) represents only a formal solution, inasmuch as the explicit form of the general solution can be given only when *all* the six integrals $I_1, \ldots, I_6$ are known. But the

---

[2]Note that eq. (B6) can be regarded either as a linear homogeneous partial differential equation for f_* or as a linear nonhomogeneous partial differential equation for Ψ_T.

equations of motion determining this integrals involve the potential $\Psi_{\mathrm{T}}(r, \theta, \varphi, t)$, which is largely unspecified. However, with appropriate restrictions on the potential function it is possible to write down the explicit form of one or more integrals of the equations of motions, although it is clear that this approach unavoidably lead to loosing some degree of generality. In any case, under no circumstance we can specify all the six integrals without complete loss of generality.

B.1 The Jeans equations for spherical systems

Since the general solution of the CBE depends on the knowledge of the orbital properties in the arbitrary potential function $\Psi_{\mathrm{T}}(r, \theta, \varphi, t)$, various technique in order to extract information from the CBE have been developed. Such technique can be divide in the construction of *particular solutions for stationary systems* and in the so-called *method of moments*. In this Section we shall present the second method, which lead us to obtain some general relations of great practical interest. These are often referred to "equation of stellar hydrodinamics", obtained by integrating the CBE over all the velocities after have multiplied it by appropriate factors.

Multiply eq. (B6) by $dv_r dv_\theta dv_\varphi$, and integrating over these variables. By using the fact that the DF goes to zero for sufficiently large values of the velocities, we obtain

$$\frac{\partial \rho_*}{\partial t} + \frac{1}{r^2}\frac{\partial r^2 \rho_* \overline{v_r}}{\partial r} + \frac{1}{r \sin\theta}\frac{\partial \rho_* \overline{v_\theta}\sin\theta}{\partial \theta} + \frac{1}{r \sin\theta}\frac{\partial \rho_* \overline{v_\varphi}}{\partial \varphi} = 0, \qquad (\text{B10})$$

where $\overline{v_r}$, $\overline{v_\theta}$, and $\overline{v_\varphi}$ denote the average values of v_r, v_θ, and v_φ, respectively[3]. Equation eq. (B10) clearly expresses the conservation of the stellar mass; it represents, therefore, the "macroscopic equation of continuity". Next, by multiplying eq. (B6) by $v_r dv_r dv_\theta dv_\varphi$, and integrating over all the velocities, we have

$$\frac{\partial \rho_* \overline{v_r}}{\partial t} + \frac{\partial \rho_* \overline{v_r^2}}{\partial r} + \frac{1}{r}\frac{\partial \rho_* \overline{v_r v_\theta}}{\partial \theta} + \frac{1}{r \sin\theta}\frac{\partial \rho_* \overline{v_r v_\varphi}}{\partial \varphi} + \frac{2\overline{v_r^2} - (\overline{v_\theta^2} + \overline{v_\varphi^2}) + \overline{v_r v_\theta}\cot\theta}{r}\rho_* = \frac{\partial \Psi_{\mathrm{T}}}{\partial r}\rho_*. \quad (\text{B11})$$

Similarly, we now multiply eq. (B6) successively by $v_\theta dv_r dv_\theta dv_\varphi$ and $v_\varphi dv_r dv_\theta dv_\varphi$, and integrate with respect to all values of v_r, v_θ and v_φ. We find, respectively,

$$\frac{\partial \rho_* \overline{v_\theta}}{\partial t} + \frac{\partial \rho_* \overline{v_\theta v_r}}{\partial r} + \frac{1}{r}\frac{\partial \rho_* \overline{v_\theta^2}}{\partial \theta} + \frac{1}{r \sin\theta}\frac{\partial \rho_* \overline{v_\theta v_\varphi}}{\partial \varphi} + \frac{3\overline{v_r v_\theta} + (\overline{v_\theta^2} - \overline{v_\varphi^2})\cot\theta}{r}\rho_* = \frac{1}{r}\frac{\partial \Psi_{\mathrm{T}}}{\partial \theta}\rho_* \quad (\text{B12})$$

and

---

[3]Let $Q = Q(\mathbf{x}, \mathbf{v}, t)$ be a *microscopic function* (i.e., defined on the phase-space). Then, the associated *macroscopic function* $\overline{Q} = \overline{Q}(\mathbf{x}, t)$ is defined as

$$\overline{Q}(\mathbf{x}, t) \equiv \frac{1}{\rho_*(\mathbf{x}, t)}\int_{\mathbb{R}^3} f_*(\mathbf{x}, \mathbf{v}, t)Q(\mathbf{x}, \mathbf{v}, t)d^3\mathbf{v},$$

i.e., as the mean value of $Q(\mathbf{x}, \mathbf{v}, t)$ over all the velocities of particles that at time t determine the density $\rho_*(\mathbf{x}, t)$. For this reason, we shall refer to the function $\overline{Q}(\mathbf{x}, t)$ as the *average value* of $Q(\mathbf{x}, \mathbf{v}, t)$. Obviously, from its definition it follows that this "bar-operator" is linear; indeed, if $Q_1 = Q_1(\mathbf{x}, \mathbf{v}, t)$, $Q_2 = Q_2(\mathbf{x}, \mathbf{v}, t)$, and $\alpha = \alpha(\mathbf{x}, t)$, we have

$$\overline{Q_1 + Q_2} = \overline{Q}_1 + \overline{Q}_2, \qquad \overline{\alpha Q} = \alpha \overline{Q}.$$

$$\frac{\partial \rho_* \overline{v_\varphi}}{\partial t} + \frac{\partial \rho_* \overline{v_\varphi v_r}}{\partial r} + \frac{1}{r}\frac{\partial \rho_* \overline{v_\varphi v_\theta}}{\partial \theta} + \frac{1}{r\sin\theta}\frac{\partial \rho_* \overline{v_\varphi^2}}{\partial \varphi} + \frac{3\overline{v_r v_\varphi} + 2\overline{v_\theta v_\varphi}\cot\theta}{r}\rho_* = \frac{1}{r\sin\theta}\frac{\partial \Psi_{\mathrm T}}{\partial \varphi}\rho_*. \quad \text{(B13)}$$

Equations (B11), (B12), and (B13), which represent the "macroscopic equations for mass motions", are the *Jeans equations.*

In a spherically symmetrical system the DF and the Newtonian potential *must* be independent of θ and φ, i.e.,

$$\frac{\partial f_*}{\partial \theta} = \frac{\partial f_*}{\partial \varphi} = 0, \qquad\qquad \frac{\partial \Psi_{\mathrm T}}{\partial \theta} = \frac{\partial \Psi_{\mathrm T}}{\partial \varphi} = 0. \qquad\qquad \text{(B14)}$$

Consequently, also the stellar mass density and any average value depend on r and t only. Moreover, by assuming that the system is in a steady state, also the dependence on time vanishes. Under these conditions, assuming further that $\overline{v_r} = \overline{v_\theta} = \overline{v_\varphi} = \overline{v_r v_\theta} = \overline{v_r v_\varphi} = \overline{v_\theta v_\varphi} = 0$, we obtain that eq. (B13) is an identity, while eq. (B11) and eq. (B12) become, respectively,

$$\frac{d\rho_*(r)\overline{v_r^2}(r)}{dr} + \frac{2\overline{v_r^2}(r) - \overline{v_\theta^2}(r) - \overline{v_\varphi^2}(r)}{r}\rho_*(r) = \frac{d\Psi_{\mathrm T}(r)}{dr}\rho_*(r), \qquad \overline{v_\theta^2}(r) = \overline{v_\varphi^2}(r). \qquad \text{(B15)}$$

Now, defining the general ij-component of the *velocity dispersion tensor* (see Binney & Tremaine 2008) as

$$\sigma_{ij}^2(\mathbf{x}, t) \equiv \overline{(v_i - \overline{v_i})(v_j - \overline{v_j})} = \overline{v_i v_j} - \overline{v_i}\,\overline{v_j}, \qquad (i, j = 1, 2, 3), \qquad \text{(B16)}$$

by virtue of the particular conditions previously assumed, eq. (B15) becomes[4]

$$\frac{d\rho_*(r)\sigma_{\mathrm r}^2(r)}{dr} + \frac{2\sigma_{\mathrm r}^2(r) - \sigma_\theta^2(r) - \sigma_\varphi^2(r)}{r}\rho_*(r) = \frac{d\Psi_{\mathrm T}(r)}{dr}\rho_*(r), \qquad \sigma_\theta^2(r) = \sigma_\varphi^2(r). \qquad \text{(B17)}$$

Finally, introducing the function

$$\beta(r) \equiv 1 - \frac{\sigma_\theta^2(r)}{\sigma_{\mathrm r}^2(r)}, \qquad\qquad\qquad \text{(B18)}$$

which describes the degree of anisotropy of the velocity distribution at each point, the Jeans equations (B17) can therefore be rewritten as

$$\frac{d\rho_*(r)\sigma_{\mathrm r}^2(r)}{dr} + \frac{2\beta(r)}{r}\rho_*(r)\sigma_{\mathrm r}^2(r) = \frac{d\Psi_{\mathrm T}(r)}{dr}\rho_*(r), \qquad \sigma_{\mathrm t}^2(r) = 2\sigma_{\mathrm r}^2(r)[1 - \beta(r)], \qquad \text{(B19)}$$

where $\sigma_{\mathrm t}^2(r) \equiv \sigma_\theta^2(r) + \sigma_\varphi^2(r)$ describes the velocity dispersion in the tangential direction.

---

[4]Following a standard convention, we define $\sigma_{rr}^2 \equiv \sigma_{\mathrm r}^2$, $\sigma_{\theta\theta}^2 \equiv \sigma_\theta^2$, and $\sigma_{\varphi\varphi}^2 \equiv \sigma_\varphi^2$.

APPENDIX C

The Function $\mathcal{H}$

In Chapter 4 we have seen that, in solving the Jeans equations, a particular function of ξ and s has to be introduced. We define this function as

$$\mathcal{H}(\xi, s) \equiv \int_s^\infty \ln\left(1 + \frac{1}{y}\right) \frac{dy}{\xi + y}, \tag{C1}$$

where $\xi > 0$, and $s \geq 0$. Unfortunately, the integral defining $\mathcal{H}(\xi, s)$ cannot be evaluated analytically via elementary functions. Indeed, with the substitution $1 + y \equiv 1/t$, eq. (C1) can be rewritten, after some minor reductions, as

$$\mathcal{H}(\xi, s) = \mathrm{Li}_2\left(\frac{1}{1+s}\right) + \mathcal{G}(\xi, s), \qquad \mathcal{G}(\xi, s) \equiv (\xi - 1) \int_0^{1/(1+s)} \frac{\ln(1-t)}{1 + (\xi - 1)t}\, dt, \tag{C2}$$

where

$$\mathrm{Li}_2(x) \equiv -\int_0^x \frac{\ln(1-t)}{t}\, dt \tag{C3}$$

is the *dilogarithm function* (see Lewin 1981, see also Gradshteyn & Ryzhik 2007). In order to find an analytical expression for $\mathcal{H}(\xi, s)$, let us focus on $\mathcal{G}(\xi, s)$.

For $\xi = 1$ the function $\mathcal{G}(\xi, s)$ vanishes, and so we have simply

$$\mathcal{H}(1, s) = \mathrm{Li}_2\left(\frac{1}{1+s}\right), \tag{C4}$$

which gives, in the special case $s = 0$, $\mathcal{H}(1, 0) = \mathrm{Li}_2(1) = \pi^2/6$.

For $\xi \neq 1$, instead, we have to distiguish the case $\xi < 1$ from the case $\xi > 1$. In the first case, the substitution $1 + (\xi - 1)t \equiv \xi/z$ yield

$$\mathcal{G}(\xi, s) = \frac{1}{2} \ln \frac{1+s}{\xi + s} \ln \frac{(1-\xi)^2(1+s)}{\xi + s} - \int_\xi^d \frac{\ln(1-z)}{z}\, dz, \qquad d \equiv \frac{\xi(1+s)}{\xi + s}, \tag{C5}$$

whence, by applying eq. (C3), we find

$$\mathcal{G}(\xi, s) = \frac{1}{2} \ln \frac{1+s}{\xi + s} \ln \frac{(1-\xi)^2(1+s)}{\xi + s} + \mathrm{Li}_2\left[\frac{\xi(1+s)}{\xi + s}\right] - \mathrm{Li}_2(\xi). \tag{C6}$$

In the second case, i.e. for $\xi > 1$, it is convenient to use the change of variable $1 + (\xi - 1)t \equiv \xi u$. By this substitution we obtain

$$\mathcal{G}(\xi, s) = \ln\frac{\xi}{\xi - 1}\ln\frac{\xi + s}{1 + s} + \int_{1/\xi}^{b}\frac{\ln(1 - u)}{u}\,du, \qquad b \equiv \frac{\xi + s}{\xi(1 + s)}, \tag{C7}$$

whence, from eq. (C3),

$$\mathcal{G}(\xi, s) = \ln\frac{\xi}{\xi - 1}\ln\frac{\xi + s}{1 + s} - \text{Li}_2\left[\frac{\xi + s}{\xi(1 + s)}\right] + \text{Li}_2\left(\frac{1}{\xi}\right). \tag{C8}$$

Summarizing, the explicit expression for the function $\mathcal{H}(\xi, s)$ reads

$$\mathcal{H}(\xi, s) = \text{Li}_2\left(\frac{1}{1 + s}\right) + \begin{cases} \dfrac{1}{2}\ln\dfrac{1 + s}{\xi + s}\ln\dfrac{(1 - \xi)^2(1 + s)}{\xi + s} + \text{Li}_2\left[\dfrac{\xi(1 + s)}{\xi + s}\right] - \text{Li}_2(\xi), & 0 < \xi < 1, \\[4mm] 0, & \xi = 1, \\[4mm] \ln\dfrac{\xi}{\xi - 1}\ln\dfrac{\xi + s}{1 + s} - \text{Li}_2\left[\dfrac{\xi + s}{\xi(1 + s)}\right] + \text{Li}_2\left(\dfrac{1}{\xi}\right), & \xi > 1. \end{cases} \tag{C9}$$

At the center, remember the identity $\text{Li}_2(1) = \pi^2/6$, we have

$$\mathcal{H}(\xi, 0) = \begin{cases} \dfrac{\pi^2}{3} + \dfrac{\ln^2\xi}{2} - \ln\xi\ln(1 - \xi) - \text{Li}_2(\xi), & 0 < \xi < 1, \\[4mm] \dfrac{\pi^2}{6}, & \xi = 1, \\[4mm] \ln^2\xi - \ln\xi\ln(\xi - 1) + \text{Li}_2\left(\dfrac{1}{\xi}\right), & \xi > 1. \end{cases} \tag{C10}$$

We shall now prove that it is possible to obtain a series representation of this particular function. For, we shall focus directly on eq. (C1). First, we rewrite $\mathcal{H}(\xi, s)$ as

$$\mathcal{H}(\xi, s) = \mathcal{H}(\xi, 0) - \int_0^s \ln\left(1 + \frac{1}{y}\right)\frac{dy}{\xi + y}, \tag{C11}$$

or, alternatively,

$$\mathcal{H}(\xi, s) = \mathcal{H}(\xi, 0) - \frac{\mathcal{D}_1(\xi, s) - \mathcal{D}_2(\xi, s)}{\xi}, \tag{C12}$$

where the following definitions apply:

$$\mathcal{D}_1(\xi, s) \equiv \int_0^s \frac{\ln(1 + y)}{1 + y/\xi}\,dy, \qquad \mathcal{D}_2(\xi, s) \equiv \int_0^s \frac{\ln y}{1 + y/\xi}\,dy. \tag{C13}$$

Now, since for $|x| \le 1$ we have, in general,

$$\ln(1+x) = \sum_{n=0}^{\infty} (-1)^n \frac{x^{n+1}}{n+1}, \qquad \frac{1}{1+x} = \sum_{n=0}^{\infty} (-1)^n x^n, \qquad \text{(C14)}$$

the functions $\mathcal{D}_1(\xi, s)$ and $\mathcal{D}_2(\xi, s)$ becomes[1], for $s < \xi$,

$$\mathcal{D}_1(\xi, s) \equiv -\int_0^s \sum_{n=1}^{\infty} \sum_{k=1}^{n} (-1)^n \frac{y^n}{k\,\xi^{n-k}}\, dy, \qquad \mathcal{D}_2(\xi, s) \equiv -\int_0^s \sum_{n=1}^{\infty} (-1)^n \frac{y^{n-1}}{\xi^{n-1}}\, \ln y\, dy. \tag{C15}$$

Then, performing the integration, we have

$$\mathcal{D}_1(\xi, s) = \sum_{n=1}^{\infty} a_n(\xi) s^{n+1}, \qquad a_n(\xi) \equiv -\frac{(-1)^n}{n+1} \sum_{k=1}^{n} \frac{1}{k\,\xi^{n-k}},$$

$$\mathcal{D}_2(\xi, s) = \sum_{n=1}^{\infty} (1 - n \ln s) b_n(\xi) s^n, \qquad b_n(\xi) \equiv \frac{(-1)^n}{n^2 \xi^{n-1}}. \tag{C16}$$

Finally, by inserting eq. (C16) in eq. (C12), and defining $a_0(\xi) \equiv 0$, we obtain the following series representation:

$$\mathcal{H}(\xi, s) = \mathcal{H}(\xi, 0) + \frac{1}{\xi} \sum_{n=1}^{\infty} [(1 - n \ln s) b_n(\xi) - a_{n-1}(\xi)] s^n, \qquad (s < \xi). \tag{C17}$$

Now, in order to find the series representation of $\mathcal{H}(\xi, s)$ for $s > \xi$, we use the change of variable $t \equiv 1/y$ in eq. (C1). This substitution readily yield

$$\mathcal{H}(\xi, s) = \int_0^{1/s} \frac{\ln(1+t)}{t(1+\xi t)}\, dt. \tag{C18}$$

Following the discussion after eq. (C12), by using eq. (C14) we find that eq. (C18) can be rewritten, for $s > \xi$, as

$$\mathcal{H}(\xi, s) = \int_0^{1/s} \sum_{n=1}^{\infty} \sum_{k=1}^{n} (-1)^{n-1} \frac{\xi^{n-k}}{k}\, t^{n-1} dt, \tag{C19}$$

---

[1]Let

$$S_a \equiv a_0 + a_1 + a_2 + \cdots + a_n + \cdots \qquad \text{and} \qquad S_b \equiv b_0 + b_1 + b_2 + \cdots + b_n + \cdots$$

be any two series whatever. By multiplying terms of the first series by terms of the second in all possible ways, we obtain a new series:

$$S \equiv S_a \times S_b = a_0 b_0 + (a_0 b_1 + a_1 b_0) + (a_0 b_2 + a_1 b_1 + a_2 b_0) + \cdots + (a_0 b_n + a_1 b_{n-1} + \cdots + a_n b_0) + \cdots,$$

or, alternatively,

$$\left(\sum_{n=0}^{\infty} a_n \right) \times \left(\sum_{n=0}^{\infty} b_n \right) = \sum_{n=0}^{\infty} c_n, \qquad c_n \equiv \sum_{k=0}^{n} a_k\, b_{n-k}.$$

If each of the series S_a and S_b is absolutely convergent, the series S converges, and its sum is the product of the sums of the two given series. This theorem, which is due to Cauchy, was generalized by Mertens, who showed that it still holds if only one of the series S_a and S_b is absolutely convergent and the other is merely convergent (see, e.g., Goursat 1904).

whence, performing the integration,

$$\mathcal{H}(\xi, s) = \sum_{n=1}^{\infty} \frac{h_n(\xi)}{s^n}, \qquad h_n(\xi) \equiv -\frac{(-1)^n}{n} \sum_{k=1}^{n} \frac{\xi^{n-k}}{k}, \qquad (s > \xi). \qquad \text{(C20)}$$

Therefore, the asymptotic expansion of the function $\mathcal{H}(\xi, s)$ for "small" and "large" values of s, useful to examine the behaviour of the velocity dispersion profile (see Section 4.2), can be written more explicitly, by retaining the first three terms of the expansion, as

$$\mathcal{H}(\xi, s) = \begin{cases} \mathcal{H}(\xi, 0) + \dfrac{s \ln s}{\xi} - \dfrac{s}{\xi} + \mathcal{O}\big(s^2 \ln s\big), & s < \xi, \\[4mm] \dfrac{1}{s} - \dfrac{2\xi + 1}{4s^2} + \dfrac{6\xi^2 + 3\xi + 2}{18s^3} + \mathcal{O}\left(\dfrac{1}{s^4}\right), & s > \xi. \end{cases} \qquad \text{(C21)}$$

For what concerns the asymptotic behaviour of the function of one variable $\mathcal{H}(\xi, 0)$, useful to study the relevant quantities entering the virial theorem (see Section 5.1), it can be obtained directly by expanding eq. (C10): such expansion gives, at the leading order,

$$\mathcal{H}(\xi, 0) \sim \begin{cases} \dfrac{\ln^2 \xi}{2}, & \xi \to 0, \\[4mm] \dfrac{1}{\xi}, & \xi \to \infty. \end{cases} \qquad \text{(C22)}$$

References

[1] An J. H., & Evans N. W., 2006, ApJ, 642, 752

[2] Bertin G., 2000, *Dynamics of Galaxies*, Cambridge University Press;

[3] Bertin G. & Stiavelli M., 1989, ApJ, 338, 723

[4] Bertin G., Pegoraro F., Rubini F. & Vesperini E., 1994, ApJ, 434, 94

[5] Bertin G., Bertola F., Buson L. M., Danzinger I. J., Dejonghe H., Sadler E. M., Saglia R. P., de Zeeuw P. T., Zeilinger W. W., 1994, A&A, 292, 381

[6] Bertin G., Ciotti L., Del Principe M., 2002, A&A, 386, 149

[7] Binney J., & Tremaine S., 2008, *Galactic Dynamics*, 2nd Ed., Princeton University Press (Binney & Tremaine 2008);

[8] de Bruijne Jos H. J., van der Marel R. P., de Zeeuw P. T., 1996, MNRAS, 282, 909

[9] Bullock J.S. & Boylan-Kolchin M., 2017, Annu. Rev. Astron. Astrophys. 55:343-87

[10] Chandrasekhar S., 1942, *Principles of Stellar Dynamics*, Chicago University Press (Chandrasekhar 1942);

[11] Chandrasekhar S., 1969, *Ellipsoidal Figures of Equilibrium*, Yale University Press (Chandrasekhar 1969);

[12] Ciotti L., 1999, ApJ, 520, 574

[13] Ciotti L., 2000, *Lecture Notes on Stellar Dynamics*, Scuola Normale Superiore Ed. (Ciotti 2000);

[14] Ciotti, L., & Lanzoni, B. 1997, A&A, 321, 724

[15] Ciotti L., & Morganti L., 2009, MNRAS, 393, 179

[16] Ciotti L. & Pellegrini S., 1992, MNRAS, 255, 561 (CP92)

[17] Ciotti L. & Pellegrini S., 2017, arXiv:1707.00741

[18] Ciotti L., & Renzini A., 1993, ApJ, 416, L49

[19] Ciotti L., Morganti L., de Zeeuw P. T., 2009, MNRAS, 393, 491 (CMZ09)

[20] Ciotti L. & Ziaee Lorzad A., 2018, MNRAS, 473, 5476 (CZ18)

[21] Czoske O., Barnabe M., Koopmans L. E. V., Treu T., Bolton, A.S. 2008, ApJ, 384, 987

[22] Dehnen W., 1993, MNRAS, 265, 250

[23] De Vaucouleurs G., 1948, Ann.Astr., 11, 247

[24] Fridman A. M., & Polyachenko V. L., 1984, *Physics of Gravitating Systems*, Springer-Verlag New York Inc.;

[25] Gavazzi R., Treu T., Rhodes J. D., Koopmans, L. V. E., Bolton A. S., Burles S., Massey R. J., Moustakas L. A., 2007, ApJ, 667, 176

[26] Gerhard O., Kronawitter A., Saglia R. P., Bender R., 2001, AJ, 121, 1936

[27] Goursat E., *A Course in Mathematical Analysis. Volume I*, New York: Ginn & Co., 1904 (Goursat 1904);

[28] Goursat E., *A Course in Mathematical Analysis. Volume II, Part Two*, New York: Ginn & Co., 1917 (Goursat 1917);

[29] Gradshteyn I. S., Ryzhik I. M., 2007, in Jeffrey A., Zwillinger D. E., eds, Table of Integrals, Series, and Products, 7th edn. Elsevier, Amsterdam

[30] Hernquist L., 1990, ApJ, 536, 359

[31] Hiotelis N., 1994, A&A, 291, 725

[32] Jaffe W., 1983, MNRAS, 202, 995

[33] Kochanek C. S., 1994, ApJ, 436, 56

[34] Koopmans L. V. E., Treu T., Bolton A. S., Burles S., Moustakas L. A., 2006, ApJ, 649, 599

[35] Kormendy J., & Ho L. C., 2013, ARA&A, 51, 511

[36] Lewin L., Polylogarithms and Associated Functions, 1981, New York: North-Holland

[37] Magorrian J., Tremaine S., Richstone D. et al. 1998, AJ, 115, 2285

[38] Merritt D. & Aguilar L. A., 1985, MNRAS, 217, 787

[39] Meza A. & Zamorano N., 1997, AJ, 490, 136

[40] Naab T. & Ostriker J. P., 2007, MNRAS, 366, 899

[41] Navarro J. F., Frenk C. S., White S. D. M., 1997, ApJ, 490, 493

[42] Nipoti C., Londrillo P. & Ciotti L., 2002, MNRAS, 332, 901

[43] Nipoti C., Treu T. & Bolton A. S., 2008, MNRAS, 390, 349

[44] Ogorodnikov K. F., 1965, *Dynamics of Stellar Systems*, Pergamon Press LTD. (Ogorodnikov 1965);

[45] Osipkov L. P., 1979, Pis'ma Astron. Zh., 5, 77

[46] Pellegrini S., 2011, ApJ, 738, 57

[47] Posacki S., Pellegrini S. & Ciotti L., 2013, MNRAS, 433, 2259

[48] Rix H. W., de Zeeuw P. T., Cretton N., van der Marel R. P., Carollo C. M., 1997, ApJ, 488, 702

[49] Rusin D. & Kochanek C. S., 2005, ApJ, 623, 666

[50] Rusin D., Kochanek C. S., Keeton C. R., 2003, ApJ, 595, 29

[51] Saslaw W. C., 1987, *Gravitational Physics of Stellar and Galactic Systems*, Cambridge University Press (Saslaw 1987);

[52] Shankar F. et al., 2017, ApJ, 840, 34

[53] Tremaine S. et al., 1994, AJ, 107, 634

[54] Treu T. & Koopmans L. V. E., 2004, ApJ, 611, 739

[55] van Hese E., Baes M., Dejonghe H., 2011 ApJ, 726, 80